Determination of boiling heat transfer coefficients in plate heat exchangers

Felix Strandström

Supervisor: Doc. Frank Pettersson

Thermal and Flow Engineering Laboratory

Faculty of Science and Engineering

Åbo Akademi University

Turku, Finland, August 2019

Abstract

Work: Master's Thesis

Title: Determination of boiling heat transfer coefficients in plate heat exchangers

Author: Felix Strandström, Thermal and Flow Engineering Laboratory, Faculty of Science and Engineering, Åbo Akademi University

Supervisors: Åbo Akademi University, Senior Lecturer, Docent Frank Pettersson

Vahterus, Customer Service Director, Valtteri Haavisto

Vahterus, Research and Development Director, Jyrki Sonninen

Place and Date: Turku, 2019

This Master's thesis deals with heat transfer in heat exchangers, with the emphasis on the modelling of flow boiling in plate heat exchangers. In co-operation with the company Vahterus, a computational tool for predicting flow boiling heat transfer coefficients in plate heat exchangers has been developed. The parameters in the models in the computational tool were obtained empirically, by minimizing the deviation from values obtained with proposed correlations and measured experimental values.

Key Words: heat transfer, flow boiling, plate heat exchanger, nucleate boiling, convective boiling

Preface

This work has been continuously educational and a “trial and error” process, because of the general weak knowledge about boiling heat transfer mechanisms presented in the literature. The work has been especially challenging because this field of research often involves many assumptions and speculations when experimental results are analyzed. I would like to express my deepest gratitude to the CEO and founder of Vahterus, Mauri Kontu, for giving me the opportunity to conduct this research in co-operation with his company. I would like to thank Valtteri Haavisto and Jyrki Sonninen at Vahterus for sharing their knowledge and practical experience in this field of science and research, as well as for their patience during this writing process. I would like to thank the laboratory personnel, Kerttu Kupiainen, Juha Karhu and Lauri Rantasalo, for their patience, guidance and practical experience during the evaporation experiments. Finally, I would like to thank my supervisor at the Laboratory of Science and Engineering at Åbo Akademi University, Docent Frank Pettersson for his valuable ideas, knowledge and support during the whole writing and calculation process.

Bestämning av värmegenomgångstalet i kokningsprocesser i plattvärmeväxlare

I dagens samhälle växer behovet av kylutrustning ständigt. Kylutrustning kommer man i kontakt med i många olika applikationer så som; kylare i bilar, kylskåp och luftkonditioneringsapparater. Andra ständigt växande marknader är ofta relaterade till energieffektivitet och miljövänlighet. För att aktörer i olika industribranscher skall uppnå energieffektiv och miljövänlig verksamhet bör till exempel spillvärme från olika industriella processer användas som energikälla. För att utvinna spillvärme bör apparatur som t.ex. värmeväxlare användas i energiutvinningsprocessen. Värmeväxlare är apparatur i vilka två medier utbyter värme med varandra utan att blandas ihop. Medierna i värmeväxlare åtskiljs med en separerande vägg mellan de värmeutbytande medierna (Shah & Sekulic, 2003). I kylutrustning i vilka värmeväxlare utnyttjas, utförs kylningen av så kallade evaporatorer. En evaporator är en värmeväxlare i vilken ett av medierna kokar eller förångas totalt under värmeöverföringsprocessen. När ett medium förångas absorberar det kokande mediet värme av de uppvärmande mediet, vilket resulterar i en kylande effekt i omgivningen.

För att förstå värmeöverföringsmekanismerna i värmeväxlare bör grundläggande värmeöverföringsteori presenteras. Värmeöverföring kan ske på tre olika grundläggande sätt. Värmeöverföring kan ske genom värmeledning, konvektion och strålning. Värmeledning sker genom ett fast material eller genom en fluid i stationära förhållanden. Konvektion sker under värmeöverföringsförhållanden där rörelse är involverad. Värmeöverföring med avseende av strålning kan ske i förhållanden där inget värmeöverförande medium finns i processen. Kravet på att värmeöverföring kan ske överhuvudtaget är att det existerar en temperaturgradient i processen (Incropera *et al.* 2007).

Värmeöverföring som sker i processer i värmeväxlare och inte involverar fasövergång för något av de värmeutbytande medierna har studerats utförligt. Exakta och generella uttryck har skapats för att uppskatta prestandan i dessa processer. Under processer där en eller båda av de värmeutbytande fluiderna byter fas är kunskapen mycket bristfällig i nuläget. Olika fenomen som bör beaktas och mekanismer som sker under kokningsprocesser är fastslagna, men hur dessa fenomen bör beaktas i beräkningar är mycket bristfälliga. Hittills har dessa olika fenomen blivit beaktade i värmeöverföringsprocesser med fasövergång genom att beakta olika parametrar som i sin tur beskriver de olika skeende fenomenen och mekanismerna i

processerna. Viktiga parametrar i kokningsprocesser har föreslagits att vara värmeöverföringsgeometrier, värmeflöde, ångfraktioner, fluidfilmens tjocklek över värmeöverföringsytan, torra lokala områden på värmeöverföringsytan, fluidernas flödesprofiler och halten av olika smörjmedel i det kokande kylmedlet (Ayub *et al.* 2019). Andra tillvägagångssätt för att förutspå kokningen är att betrakta ångbubblornas beteende över geometrin på den upphettade ytan. För att kunna uppskatta värmeöverföringsprestandan i en värmeväxlare bör värmeöverföringskoefficienten i processen uppskattas. Värmeöverföringskoefficienten uppskattas ofta genom att bestämma Nusselts tal i processen. Nusselts tal bestäms i sin tur oftast empiriskt med en ”Nusseltfunktion”. Den enklaste formen av Nusseltfunktioner beaktar Reynolds tal och Prandtls tal. Den enklaste formen av Nusseltfunktioner ger oftast upphov till tillfredsställande och tillräckligt noggranna resultat för värmeöverföringskoefficienterna i värmeöverföringsprocesser där ingen fasövergång sker. I kokning är fallet dock mycket mera komplext. Komplext i avseende på att mycket kokningsdata inte finns allmänt tillgängligt och delvis i avseende på att de som presenterar data vanligen inte presenterar tillräckligt med bakgrundsinformation för att en god uppskattning på värmeöverföringskoefficienten kan utföras. Brister i bakgrundsinformationen är ofta relaterade till geometrier, driftstryck, driftstemperatur och volymflöde kylmedel i värmeväxlaren där kokningen sker (Mahmoud & Karayiannis, 2013; Chen *et al. 2019)*.

Tre egna kokningsexperiment har utförts i olika plattvärmeväxlarkonfigurationer, på grund av den stora utmaningen att få tillräckligt omfattande data för att kunna utföra en analys på kokningsfenomen som sker i värmeväxlare. Efter att experimenten var utförda gjordes en analys på fenomen som sker under kokningen i mellanrummen mellan plattorna i plattvärmeväxlaren. Värmeöverföringskoefficienten beräknades först exakt på basen av termodynamiska egenskaperna vid inloppet och vid utloppet, varefter fem stycken olika modeller skapades för att förutspå kokningens förlopp. Modellerna var empiriskt framställda och byggde på att försöka uppskatta bubbelbeteende i plattvärmeväxlarmellanrummen indirekt genom att beakta olika mekanismer och fenomen med dimensionslösa tal som till exempel Reynolds tal, Prandtls tal, Jakobs tal, Grashofs tal, Webers tal och bonds tal (Brooks & Hibiki, 2015). Ingen av modellerna beaktade ångfraktionens ökning under kokningsprocessen, på grund av att denna inte kunde mätas under experimenten.

Parametrarna i de skapade empiriska modellerna anpassades slutligen till uppmätta värdena på värmeöverföringskoefficienterna, genom att minimera den kvadratiska avvikelsen mellan de empiriskt uppskattade värdena och de verkliga uppmätta värdena på värmegenomgångstalen. Minimeringen av avvikelsen utfördes med MS Excels GRG-optimeringsverktyg. Varje enskild modell anpassades först till kokningsdata för ett experiment i taget. Den modellen som visade högst grad av noggrannhet i varje experiment blev sedan närmare analyserad, för att identifiera de viktigaste mekanismerna under de enskilda kokningsprocesserna. För att verifiera modellerna testades även de mest noggranna modellerna, som var skräddarsydda för de enskilda experimenten, på de andra utförda experimenten. Andra orsaker varför de föreslagna empiriska modellerna testades på experimentella data erhållet från de andra experimenten var för att se ifall de visade en godtagbar grad av noggrannhet och för att se ifall liknande kokningsmekanismer kunde identifieras.

Table of Contents

Nomenclature

Symbol	Description
A	Area
Bi	Biot number
Bl	Boiling number
Bo	Bond number
C	Concentration, heat capacity
C_f	Friction coefficient
c_p	Specific heat capacity
d	Diameter
D_{AB}	Diffusion coefficient
d_h	Hydraulic diameter
E	Emissive power
f	Friction coefficient
g	Gravity
G	Mass flux
Gr	Grashof number
h	Convective heat transfer coefficient
h_m	Convective mass transfer coefficient
i	Specific enthalpy
j	Colburn j factor
Ja	Jakob number
k	Thermal conductivity
L	Length
Le	Lewis number
$\dot{m}$	Mass flow
N_A''	Molar flux
Nu	Nusselt number
NTU	Number of transfer units

Symbol	Description
p	Pressure
P	Perimeter
Pr	Prandtl number
q	Heating power
q''	Heat flux
R	Thermal resistance
Re	Reynolds number
r	Radius
Sc	Schmidt number
Sh	Sherwood number
St	Stanton number
T	Temperature
U	Overall heat transfer coefficient
u	Velocity
v	Kinematic viscosity, velocity
V	Volume, velocity
We	Weber number
x	Mass fraction
X	Lockhart-Martinelli parameter

Greek symbols

Symbol	Description
α	Thermal diffusivity
β	Volumetric thermal expansion coefficient
ε	Effectiveness, emissivity
μ	Dynamic viscosity
σ	Surface tension, Stefan Boltzmann constant

Symbol	Description
τ	Shear stress
ρ	Density

Indexes

Symbol	Description
ave	Average
c	Crossflow, cold
$cond$	Conduction
$conv$	Convection
f	Fluid
fb	Film boiling
fg	Liquid-vapor
h	Hot
i	In
l	Liquid
lm	Logarithmic
m	Mean, mass
max	Maximum
min	Minimum
nb	Nucleate boiling
o	Out
ref	Refrigerant
rad	Radiation
s	Surface
sh	Shell
sat	Saturation
sur	Surroundings
tb	Transition boiling
tp	Two-phase

Symbol	Description
tt	Turbulent-turbulent flow
tu	Tube
v	Vapor
vv	Laminar-laminar flow
w	Wall, water

1 Introduction

1.1 Vahterus

Vahterus was founded in 1990 by Mauri Kontu as a family business in the region of Vakka-Suomi in the western part of Finland. Vahterus is known worldwide as a company that is a pioneer in the heat exchanger industry. The company is the inventor of the so called plate and shell heat exchanger technology. The benefits in the heat exchanger design of Vahterus is the small size and high heat transfer performance compared to conventional shell and tube heat exchangers. Compared to other plate heat exchanger configurations the plate and shell configuration is much more durable, because of its fully welded structure. The headquarters and the manufacturing facilities of the company are located in Finland at the same location in which the company was founded. The innovative heat exchanger design of the company has allowed it to expand globally to the extent that subsidiaries are established in China, in Germany, in the UK and in the US. Vahterus is known as a company where research is conducted continuously internally in the company as well as in cooperation with the customer in order to find unique solutions tailored to the need of every single customer. The heat exchangers manufactured by Vahterus are used in different industries with extremely demanding process conditions such as the oil and gas, chemical process, power production and refrigeration industries worldwide.

1.2 Scope of the work

The market for cooling devices is continuously growing in the modern society. Cooling devices are present in many applications that are used on daily bases, such as the radiators in the cars, fridges and air conditioning devices. Other growing markets in the modern society are strongly linked with continuously growing concepts such as energy efficiency and environmental friendliness in the heavy industry. In order to fulfil these expectations in the context of environmental friendliness, the heavy industry must create more energy efficient solutions, such as waste heat recovery systems. In both cooling applications and in waste heat recovery systems, there are often devices called heat exchangers. Heat exchangers are devices where fluids exchange heat with each other but do not mix together during the heat transfer process (Shah & Sekulic, 2003). In cooling applications, the heat exchangers that perform the actual cooling are often evaporators. During evaporation of a refrigerant in an evaporator the evaporated medium absorbs heat from the heating medium, in other words cools down its surroundings. The theories about occurring phenomena and heat transfer mechanisms are to

some extent in conflict with each other and somewhat vaguely expressed when boiling is considered.

Heat transfer can occur in three major ways: in the context of conduction, in the context of convection and in the context of radiation (Incropera *et al.* 2007). This thesis will present the basics of heat transfer mechanisms that occur in the context of conduction and convection. Radiation heat transfer will only be introduced. After the basic heat transfer theory is presented, the concept of heat exchangers and single phase heat transfer performance calculation methods will be discussed, followed by two-phase heat transfer and boiling theory.

The mechanisms of single-phase heat transfer in shell and tube heat exchangers as well as in plate heat exchangers have been studied widely and accurate expressions have been obtained. Viscous effects have been determined to be of huge importance when liquid heat transfer is predicted. Generally the heat transfer can be predicted satisfactorily with empirical Nusselt functions that account for the Reynolds number and the Prandtl number (Khan *et al.* 2010). The situation is totally different when two-phase heat transfer is considered. Different occurring phenomena have been proposed and are to some extent known. The heat transfer during phase change is strongly dependent on operating conditions and the boiled substance, as well as by the trend of switching boiling mechanism during the phase change. To make the two-phase flow even more complex, the proposed correlations for heat transfer calculations are always developed to a previously specified data set, resulting in no existing accurate general correlations for two-phase heat transfer. Important parameters in the prediction of the heat transfer coefficient during boiling phenomena have been determined to be heat transfer geometry, heat flux, mass flux, vapor quality, the thickness of the liquid or vapor film on the surface, effects of dry out, flow regime and the possible presence of lubricants in the system (Ayub *et al.* 2019).

The emphasis of this thesis will lie on the boiling and phase change heat transfer calculations. In order to gather boiling heat transfer data, three experiments with similar heat transfer geometries but different operating conditions have been conducted with plate and shell heat exchangers. Based on the data from the conducted experiments the different dominating mechanisms will be determined in the boiling processes. After the mechanisms are determined, empirical correlations will be proposed for predicting the heat transfer during boiling processes.

2 Heat transfer theory

There are three types of heat transfer: Conduction, convection and radiation. Conduction occurs across a stationary solid or a fluid. Convection occurs between a moving fluid and a surface, with the prerequisite that the surface and the moving fluid are at different temperatures. Radiation heat transfer occurs due to surfaces emitting electromagnetic waves. Radiation occurs also in the absence of a heat transferring medium between two surfaces at different temperatures. The prerequisite for heat transfer to occur is a temperature gradient existing in the process.

Fourier's law expresses the conduction heat flux according to:

$$q_x'' = k\frac{dT}{dx} = k\frac{\Delta T}{L}, \tag{1}$$

where L is the thickness of the conducting material and k is the thermal conductivity of the material. The heat transfer direction x is perpendicular to the isotherms.

As mentioned before, convection occurs between a moving fluid and a surface if a temperature difference exists between them. The temperatures within the moving fluid are different at different distances from the stationary surface. The section where the temperatures are different in the fluid is called the thermal boundary layer. Generally, the phenomenon of convection is dominated by random molecular movement at the surface, due to a flow velocity assumed to be close to 0. The random molecular movement is called diffusion. The boundary layer thickness grows with larger distances along the heat conducting surface and with increasing fluid velocity. The heat is finally conducted through the thermal boundary layer to the surrounding fluid. There are two types of convection: forced and natural convection. Forced convection is flow motion in the fluid created by external means, such as by gravity, by a pump, by a fan or by atmospheric winds. Natural convection is movement created by internal density differences in a fluid. Newton's law of cooling describes the heat flux created by convection according to:

$$q'' = h(T_s - T_\infty), \tag{2}$$

where q'' is the heat flux, h is the convection heat transfer coefficient, T_s is the temperature at the surface and T_∞ is the temperature outside the boundary layer.

Radiation heat flux can be expressed as

$$q''_{rad} = \frac{q}{A} = \varepsilon \cdot E_b(T_s) - \alpha \cdot G, \tag{3}$$

where $G = \sigma \cdot T_{sur}^4$. If a gray surface ($\varepsilon = \alpha$) is considered, the radiation heat flux can be written as:

$$q''_{rad} = \frac{q}{A} = \varepsilon \cdot \sigma \cdot (T_s^4 - T_{sur}^4). \tag{4}$$

In summary, the prerequisite for heat transfer to occur is a temperature gradient existing in the process. An energy balance around a surface can be written as:

$$q''_{cond} - q''_{conv} - q''_{rad} = 0$$

(Incropera *et al.* 2007).

2.1 Conduction

The conduction heat transfer rate is defined according to:

$$q_x = -k \cdot A \cdot \frac{dT}{dx}. \tag{5}$$

If the conduction heat flux occurs in three dimensions, it can be written as:

$$q'' = -k\nabla T = -k\left(i\frac{\partial T}{\partial x} + j\frac{\partial T}{\partial y} + z\frac{\partial T}{\partial z}\right) \tag{6}$$

where,

$$q''_x = -k\frac{\partial T}{\partial x}$$

$$q''_y = -k\frac{\partial T}{\partial y}$$

$$q''_z = -k\frac{\partial T}{\partial z}.$$

The thermal conductivity k is a constant that indicate how well a specific material conduct heat. Another constant that can be taken into consideration when selecting materials for a heat transfer process is the thermal diffusivity α, which indicate how fast a material respond to thermodynamic changes in the surroundings. The properties of a material with a large α will respond rapidly to thermodynamic changes in the surrounding environment, while a

material with a small α will respond more slowly to thermodynamic changes in the environment. The thermal diffusivity is defined as:

$$\alpha = \frac{k}{\rho \cdot c_p}. \tag{7}$$

2.2 Heat transfer over a surface

Heat transfer processes can include conduction, convection and radiation. Generally, it is most common to neglect the heat transfer in the context of radiation in heat transfer processes that occur in heat exchangers.

The thermal heat resistance is a phenomenon that describes how well a material, or a fluid will resist heat absorption. For conduction the thermal resistance is defined as:

$$R_{t,cond} = \frac{T_{s,1} - T_{s,2}}{q_x} = \frac{L}{k \cdot A}, \tag{8}$$

for convection the thermal resistance is defined as:

$$R_{t,conv} = \frac{T_s - T_\infty}{q} = \frac{1}{h \cdot A} \tag{9}$$

and for radiation the thermal resistance is defined as:

$$R_{t,rad} = \frac{T_s - T_{sur}}{q_{rad}} = \frac{1}{h_r \cdot A}, \tag{10}$$

where the radiation heat transfer coefficient is

$$h_r = \varepsilon \cdot \sigma \cdot (T_s + T_{sur})(T_s^2 + T_{sur}^2). \tag{11}$$

If an overall heat transfer coefficient U is introduced, the thermal resistance can be written in a general form such as:

$$R_{tot} = \sum R_t = \frac{\Delta T}{q} = \frac{1}{UA}. \tag{12}$$

The overall heat transfer coefficient, U, describes how well heat is transferred in a system. In cases of heat exchangers the dominating heat transfer mechanisms are often considered to be conduction and convection over a surface according to:

$$R_{tot} = \frac{1}{h_1 A} + \frac{L}{k \cdot A} + \frac{1}{h_2 \cdot A}, \tag{13}$$

where the indexes 1 and 2 refer to the different sides of a separating wall in a heat exchanger.

There are several options to increase the convection-conduction heat transfer between a fluid and a solid surface. If a plain surface, with a fixed surface temperature T_s is considered, one option is to increase the flow velocity of the fluid. Another option is to reduce the temperature outside the heat transfer boundary layer T_∞. The heat transfer coefficient increases with increasing fluid flow velocities which, in turn, results in increasing heat transfer rates. Increasing temperature differences between the temperature at the surface and the temperature outside the boundary layer also improves the heat transfer rate. However, when the fluid velocity is increased under the aforementioned conditions, the pump or fan power demand is also increased. An increase in pump or fan power demand results in higher operating costs of the process, which may be unattractive. The second option, suggesting to decrease the temperature outside the boundary layer T_∞, is often considered impractical, as the goal could be to heat the fluid flowing over the surface. A third option to enhance the conduction-convection heat transfer between a solid and a fluid is to extend the contact surface between the media by implementing fins at the surface. By implementing fins, the heat transfer area increases, which results in an improved heat transfer rate. The fins may also generate turbulence, which induces mixing and improves the heat transfer rate. Ideally, the fins would be constructed of materials with high thermal conductivity, with the purpose to achieve minimum temperature variations between the attached fin and the base surface. The design of the fins and the surface depends on space, weight, manufacturing and cost considerations as well as the convective heat transfer reduction properties of the fins and the additional pressure drop created by them.

The convective heat transfer is in theory two dimensional in transverse directions to the fin. In practice, the temperature differences in the fins are small compared to the differences between the fins and the surroundings due to thin fins. This knowledge of the practical case allows the assumption of one-dimensional heat transfer. If one-dimensional conditions are assumed in the x-direction with a constant thermal conductivity, negligible radiation from the surface, a uniform convection heat transfer coefficient, no heat generation and steady state conditions, a general energy equation for an extended surface can be derived as:

$$\frac{d}{dx}\left(A_c \frac{dA_c}{dx}\right) - \frac{h}{k}\frac{dA_s}{dx}(T - T_\infty) = 0 \tag{14}$$

or

$$\frac{d^2T}{dx^2} + \left(\frac{1}{A_c}\frac{dA_c}{dx}\right)\frac{dT}{dx} - \left(\frac{1}{A_c}\frac{h}{k}\frac{dA_s}{dx}\right)(T - T_\infty) = 0. \quad (15)$$

A_c refers to the crossflow area and A_s refers to the heat transfer surface area in equations (14) and (15). The solution for equation (15), for appropriate boundary conditions, provides the temperature distribution for equation (1) which, in turn, may be used for determining the conduction heat transfer rate of any x, namely at any position in the surface.

2.3 Convection

The ratio between the conductive and the convective heat transfer resistance is defined by the Biot number Bi. The mathematical expression is defined as:

$$\frac{T_{s,1}-T_{s,2}}{T_{s,2}-T_\infty} = \frac{(L/kA)}{(1/hA)} = \frac{R_{cond}}{R_{conv}} = \frac{hL}{k} = \mathrm{Bi}. \quad (16)$$

If $\mathrm{Bi} \ll 1$ the resistance against conductive heat transfer is much lower compared to the resistance of convective heat transfer in the boundary layer. This indicates that the temperature gradient in the solid is small. For large Bi numbers, the temperature gradient is significant in the solid.

The following condition indicates a small Bi number:

$$\mathrm{Bi} = \frac{hL_c}{k} < 0.1,$$

where the characteristic length L_c is defined by:

$$L_c \equiv \frac{V}{A_s}.$$

2.3.1 Convection boundary layers and convection transfer coefficients

The velocity boundary layer thickness is defined by the value of the velocity u at an orthogonal distance from the surface where:

$$u = 0.99u_\infty \quad (17)$$

and u_∞ is the temperature outside the boundary layer. For external flows, the friction coefficient is defined by:

$$C_f \equiv \frac{\tau_s}{\rho u_\infty^2/2}, \quad (18)$$

where τ_s is the shear stress of the surface, and is defined as:

$$\tau_s = \mu \frac{\partial u}{\partial y}\Big|_{y=0}. \quad (19)$$

Thermal boundary layers develop if the temperature of a fluid stream at a given distance of a surface is different compared to the temperatures of the fluid stream near the surface. At the edge of the thermal boundary layer the temperature at a distance y, $T(y) = T_\infty$, is uniform. The particles in the boundary layer exchange energy with the particles outside the boundary layer and heat exchange occur. The thickness of the thermal boundary layer is then typically defined by:

$$\frac{T_s - T(y)}{T_s - T_\infty} = 0.99, \quad (20)$$

where T_s is the temperature at the surface, $T(y)$ is the temperature at a distance y from the surface and T_∞ is the temperature outside the thermal boundary layer.

At the solid surface, where the fluid velocity is assumed to be 0, only conductive heat transfer occurs. According to Fourier's law, the conductive heat flux to the fluid is:

$$q_s'' = -k_f \frac{\partial T}{\partial y}\Big|_{y=0}. \quad (21)$$

The convective heat flux is defined according to Newton's law of cooling, according to equation (2). If equations (2) and (21) are combined, the following expression for the convective heat transfer coefficient is obtained (with the conditions that heat transfer only occurs from a surface to a fluid):

$$h = \frac{-k_f \frac{\partial T}{\partial y}\Big|_{y=0}}{T_s - T_\infty}. \quad (22)$$

Convection is not a phenomenon that only cover heat transfer, but also in different cases mass transfer. If a mixture of two chemical species, A and B, which are flowing over a surface is considered, a concentration boundary layer exists if the concentration of one of the species is different at the surface and at a given distance from the surface. The concentration can be different due to, for example, evaporation and sublimation of a fluid on a solid surface. The thickness of the layer, where the concentration gradient exists, is usually defined by:

$$\frac{C_{A,s} - C_A(y)}{C_{A,s} - C_{A,\infty}} = 0.99, \quad (23)$$

where $C_{A,s}$ refers to the concentration of species A at the surface, $C_A(y)$ refers to the concertation at a distance y from the surface and $C_{A,\infty}$ refers to the concentration outside the boundary layer. The molar flux is defined by Fick's law as:

$$N_A'' = -D_{AB} \frac{\partial C_A}{\partial y}\Big|_{y=0}, \tag{24}$$

with the condition that only species transfer by diffusion mechanism occurs at the surface. Newton's law of cooling can also be applied to the diffusion mechanism according to:

$$N_{A,s}'' = h_m\big(C_{A,s} - C_{A,\infty}\big). \tag{25}$$

If equations (24) and (25) are combined, the convection mass transfer coefficient can be obtained according to:

$$h_m = \frac{-D_{AB}\frac{\partial C_A}{\partial y}\Big|_{y=0}}{(C_{A,s} - C_{A,\infty})}. \tag{26}$$

If a surface is considered to be isotherm and the temperature outside the boundary layer differs from the temperature inside the boundary layer, convection heat transfer will occur. The total heat transfer rate can be obtained if the heat flux is integrated over the surface area according to:

$$q = \int_{A_s} q''\, dA_s. \tag{27}$$

If an average coefficient is used, the heat transfer rate can be written as:

$$q = \bar{h} A_s (T_s - T_\infty). \tag{28}$$

The average heat transfer coefficient, used in equation (28), is obtained by integrating the local heat transfer coefficients over the surface area according to:

$$\bar{h} = \frac{1}{A_s}\int_{A_s} h\, dA_s. \tag{29}$$

In the special case, where the surface is considered to be a flat plate, the convection heat transfer coefficient will only vary by the distance x to the plate according to:

$$\bar{h} = \frac{1}{L}\int_0^L h\, dx. \tag{30}$$

A similar approach can be made when determining molar mass transfer of a surface. The result is:

$$N_A = \overline{h_m} A_s \left(C_{A,s} - C_{A,\infty}\right), \tag{31}$$

where

$$\overline{h_m} = \frac{1}{A_s} \int_{A_s} h_m \, dA_s. \tag{32}$$

In the special case, where a flat plate is considered, the result is equally:

$$\overline{h_m} = \frac{1}{L} \int_0^L h_m \, dx, \tag{33}$$

compared to the heat transfer case.

The mass transfer equations can also be modified by multiplying the concentrations of the species with their molar mass M_i:

$$\rho_A = M_A C_A. \tag{34}$$

The following results are obtained:

$$n''_{A,s} = h_m \left(\rho_{A,s} - \rho_{A,\infty}\right) \tag{35}$$

and

$$N_A = \overline{h_m} A_s \left(\rho_{A,s} - \rho_{A,\infty}\right), \tag{36}$$

which in turn result in:

$$N''_A = -D_{AB} \left. \frac{\partial \rho_A}{\partial y} \right|_{y=0} \tag{37}$$

and

$$h_m = \frac{-D_{AB} \left. \frac{\partial \rho_A}{\partial y} \right|_{y=0}}{\left(\rho_{A,s} - \rho_{A,\infty}\right)}. \tag{38}$$

The problems linked to convection heat transfer, are the determination of the convection heat and mass transfer coefficients. The coefficients are dependent on fluid properties such as: thermal conductivity, specific heat, viscosity as well as surface geometry (Incropera *et al.* 2007). An example when convective mass transfer is relevant to take into consideration, is

during phase change phenomena, because the properties of the fluid change along with increasing or decreasing vapor fractions in the fluid. Another remarkable case when convective mass transfer needs to be considered is when a mixture of substances is boiled or condensed. The phase change of mixtures often results in that one of the components will condense or evaporate before the others which, in turn, will change the properties of the boiled or condensed mixture, which also will affect the heat transfer rate in the process.

2.3.2 Single phase flow conditions

There are three types of single phase flow conditions: Laminar, transition and turbulent flow conditions. In laminar flow conditions, the flow profile is well organized. In turbulent flow conditions, the flow profile is characterized by irregular and random movement. The transition flow profile is something of a crossing between laminar and turbulent flows, where both well-organized flow patterns and highly irregular flow patterns can be observed in the flow profile. The flow conditions are determined by the Reynolds number, Re, which is defined by:

$$\mathrm{Re}_x = \frac{\rho u_\infty x}{\mu}. \tag{39}$$

The flow conditions have an influence on the convective heat and mass transfer. Turbulent flow conditions promote large temperature and species concentration gradients within the fluid flowing on a surface. The large temperature and species concentration gradients result in increasing convective heat and mass transfer coefficients. The turbulent flow induces mixing. Mixing decreases the importance of taking into consideration conduction and diffusion when determining the boundary layer thickness, because the differences in the velocity, concentration and thermal boundary layer thicknesses tend to be much smaller in turbulent flow conditions compared to laminar flow conditions (Incropera *et al.* 2007).

In order to determine if the flow regime is laminar, transient or turbulent, one has to consider the geometry and what type of calculation is to be made. Now the limits for different flow regimes for smooth circular pipes will be presented. When Reynolds numbers are below 2000, the flow regime is considered stable and the flow laminar. When Reynolds numbers are above 2100, pressure drop calculations can be made for turbulent flows. For heat transfer calculations the criterion for turbulent flow conditions is considered to be above 10,000 (Bell & Mueller, 2001). Figure 1 illustrates the flow patterns for the different flow regimes.

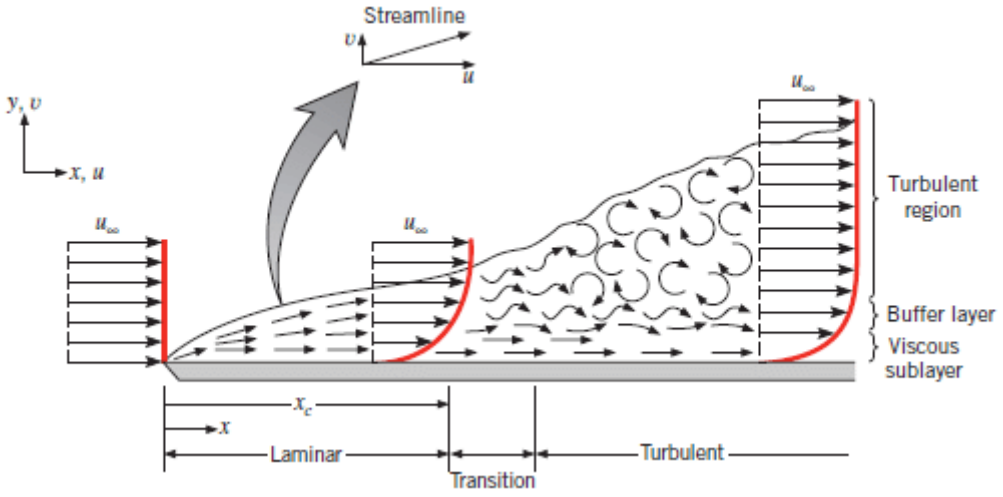

Figure 1: The development of the single phase flow profile over a flat plate (Incropera et al. 2007).

2.3.3 Dimensionless boundary similarity parameters, variables and equations

In order to obtain equations that are applicable for different types of surfaces, and hence how the surface geometry affects the convective mass and heat transfer in different situations, boundary similarity parameters, variables and equations are introduced. The boundary similarity equations are dimensionless independent variables that can be defined as:

$$x^* \equiv \frac{x}{L} \tag{40}$$

$$y^* \equiv \frac{y}{L} \tag{41}$$

where L is the characteristic length of the surface. Other dimensionless variables may be related to the velocity such as

$$u^* \equiv \frac{u}{V} \tag{42}$$

$$v^* \equiv \frac{v}{V} \tag{43}$$

where V is the upstream velocity of the surface, and also

$$T^* \equiv \frac{T-T_s}{T_\infty - T_s} \tag{44}$$

$$C_A^* \equiv \frac{C_A - C_{A,s}}{C_{A,\infty} - C_{A,s}} \tag{45}$$

$$p^* \equiv \frac{p_\infty}{\rho V^2}\,. \tag{46}$$

After the dimensionless variables are introduced, boundary layer equations can be presented as conservation equations for the surface.

The conservation equations for the velocity, heat and concentration at the boundary layer are presented as:

$$u^* \frac{\partial u^*}{\partial x^*} + v^* \frac{\partial v^*}{\partial y^*} = -\frac{dp^*}{dx^*} + \frac{1}{\mathrm{Re_L}} \frac{\partial^2 u^*}{\partial y^{*2}} \tag{47}$$

$$u^* \frac{\partial T^*}{\partial x^*} + v^* \frac{\partial T^*}{\partial y^*} = \frac{1}{\mathrm{Re_L Pr}} \frac{\partial^2 T^*}{\partial y^{*2}} \tag{48}$$

$$u^* \frac{\partial C_A^*}{\partial x^*} + v^* \frac{\partial C_A^*}{\partial y^*} = \frac{1}{\mathrm{Re_L Sc}} \frac{\partial^2 C_A^*}{\partial y^{*2}}, \tag{49}$$

with the boundary conditions at the surface:

$$u^*(x^*, 0) = 0$$

$$v^*(x^*, 0) = 0$$

$$T^*(x^*, 0) = 0$$

$$C_A^*(x^*, 0) = 0$$

and outside the boundary layer as:

$$u^*(x^*, \infty) = \frac{u_\infty(x^*)}{V}$$

$$T^*(x^*, \infty) = 1$$

$$C_A^*(x^*, \infty) = 1$$

with the similarity parameters:

$$\mathrm{Re}_L = \frac{VL}{v} \tag{50}$$

$$\mathrm{Pr} = \frac{v}{\alpha} \tag{51}$$

$$\mathrm{Sc} = \frac{v}{D_{AB}}. \tag{52}$$

As a result, from the dimensionless equations (47)-(49), variables (40)-(46) and parameters (50)-(52), it is possible to determine which variables are affected by changes in other variables, according to:

$$u^* = f\left(x^*, y^*, \mathrm{Re_L}, \frac{dp^*}{dx^*}\right). \tag{53}$$

The shear stress at the surface can be expressed as

$$\tau_s = \mu \frac{\partial u}{\partial y}\Big|_{y=0} = \left(\frac{\mu V}{\mathrm{Re_L}}\right) \frac{\partial u^*}{\partial y^*}\Big|_{y^*=0}, \tag{54}$$

with

$$\frac{\partial u^*}{\partial y^*}\Big|_{y^*=0} = f\left(x^*, \mathrm{Re_L}, \frac{dp^*}{dx^*}\right). \tag{55}$$

The friction coefficient can further be expressed as:

$$C_f = \frac{2}{\mathrm{Re_L}} f(x^*, \mathrm{Re_L}). \tag{56}$$

The dimensionless variable referring to the temperature can be expressed as:

$$T^* = f\left(x^*, y^*, \mathrm{Re_L}, \mathrm{Pr}, \frac{dp^*}{dx^*}\right) \tag{57}$$

and the convective heat transfer coefficient can be written as:

$$h = -\frac{k_f}{L} \frac{(T_\infty - T_s)}{(T_s - T_\infty)} \frac{\partial u^*}{\partial y^*}\Big|_{y^*=0} = \frac{k_f}{L} \frac{\partial u^*}{\partial y^*}\Big|_{y^*=0} \tag{58}$$

(Incropera *et al.* 2007).

2.3.4 Nusselt and Sherwood number

A dimensionless temperature gradient on a surface is described by the Nusselt number, Nu, according to:

$$\mathrm{Nu} = \frac{hL}{k_f} = \frac{\partial T^*}{\partial y^*}\Big|_{y^*=0}. \tag{59}$$

The Nusselt number can also be written as a function as:

$$\mathrm{Nu} = f(x^*, \mathrm{Re_L}, \mathrm{Pr}). \tag{60}$$

If only an average Nusselt number is taken into consideration, it can be defined as:

$$\overline{\mathrm{Nu}} = \frac{\bar{h}L}{k_f} = f(\mathrm{Re_L}, \mathrm{Pr}). \tag{61}$$

Similarly, the concentration at different distances of the surface and the mass transfer coefficient can be described as:

$$C_A^* = f\left(x^*, y^*, \mathrm{Re_L}, \mathrm{Sc}, \frac{dp^*}{dx^*}\right) \tag{62}$$

and

$$h_m = -\frac{D_{AB}}{L}\frac{C_{A,\infty}-C_{A,S}}{C_{A,S}-C_{A,\infty}}\frac{\partial C_A^*}{\partial y^*}\bigg|_{y^*=0} = \frac{D_{AB}}{L}\frac{\partial C_A^*}{\partial y^*}\bigg|_{y^*=0}. \tag{63}$$

From the aforementioned relationships, the Sherwood number, Sh, can be defined as:

$$\mathrm{Sh} = \frac{h_m L}{D_{AB}}, \tag{64}$$

with

$$\mathrm{Sh} = f(x^*, \mathrm{Re_L}, \mathrm{Sc}) \tag{65}$$

$$\overline{\mathrm{Sh}} = \frac{\overline{h_m} L}{D_{AB}} = f(\mathrm{Re_L}, \mathrm{Sc}) \tag{66}$$

(Incropera *et al.* 2007).

2.3.5 Interpretation of the dimensionless parameters

The Reynolds number describes the ratio between inertia forces and viscous forces in a fluid. The Reynolds number is defined by:

$$\mathrm{Re_L} = \frac{\rho V L}{\mu} = \frac{VL}{\nu}, \tag{67}$$

which indicates that inertia forces dominate at large Reynolds numbers and viscous forces dominate at small Reynolds numbers.

The Prandtl number, Pr, is defined as the ratio of momentum diffusivity ν compared to the thermal diffusivity α. The Prandtl numbers obtain values near unity for gases, which indicate that momentum and thermal diffusivity are of equal importance. For liquids the case can be totally different, where thermal diffusivity can be a dominating phenomenon.

$$\mathrm{Pr} = \frac{\nu}{\alpha} = \frac{c_p \mu}{k} \tag{68}$$

Similarly, the Schmidt number, Sc, provides information about the ratio between the momentum and mass diffusion rate in the velocity and the concentration boundary layers, according to:

$$\mathrm{Sc} = \frac{v}{D_{AB}}\,. \tag{69}$$

A ratio between the thermal and concentration boundary layer thicknesses is provided by the Lewis number Le:

$$\mathrm{Le} = \frac{\alpha}{D_{AB}} = \frac{\mathrm{Sc}}{\mathrm{Pr}}\,. \tag{70}$$

2.3.6 Relevant dimensionless groups for convective heat and mass transfer

In mass and heat transfer calculations, dimensionless groups are often utilized in order to gather information about the process conditions. This section will summarize all of the most common dimensionless groups that are used in such calculations.

The ratio between the thermal resistance of the boundary layer compared to the resistance of the solid surface is defined by the Biot number, Bi, according to equation (16).

The ratio of gravitational and surface tension forces of an upwards flowing fluid, is described by the Bond number, Bo, according to:

$$\mathrm{Bo} = \frac{g(\rho_l - \rho_v)L^2}{\sigma}\,. \tag{71}$$

Surface shear stress is expressed by the coefficient of friction, defined in equation (18).

The pressure drop of internal flows is expressed by the friction factor:

$$f = \frac{\Delta p}{\left({}^{L}/_{D}\right)\left({}^{\rho u_m^2}/_{2}\right)}\,. \tag{72}$$

The ratio between buoyancy forces and viscous forces is described by the Grashof number, Gr, according to:

$$\mathrm{Gr} = \frac{g\beta(T_s - T_\infty)L^3}{v^2}\,. \tag{73}$$

Natural convection is considered to be strongly linked with the Grashof number as a phenomenon.

The ratio between the sensible heat absorbed and the latent heat, during a liquid-vapor phase change, is defined by the Jakob number, Ja, according to:

$$\mathrm{Ja} = \frac{c_p(T_s - T_{sat})}{i_{fg}}. \tag{74}$$

Dimensionless heat and mass transfer coefficients are defined by the Colburn *j* factors, j_H and j_m

$$j_H = \mathrm{StPr}^{2/3} \tag{75}$$

$$j_m = \mathrm{StSc}^{2/3}. \tag{76}$$

The Lewis number describes the ratio between thermal and mass diffusion as defined by equation (70).

The Nusselt number, which describes the ratio between convection to pure conduction in a fluid, is defined by equation (59).

The ratio between the momentum and the thermal diffusivities, is defined by the Prandtl number according to equation (68).

In order to determine whether to assume turbulent or laminar flow regimes, knowledge about the ratio between inertia and viscous forces is needed. The flow regimes are assumed with the Reynolds number that is calculated with equation (67).

The ratio between momentum and mass diffusivities is defined by the Schmidt number, expressed by equation (69).

Concentration gradients in the boundary layer are expressed in equation (64) by the Sherwood number.

The Stanton number is a modified form of the Nusselt number and is defined by:

$$\mathrm{St} = \frac{h}{\rho V c_p} = \frac{\mathrm{Nu_L}}{\mathrm{Re_L Pr}} \tag{77}$$

for heat transfer. For mass transfer the Stanton number can similarly be expressed as a modification of the Sherwood number:

$$\mathrm{St}_m = \frac{h_m}{V} = \frac{\mathrm{Sh}_L}{\mathrm{Re}_L Sc}. \tag{78}$$

The ratio between the surface tension forces and the inertia forces in a fluid is defined by the Weber number:

$$\mathrm{We} = \frac{\rho V^2 L}{\sigma}. \tag{79}$$

If equation (77) and (78) are analyzed, a proportional correlation can be obtained between the Nusselt number and the Sherwood number according to:

$$\frac{\mathrm{Nu}}{\mathrm{Pr}^n} = \frac{\mathrm{Sh}}{\mathrm{Sc}^n}. \tag{80}$$

Equation (80) can further be developed to:

$$\frac{h}{h_m} = \frac{k}{D_{AB}\mathrm{Le}^n} = \rho c_p \mathrm{Le}^{n-1}. \tag{81}$$

Equation (81) can be utilized to determine either the convective mass transfer or the convective heat transfer coefficient, if one of them is known. Equation (81) can be applied on both turbulent or laminar flow conditions and average convective heat and mass transfer coefficients (Incropera *et al.* 2007).

2.3.7 Empirical determination of the dimensionless groups

It is possible to determine the average Nusselt and Sherwood number empirically, if experimental data is available for the specific conditions. The average convective heat and mass transfer coefficients can often be determined based on the following correlations according to:

$$\overline{\mathrm{Nu_L}} = C\mathrm{Re}_L^m \mathrm{Pr}^n \tag{82}$$

and

$$\overline{\mathrm{Sh_L}} = C\mathrm{Re}_L^m \mathrm{Sc}^n. \tag{83}$$

The Prandtl number is only dependent on the fluid and not on the surface geometry. The coefficients *C*, *m* and *n* could then be determined by plotting $\mathrm{Nu_L}$ against $\mathrm{Re_L}$ in a log-log diagram and minimizing the deviation from the test results. The equations could further be made more accurate by multiplying with a correction factor:

$$\left(\frac{\mathrm{Pr}_\infty}{\mathrm{Pr}_s}\right)^r$$

or

$$\left(\frac{\mu_\infty}{\mu_s}\right)^r.$$

Another option is to calculate the fluid properties at a mean temperature within the boundary layer according to:

$$T_f = \frac{(T_s - T_\infty)}{2} \tag{84}$$

(Incropera *et al.* 2007). The aforementioned correlations are typical empirical correlations presented in the literature in the form of:

$$\overline{\mathrm{Nu}} = \frac{\bar{h}L}{k_f} = f(\mathrm{Re_L}, \mathrm{Pr}).$$

There exist numerous variants, all depending on the dominating phenomena that occur in the heat transfer processes. The different phenomena are represented by the dimensionless numbers included in the empirical equations. The equations are often of one of the following types:

$$\overline{\mathrm{Nu}} = \frac{\bar{h}L}{k_f} = f(\mathrm{Gr}, \mathrm{Re}_L, \mathrm{Pr} \dots)$$

$$\overline{\mathrm{Nu}} = \frac{\bar{h}L}{k_f} = f(\mathrm{Gr}, \mathrm{Re}_L, \mathrm{Pr}, \mathrm{Ja} \dots)$$

$$\overline{\mathrm{Nu}} = \frac{\bar{h}L}{k_f} = f(\mathrm{Gr}, \mathrm{Pr})$$

(Incropera *et al.* 2007).

2.3.8 Internal single phase flows

For internal flows, the Reynolds number is defined by:

$$\mathrm{Re}_D = \frac{\rho u_m D}{\mu} = \frac{u_m D}{v}, \tag{85}$$

where the mean flow velocity is

$$u_m = \frac{\dot{m}}{\rho A_c} \tag{86}$$

(Incropera *et al.* 2007).

Equation (85)-(86) can be combined and the following result is obtained:

$$\mathrm{Re} = \frac{\dot{m} d_h}{\mu A_c} = \frac{G d_h}{\mu}, \tag{87}$$

where

$$G = \frac{\dot{m}}{A_c} \tag{88}$$

(Hesselgreaves, 2001). The hydraulic diameter, d_h, is defined as:

$$d_h = 4 \frac{\text{wetted flow area}}{\text{wetted perimeter}} = 4 \left(\frac{A_c}{P} \right) \tag{89}$$

(Clark, 1969). An energy balance over an internal flow can be described by:

$$\dot{m} c_p T_m = \int_{A_c} \rho u c_p T dA_c. \tag{90}$$

If equation (90) is further manipulated, the mean temperature of an internal flow can be obtained by:

$$T_m = \frac{\int_{A_c} \rho u c_p T dA_c}{\dot{m} c_p} \tag{91}$$

(Incropera *et al.* 2007).

2.3.9 Crossflow over a tube

The convective heat transfer of a crossflow of a fluid over a tube can be calculated by:

$$q_{conv} = \bar{h} A_s \Delta T_{lm}. \tag{92}$$

If the surface temperature $T_s =$ constant, or if the temperature of the external fluid $T_\infty =$ constant, equation (90) can further be developed to:

$$q = \overline{U} A_s \Delta T_{lm}. \tag{93}$$

The logarithmic mean temperature is defined by:

$$\Delta T_{lm} = \frac{\Delta T_o - \Delta T_i}{\ln\left(\frac{\Delta T_o}{\Delta T_i}\right)} \tag{94}$$

and

$$\frac{\Delta T_o}{\Delta T_i} = \frac{T_\infty - T_{m,o}}{T_\infty - T_{m,i}} = e^{\left(-\frac{\bar{U}A_S}{\dot{m}c_p}\right)} \quad (95)$$

(Incropera *et al.* 2007).

3 Heat exchangers

A heat exchanger is an apparatus in which two fluids exchange heat with each other through a separating wall that prevents them from mixing together (Shah & Sekulic, 2003). Heat exchangers are often classified according to their fluid flow arrangements, namely: parallel flow or co-current flow, counterflow or crossflow. In parallel flow heat exchangers, the fluids flow alongside in the same direction with each other and the fluids enter and exit at the same ends. In counterflow heat exchangers, the fluids enter and exit at opposite ends of the exchanger which, in turn, result in that the fluids flow in opposite directions. In crossflow heat exchangers, the fluids move in a perpendicular direction compared to each other (Incropera *et al*. 2007). Heat exchangers can also be classified according to the construction and their construction methods. Generally the exchangers are considered to be of plate type or of tube type classification according to their construction. The heat transfer surfaces can be provided by fins in order to extend the surface or to promote the flow of the fluid by preventing the fluid from flowing in a transverse direction from the surface. Fluid motion in a heat exchanger can either be considered mixed or unmixed. Unmixed fluid motion is defined by an existing temperature gradient at different distances of the surface as well as along the heat conducting surface. Mixed fluid motion is defined by a temperature gradient that exists only in the flow direction along the heat conducting surface (Incropera *et al.* 2007). The most common heat exchanger configurations are: shell and tube heat exchangers, finned tube heat exchangers, bare tube heat exchangers, plate and frame heat exchangers, spiral heat exchangers, helical coil heat exchangers and plate coil heat exchangers (Hall, 2018). This work will focus on the plate heat exchangers and, more specifically, on plate and shell evaporating heat exchanger configurations.

A shell and tube exchanger is a heat exchanger where a tube bundle is inserted into a pressure vessel. One fluid flows in the tubes and another outside the tubes. Shell and tube heat exchangers are considered to be the most common configuration in the chemical process industries (Hall, 2018). A plate and shell heat exchanger is constructed of a plate pack that is inserted into a pressure vessel. The plate pack has the same function as the tube bundle in the shell and tube configuration. The plate pack consists of plates that are pairwise welded together, which results in passages in which the different fluids flow and exchange heat but do not mix with each other according to figure 2. The plates are often provided with a

corrugated pattern on the surface, which promotes mixing and turbulent flows of the fluids (Shah & Sekulic, 2003).

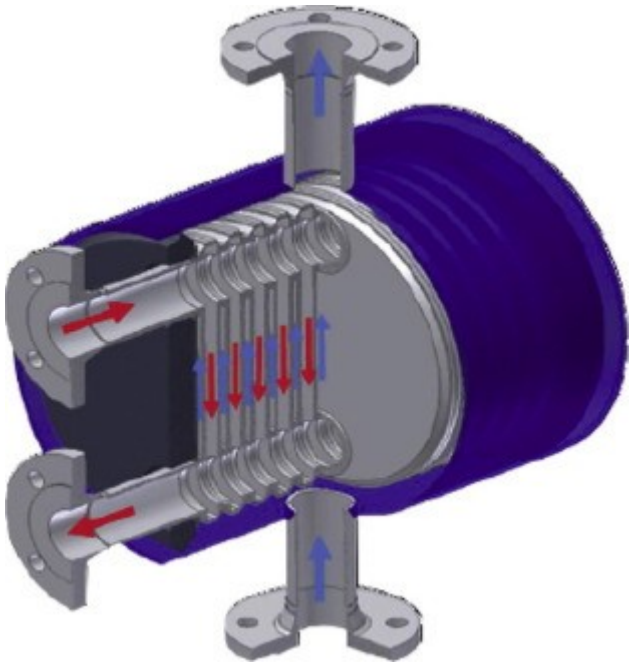

Figure 2: Typical structure and flow arrangement in a plate and shell heat exchanger (Tovazhnyanskyy et al. 2016*).*

The performance of a heat exchanger can suddenly decrease to a not desirable level because of fouling. The most common types of fouling are called: sedimentation fouling, inverse solubility fouling, chemical reaction fouling and corrosion product fouling. Sedimentation fouling occurs when solids inside a heat transfer fluid form a restricting layer on the heat transfer surface. The formation of the restricting layer is dependent on the fluid velocities and operating temperatures. Inverse solubility fouling occurs typically when salts containing fluids are used as heat transfer fluids. Some salts are more soluble in different fluids at low temperatures than at high temperatures. Thus, when the temperatures in the fluid increase, the salts start to crystallize at the heat transfer surfaces and decrease the heat transfer in the system. Chemical reaction fouling can occur if a fouling layer is formed on the heat transfer surface due to a chemical reaction that occurs in the heat exchanger. Chemical reaction fouling can typically occur during film boiling (presented later in the boiling section of this thesis) when a fluid is thermally degraded due to extremely high heat transfer surface temperatures. Corrosion product fouling occurs because of corroded surfaces. Corrosion affects the smoothness of the heat transfer surfaces. Rough surfaces may attach particles that are brought in with the fluid streams. The particles that are stuck to the heat transfer surfaces

will, in turn, worsen the heat transfer from the surfaces to heat heated fluid. Fouling can also occur as combinations of the aforementioned mechanisms (Bell & Mueller, 2001). Other authors mention that the most common fouling mechanisms are: Crystallization or precipitation fouling, particulate fouling or silting, biological fouling, corrosion fouling, chemical reaction fouling and freezing or solidification fouling. Crystallization fouling occurs when crystals are formed directly on the heat transfer surface or in the heat transfer fluid in a heat exchanger. Crystallization fouling is a phenomenon that also covers the aforementioned inverse solubility fouling. Particulate fouling is a phenomenon that occurs when particles cover the heat transfer surface at one or many locations in a heat exchanger which, in turn, results in worse heat transfer. Biological fouling is a result of the presence and growth of organisms on the heat transfer surface. Biological fouling may promote the aforementioned corrosion fouling. Chemical reaction fouling may also promote corrosion of the heat transfer surfaces. Solidification fouling occurs when the operating temperatures in the heat exchanger drop too low and a solid insulating layer is formed on the heat transfer surface (Hesselgreaves, 2001).

Now two overall calculation methods for dimensioning heat exchangers will be presented. The first is the logarithmic mean temperature difference method (LMTD-method) and the second is called the number of transfer unit method (NTU-method). None of the presented methods will provide any information about local thermal performance within the exchanger, only information about global thermal performance (Incropera *et al.* 2007).

3.1 LMTD-method

If an energy balance is introduced over a heat exchanger, it can be described as:

$$q = \dot{m}_h\left(i_{h,i} - i_{h,o}\right) \tag{96}$$

or

$$q = \dot{m}_c\left(i_{c,o} - i_{c,i}\right). \tag{97}$$

If there are no phase changes in the fluids during the heat transfer process and their specific heat is assumed to be constant, the energy balance can be written as:

$$q = \dot{m}_h c_{p,h}\left(T_{h,i} - T_{h,o}\right) \tag{98}$$

and

$$q = \dot{m}_c c_{p,c}\left(T_{c,o} - T_{c,i}\right). \tag{99}$$

If the aforementioned expressions are interpreted by Newton's law of cooling, the result is:

$$q = UA_s \Delta T_m\,, \tag{100}$$

where the mean temperature difference T_m can be estimated by the logarithmic mean temperature difference ΔT_{lm} according to:

$$\Delta T_m \approx \Delta T_{lm} = \frac{\Delta T_2 - \Delta T_1}{\ln\left(\frac{\Delta T_2}{\Delta T_1}\right)}\,. \tag{101}$$

The temperature differences ΔT_2 and ΔT_1 are described according to the flow configuration existing in the heat exchanger. For parallel flow configurations the temperature differences are described by:

$$\Delta T_1 = T_{h,1} - T_{c,1} = T_{h,i} - T_{c,i} \tag{102}$$

and

$$\Delta T_2 = T_{h,2} - T_{c,2} = T_{h,o} - T_{c,o}. \tag{103}$$

For counterflow heat exchangers the temperature differences are described by:

$$\Delta T_1 = T_{h,1} - T_{c,1} = T_{h,i} - T_{c,o} \tag{104}$$

and

$$\Delta T_2 = T_{h,2} - T_{c,2} = T_{h,o} - T_{c,i}. \tag{105}$$

It is remarkable that in the two different heat exchanger configurations, $T_{c,o}$ can be a higher temperature than $T_{h,o}$ in counterflow configurations but not in parallel flow configurations. The temperature distribution for single-phase flows is presented in figure 3 and figure 4.

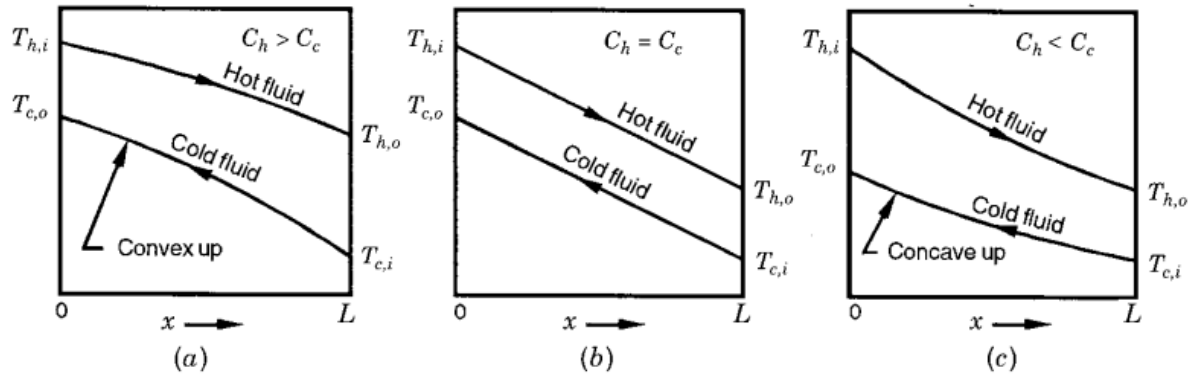

Figure 3: Temperature distribution for single-phase counterflow flow configurations, C_h and C_c refers to the heat capacities of the hot and the cold streams (Shah & Sekulic, 2003).

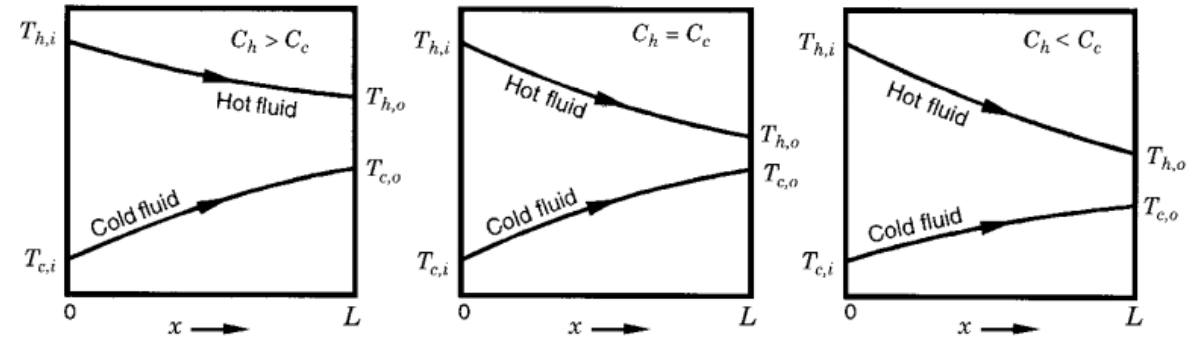

Figure 4: Temperature distribution for single-phase parallel flow configurations, C_h and C_c refers to the heat capacities of the hot and the cold streams (Shah & Sekulic, 2003).

The expressions used in the LMTD-method are only valid if the following assumptions are made:

1. The only heat exchange that occurs is between the hot and the cold fluid, which means that the heat exchanger is totally insulated from the surroundings.
2. Axial conduction along the surface is negligible
3. Negligible differences in potential and kinetic energy
4. The specific heats of the fluids are constant
5. The overall heat transfer coefficient U is constant
6. Parallel or counterflow flow configuration in the heat exchanger

(Incropera *et al.* 2007; Bell & Mueller, 2001).

In order to account for different flow configurations in different types of heat exchangers, a temperature correction factor F is introduced. The temperature correction factor F expresses

the deviation from the behavior in a pure counterflow heat exchanger in the aspect of performance. The expression for Newton's law of cooling is further developed to:

$$q = FUA_s\Delta T_{lm} \tag{106}$$

(Hesselgreaves, 2001). The temperature correction factor F is defined by:

$$F = \frac{\Delta T_m}{\Delta T_{lm}}, \tag{107}$$

where ΔT_{lm} is the logarithmic mean temperature difference predicted for pure counterflow configurations and ΔT_m is the real mean temperature difference (Bell & Mueller, 2001).

3.2 NTU-method

In this section, the NTU-effectiveness method will be introduced, as an alternative approach to predict the performance to the LMTD-method presented previously. The aim of the NTU-effectiveness method is to anticipate the most economic design of a heat exchanger. The energy balance is equal to the one presented in the LMTD-method, according to:

$$q = \dot{m}_h c_{p,h}\left(T_{h,i} - T_{h,o}\right) \tag{98}$$

and

$$q = \dot{m}_c c_{p,c}\left(T_{c,o} - T_{c,i}\right). \tag{99}$$

The product $\dot{m}_h c_{p,h}$ and $\dot{m}_c c_{p,c}$ will now be denoted as C_h and C_c. Equally the maximum heat transfer capacity of the streams in a heat exchanger will be named C_{max} and the minimum heat transfer capacity of the streams in a heat exchanger will be named C_{min}. The ratio between the maximum and minimum heat transfer capacities will now be denoted C_r according to:

$$C_r = \frac{C_{min}}{C_{max}}. \tag{108}$$

The maximum possible amount of heat transferred in a heat exchanger, or the heat transferred in an infinite long heat exchanger can now be defined as:

$$q_{max} = C_{min}\left(T_{h,i} - T_{c,i}\right)$$

At this stage, enough new variables are presented to introduce the definition of the effectiveness ε:

$$\varepsilon = \frac{q}{q_{max}} = \frac{C_h(T_{h,in}-T_{h,out})}{C_{min}(T_{h,in}-T_{c,in})} = \frac{C_c(T_{c,out}-T_{c,in})}{C_{min}(T_{h,in}-T_{c,in})}. \quad (109)$$

The effectiveness, ε, of a heat exchanger describes the ratio between heat transferred in reality and the theoretical maximum of heat transferred in a process. Now a new parameter for the thermal design problems will be introduced, namely the number of transfer units, NTU, which describes the thermal length of a heat exchanger. NTU is defined according to:

$$NTU = \frac{UA_S}{C_{min}}. \quad (110)$$

There are correlations between the NTU and the effectiveness ε. The correlations are dependent on the flow configuration as well as of the presence of mixing of the fluids. The most common correlations are presented in equations (111)-(126).

Counterflow:

$$\varepsilon = \frac{1-e^{((-NTU)(1-C_r))}}{1-C_r e^{((-NTU)(1-C_r))}} \quad (111)$$

Unmixed crossflow:

$$\varepsilon = 1 - e^{\left(\left(e^{(-NTU^{0.78}C_r)}-1\right)NTU^{0.22}/C_r\right)} \quad (112)$$

Parallel or cocurrent flow:

$$\varepsilon = \frac{1-e^{(-NTU(1+C_r))}}{1+C_r} \quad (113)$$

Crossflow, C_{min} unmixed:

$$\varepsilon = \frac{1}{C_r}\left[1 - e^{\{-C_r[1-e^{(-NTU)}]\}}\right] \quad (114)$$

Crossflow, C_{max} unmixed:

$$\varepsilon = 1 - e^{\left\{\frac{1}{C_r}\times\left[1-e^{(-NTUC_r)}\right]\right\}} \quad (115)$$

Crossflow, both fluids mixed:

$$\varepsilon = \frac{1}{\frac{NTU}{1-e^{(-NTU)}}+\frac{NTUC_r}{1-e^{(-NTUC_r)}}-1} \quad (116)$$

Multipass overall counterflows, fluids mixed between passes:

$$\varepsilon = \frac{\left(\frac{1-\varepsilon_p C_r}{1-\varepsilon_p}\right)^n - 1}{\left(\frac{1-\varepsilon_p C_r}{1-\varepsilon_p}\right)^n - C_r} \quad (117)$$

$n =$ number of identical passes, ε_p = effectiveness of each pass

$$\varepsilon_p = \frac{\left(\frac{1-\varepsilon C_r}{1-\varepsilon}\right)^n - 1}{\left(\frac{1-\varepsilon C_r}{1-\varepsilon}\right)^{1/n} - C_r} \tag{118}$$

Multipass overall parallel flow, fluids mixed between passes:

$$\varepsilon = \frac{1}{1+C_r}\left[1 - \left\{1 - (1+C_r)\varepsilon_p\right\}^n\right] \tag{119}$$

All configurations for pure evaporation and condensation $C_r = 0$:

$$\varepsilon = 1 - e^{(-NTU)}. \tag{120}$$

The following section presents inverse relationships between the NTU and the ε, if the terminal temperatures are known.

Counterflow:

$$NTU = \frac{1}{C_r - 1} ln\left(\frac{\varepsilon - 1}{\varepsilon C_r - 1}\right) \tag{121}$$

Counterflow $C_r = 1$:

$$NTU = \frac{\varepsilon}{1-\varepsilon} \tag{122}$$

Parallel flow:

$$NTU = \frac{-ln[1-(1+C_r)\varepsilon]}{1+C_r} \tag{123}$$

Crossflow:

C_{max} mixed, C_{min} unmixed:

$$NTU = -ln\left[1 + \frac{1}{C_r} ln(1 - C_r\varepsilon)\right] \tag{124}$$

C_{max} unmixed, C_{min} mixed:

$$NTU = \frac{-1}{C_r} ln[1 + ln(1-\varepsilon)] \tag{125}$$

All configurations, $C_r = 0$:

$$NTU = -ln(1-\varepsilon) \tag{126}$$

(Hesselgreaves, 2001).

3.3 Determination of the temperature correction factor F

There are some analytical expressions that can be used to calculate the correction factor F for some specific configurations, but charts presented in the literature are usually used. In order to use the charts, two new parameters, P and R, need to be introduced. For shell and tube heat exchangers, the parameters are defined by:

$$R = \frac{\Delta T_{sh}}{\Delta T_{tu}} \tag{127}$$

and

$$P = \frac{\Delta T_{tu}}{\Delta T_{max}}, \tag{128}$$

where ΔT_{sh} refers to the temperature range of the shell side, ΔT_{tu} refers to the temperature range on the tube side and ΔT_{max} refers to the maximum temperature difference in a heat exchanger (Bell & Mueller, 2001).

4 Boiling

Boiling and condensation are considered to be convective heat transfer, because both of them include fluid motion as phenomena. Important parameters in boiling and condensation processes are the latent heat, i_{fg}, surface tension between the vapor-liquid interface, σ, and density differences between vapor and liquid.

There are two major types of boiling: pool-boiling and convective boiling. Pool-boiling occurs when a heated surface generates bubbles in a fluid which, in turn, creates motion in the fluid. The fluid motion in pool-boiling is created by temperature gradients within the fluid and density gradients between the vapor bubbles and the liquid. The density gradients create buoyancy motion. In convective boiling, the fluid flow is generated externally by for example a pump and the mechanism is forced convection, or by buoyancy motion created by a heated surface, which results in the natural convection mechanism (Incropera F.P. *et al.* 2007).

4.1 Pool boiling

Pool boiling is a phenomenon that occurs when a surface heats a fluid and the fluid starts to boil. The fluid motion is created due to density differences between liquid and vapor, and temperature gradients within the fluid. The heat flux is dependent on the temperature difference between the saturation temperature of the fluid and the temperature of the heated surface. The mechanism of pool boiling is divided into four different boiling regimes, namely: natural convection, nucleate boiling, transition boiling and film boiling according to the temperature difference between the saturation temperature of the fluid and the heated surface (Incropera F.P. *et al.* 2007). Figure 5 illustrates the different pool boiling regimes and the principal correlation between the heat flux and the temperature difference between the heating wall and the saturation temperature of the fluid.

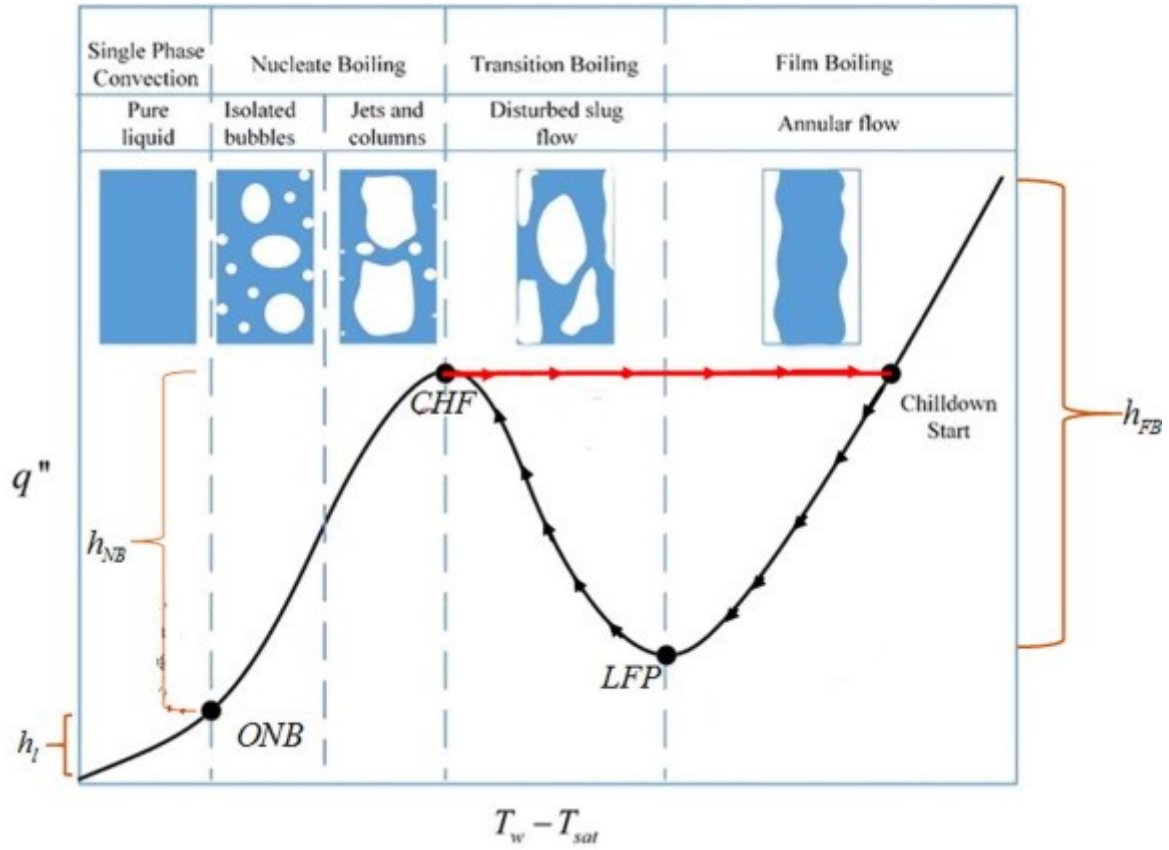

Figure 5: A boiling curve that illustrates different boiling regimes. The temperature difference between the surface and the saturation temperature is compared to the heat flux into the liquid (Hartwig et al. 2016).

At low temperature differences the dominating heat transfer regime is natural convection. Visually the flow regime is characterized by the formation of small bubbles in the heated liquid.

When the temperature differences increase, larger bubbles are formed at nucleation sites (scratches or pitches at the heated surface) in the fluid. The bubbles grow rapidly at the nucleation sites and start to move due to buoyant forces. The heat flux increases with increasing temperature differences between the heated surface and the saturation temperature of the fluid. This boiling regime is called nucleate boiling.

When the temperature difference is further increased a new boiling regime starts to dominate, namely the transition boiling. Transition boiling is characterized by a decreased heat flux with increasing temperature differences between the surface and the saturation temperature of the fluid.

Film boiling is the dominating boiling regime at huge temperature differences between the surface and the saturation temperature of the fluid. Large fouling, low heat fluxes and low heat transfer coefficients often feature this boiling regime. A vapor film is generated along the heated surface, resulting in the liquid floating over the vapor film. The boiled substance can be thermally degraded during these kinds of boiling regimes (Bell & Mueller, 2001). The possible increase in heat flux is due to radiation from the heated surface to the liquid over the vapor film formed on the surface (Coulson *et al.* 2000).

4.2 Vaporization during flow

4.2.1 Multiphase flow patterns

The flow patterns in multiphase flows cannot be distinguished to be of type laminar, transition or turbulent as the single phase flows presented previously in the section concerning flow conditions, due to different flow velocities of the vapor phase and the liquid phase. The flow patterns can be classified as bubble flow, plug flow, stratified flow, wavy flow, slug flow, annular flow and mist flow in horizontal flows in ducts. In horizontal bubble flow, the vapor and liquid have the same relative velocity and vapor bubbles are typically formed at the top of the duct. Horizontal plug flow indicates that the vapor forms plugs that are surrounded by liquid in the flowing fluid at the top of the duct. In stratified horizontal flows, the liquid flows at the bottom of the duct and the vapor flows at the top of the duct, resulting in a vapor-liquid interface being clearly distinguished. High vapor flow velocities compared to liquid flow velocities result in waves of vapor and so-called wavy flows. Horizontal annular flows mean that a liquid film is formed at the surface of the duct while vapor flows in the center. At the highest vapor velocities compared to the liquid, the flow turns into mist flow. Mist flow means that the liquid is only present as droplets in the vapor (Perry *et al.* 1997). The horizontal two-phase flow patterns are presented in figure 6.

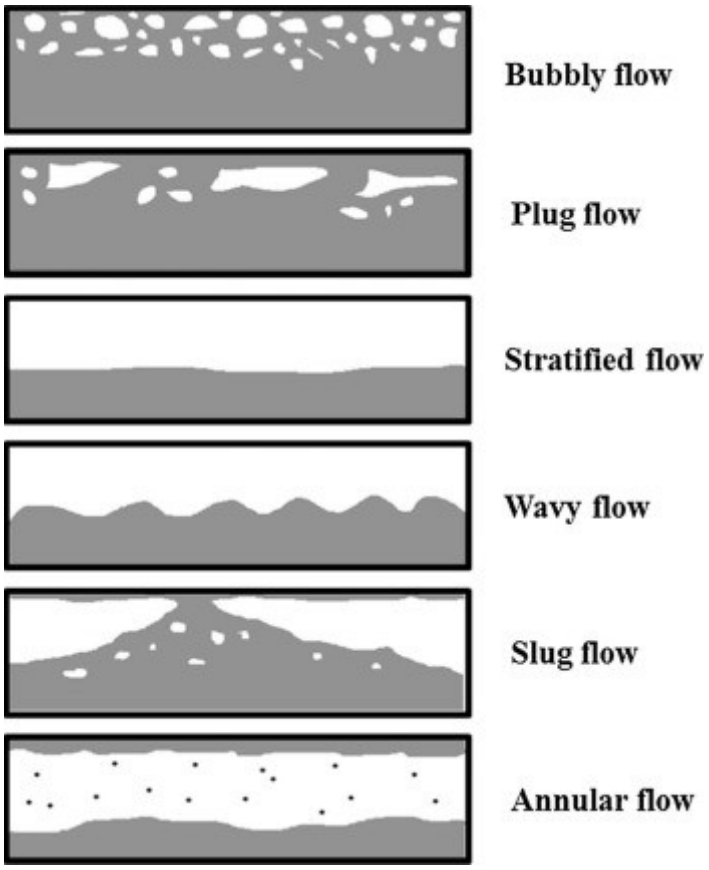

Figure 6: Horizontal two-phase flow patterns (Kumar Singh *et al.* 2018*).*

In vertical flows in ducts the flow patterns can generally be described as bubble flow, slug flow, churn flow, annular flow and mist flow according to figure 7. Vertical bubble flow is obtained when vapor bubbles are dispersed throughout the liquid and most of the vapor bubbles are typically present in the center of the duct. Vertical multiphase slug flow occurs when small vapor bubbles merge together and form vapor bubbles with nearly the same diameter as the duct. The large bubbles are surrounded by liquid and smaller vapor bubbles in multiphase vertical slug flow. Churn flow can be described as flows where neither the vapor phase nor the liquid phase can be distinguished as continuous or dispersed, due to intense mixing. Annular and mist flow can be described in the same way as for horizontal ducts (Perry *et al.* 1997).

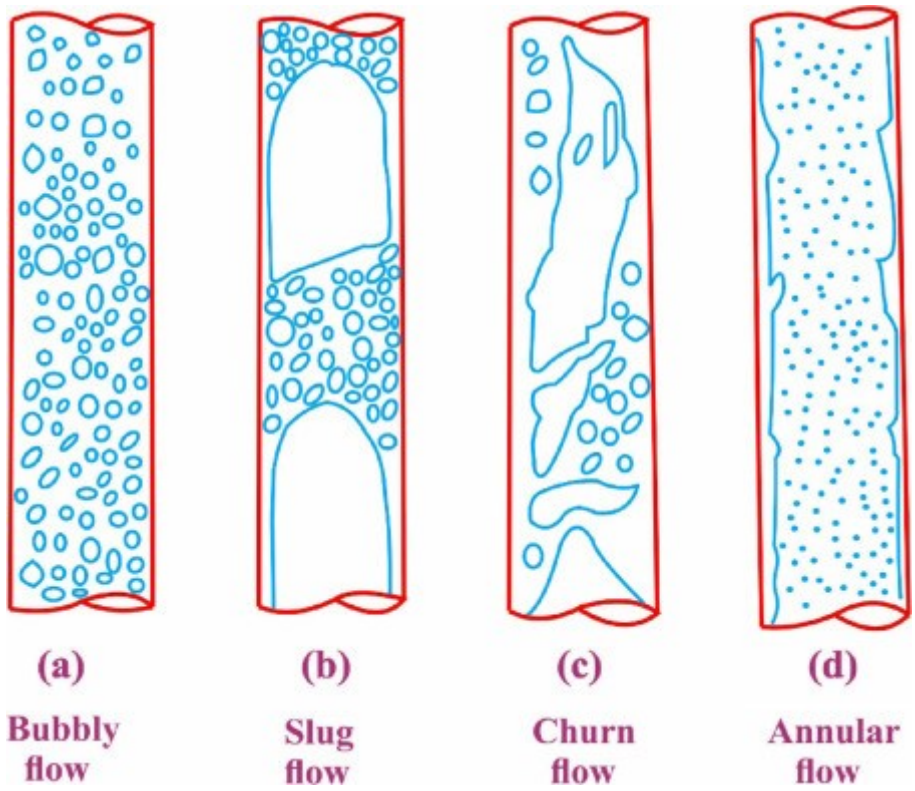

Figure 7: Different flow patterns of vertical two-phase flows (Ebrahimi-Mamaghani *et al.* 2019*).*

4.2.2 Flow boiling heat transfer mechanisms

Forced convection usually dominates the heat transfer during flow boiling phenomena. Nucleate and film boiling are common boiling regimes that occur in heat transfer processes in heat exchangers (Bell & Mueller, 2001).

Flow boiling and vaporization are often investigated in two major ways: either by the increased vapor fraction in the fluid or by vapor bubble behavior in the fluid. Flow boiling in a heat exchanger can be divided into different heat transfer regions according to the conditions at the specific levels in the exchanger, if the flow of the boiled fluid is directed vertically upwards or downwards. The regions are called: the region for subcooled boiling, the region for saturated boiling and the region for nucleate boiling. Many empirical correlations have been proposed for predicting the heat transfer coefficient in different boiling regimes at different kinds of process conditions and geometries. The problems with the existing empirical formulas are that they have a totally different level of accuracy at, for example, different flow rates and heat flux rates. Problems have especially been encountered at conditions with low flow rates of the boiled medium, because buoyancy forces have not been taken into

consideration when the empirical correlations have been determined. It has been determined that buoyancy strongly affects the behavior of a refrigerant vapor bubble and the vapor accumulation of the refrigerant at low refrigerant flow rates.

Flow boiling is known to be governed by two general mechanisms simultaneously, namely nucleate boiling and convective boiling. The two-phase heat transfer coefficient is then often expressed as of types:

$$h_{tp} = S \cdot h_{nb} + F \cdot h_{sp,l}\ , \tag{128}$$

$$\left(h_{tp}\right)^2 = (S \cdot h_l)^2 + \left(F \cdot h_{pool}\right)^2 \tag{129}$$

and

$$\left(h_{tp}\right)^3 = (S \cdot h_l)^3 + \left(F \cdot h_{pool}\right)^3, \tag{130}$$

where S is a suppression factor that takes into account an increasing vapor fraction during a boiling process. F is an enhancement factor that takes into account an increasing fluid velocity during a vaporization process. The enhancement factor, F, is in some expressions based on the Lockhart-Martinelli parameter, which is further based on the vapor fraction at a specified height in the evaporator. In other expressions the enhancement factor F is based on the boiling number, Bl, which expresses the dependence of the ratio of heat flux brought into the system and the heat flux needed for total evaporation of the fluid, the Jakob number, which takes into account subcooling of the fluid and the Prandtl number that takes into account thermophysical properties of the fluid at specified states. The single-phase heat transfer coefficient is usually determined by the common Dittus-Boelter correlation. The indices *nb, tp* and *l* stands for nucleate boiling, two-phase and liquid in the aforementioned equations (128)-(130). Empirical correlations for two-phase flows have been presented to be of type:

$$\frac{\mathrm{Nu}_{tp}}{\mathrm{Nu}_l} = a\mathrm{Bl}^b\mathrm{Ja}^c\mathrm{Pr}^d \tag{131}$$

(Chen *et al.* 2019).

The boiling number is defined according to (Chen, 1966):

$$\mathrm{Bl} = \frac{q_{in}}{\dot{m}\, i_{fg}}. \tag{132}$$

The Lockhart-Martinelli parameter is defined according to the flow conditions in a heat transfer process. For laminar-laminar flows of the two phases, the Lockhart-Martinelli parameter is defined according to:

$$X_{vv} = \left(\frac{1-x}{x}\right)^{0.5} \left(\frac{\rho_v}{\rho_l}\right)^{0.5} \left(\frac{\mu_l}{\mu_v}\right)^{0.5} \tag{133}$$

(Koyama *et al*. 2014). For turbulent-turbulent flows of the two phases, the parameter is defined according to:

$$X_{tt} = \left(\frac{1-x}{x}\right)^{0.9} \left(\frac{\rho_v}{\rho_l}\right)^{0.5} \left(\frac{\mu_l}{\mu_v}\right)^{0.1} = \left(\frac{\dot{m}_l}{\dot{m}_v}\right)^{0.9} \left(\frac{\rho_v}{\rho_l}\right)^{0.5} \left(\frac{\mu_l}{\mu_v}\right)^{0.1} \tag{134}$$

(Nitsche & Gbadamosi, 2016). The Dittus-Boelter correlation is defined as:

$$\mathrm{Nu}_l = 0.023 \mathrm{Re}_l^{0.8} \mathrm{Pr}_l^{0.4} \tag{135}$$

(Chen *et al.* 2019).

Other approaches for predicting heat transfer coefficients during flow boiling, are to calculate the heat transfer coefficient based on both the mechanisms of nucleate boiling and convective boiling. After the heat transfer coefficients have been calculated, the boiling heat transfer coefficients will be compared with each other and the one with the largest value will be selected. In order to generate more accurate correlations, the heat transfer is often divided into specific regions in order to determine the dominating mechanisms. The final general approach for predicting boiling heat transfer coefficients is to conduct an analysis of the dimensionless groups, followed by the determination of the most important ones and creating an empirical correlation based on the selected dimensionless groups (Mahmoud & Karayiannis, 2013).

Wall nucleation is a phenomenon that occurs during a liquid-vapor phase change when a surface is superheated compared to the saturation point of a heated liquid and the vapor starts to form in small cavities on the heated surface. The roughness in the surface traps gas, which in turn results in the formation and growth of bubbles. If the surface is wet and the wall remains superheated, the bubbles can remain growing up to their critical size or collapse and condensate in the surrounding bulk fluid (Brooks & Hibiki, 2015).

The required surface superheat has been determined to be an important factor in the bubble and boiling behavior of fluids. Rough surfaces tend to promote the formation of bubbles and decrease the required temperature difference that launches the boiling phenomena compared to smooth surfaces. The heated surfaces can be divided into three different categories based on the roughness and bubble behavior they cause during boiling. The different types of surfaces can be classified as non-wettable, partially wettable or entirely wetted surfaces. Boiling at non-wettable surfaces results in the vapor spreading out over the surface and reducing the area that the liquid can be in contact with the surface. Boiling at non-wettable surfaces tends to result in worse heat transfer during the process compared to boiling at other surface types. Partially wettable surfaces are surfaces with many nucleation sites where the formation of bubbles can occur. The heat transfer is higher when boiling occurs at partially wettable surfaces compared to non-wettable surfaces due to a larger contact area between the liquid and the heated surface. Boiling at entirely wetted surfaces results in a minimum contact area between the vapor and the heated surface. The bubbles are formed and released rapidly from the surface. Boiling at entirely wetted surfaces often results in many nucleation sites and in the generated bubbles being small in size. Boiling at entirely wetted surfaces results in the highest heat transfer compared to the other surface configurations (Coulson *et al.* 2000).

Nucleate boiling has generally been characterized as a boiling regime where the boiling heat transfer coefficient is strongly dependent on the heat flux brought into the system. The convective boiling heat transfer coefficient has been determined to be more dependent on the mass flux of the boiled refrigerant. Although these characteristic properties of the boiling heat transfer coefficient for the specific boiling regimes have been presented, it is not yet clear if nucleate boiling or convective boiling governs the heat transfer in plate heat exchangers during boiling processes. The boiling heat transfer regime has been reported to be strongly dependent on the operating conditions. It has been reported that the nucleate boiling regime governs when the boiled fluid contains small amounts of vapor fractions. When the vapor fraction increases, the boiling heat transfer mechanism switches from nucleate boiling to convective boiling. Generally, the nucleate boiling regime governs at low mass fluxes while convective boiling governs at large mass fluxes. The pressure in the system and the reduced pressure that is generated during the boiling process are reported to have negligible impacts

on the local heat transfer boiling coefficients in both the nucleate and convective boiling regimes (Táboas *et al.* 2010). Low mass fluxes often occur in direct expansion evaporators, which results in the nucleate boiling regime dominating over the convective boiling regime. In flooded evaporators the mass flux is usually high which, in turn, results in convective boiling dominating over nucleate boiling (Eldeeb *et al.* 2016).

It has been reported that important parameters to be considered when determining the heat transfer coefficient in a plate heat exchanger are the plate geometry (including chevron angles), heat and mass flux, vapor quality, film thickness on the surface, flow regime, the phenomenon of dry out and the effects of lubricants in the system. It is complicated to account for all the phenomena in an empirical correlation, and therefore the most important are often attempted to be selected based on the accuracy of the different empirical correlations. There are differences between evaporation inside tubes and evaporation inside channels in plate heat exchangers. Evaporation inside tubes is considered to be dominated by three mechanisms: nucleate boiling, convective boiling and dry out. The dominating boiling regime in plate heat exchangers is often determined to be convective boiling due to high mass fluxes in the narrow plate gaps (Ayub *et al.* 2019). Higher chevron angles are often associated with higher heat transfer coefficients than in heat exchangers provided with plates with lower chevron angles. Disadvantages with higher chevron angles are that they tend to increase the frictional pressure drop over the heat exchanger. Both the heat transfer coefficient and the pressure drop tend to increase with increasing vapor quality, and decrease with decreasing saturation temperatures of the refrigerant as well as with decreasing chevron angels (Eldeeb *et al.* 2016).

The Nusselt number describes the ratio between convective and conductive heat transfer, often in terms of the Reynolds number and the Prandtl number. The Reynolds number is dependent on the density of the fluid, the viscosity of the fluid, the velocity of the fluid and the characteristic length of the duct or channel the fluid is flowing in. The velocity of the fluid is further proportional to the bubble size, the bubble departure frequency and to the length the liquid is required to flow in order to replace the formed vapor bubbles on the surface. The Jakob number, which describes the maximum available sensible heat compared to the latent heat in a fluid in a heat transfer process, has been confirmed to have a large impact on the bubble departure frequency in the fluid and the bubble size, which in turn have an impact on

the fluid velocity. The bubble size is affected and the bubble diameter is strongly dependent on the Prandtl number. With increasing Prandtl numbers the thermal boundary layer will increase proportionally to the velocity boundary layer which, in turn, will allow the vapor bubbles to grow to a larger size, before mixing with the bulk fluid (Brooks & Hibiki, 2015).

5 Empirical determination of boiling heat transfer coefficients

Three experiments have been conducted with the purpose to investigate different approaches to calculate heat transfer coefficients during boiling and evaporation phenomena in plate and shell heat exchangers. In the first experiment, a flooded evaporator was investigated in a thermosiphon configuration. In the second experiment, the performance of an evaporator operating between saturated liquid and vapor in a cascade refrigeration cycle was investigated. In the third experiment, a superheating direct expansion evaporator was investigated in a refrigeration cycle. The aim of the experiments was to determine a two-phase heat transfer coefficient on the evaporating side of the evaporators. The LMTD-method was used to determine the overall heat transfer coefficient of the different heat exchangers. Warm water was used as heat source in all of the different experiments. Accurate calculation methods had been determined previously for the heating warm water side in all configurations. The geometries of the heat transfer plates in the evaporators were similar in all of the different experiments, which meant that only the operating conditions in the experiments could be focused on and deviations in plate geometries could be neglected.

In order to determine a heat transfer coefficient, one must determine the Nusselt number, which defines the ratio of convective and conductive heat transfer in a system according to:

$$\mathrm{Nu} = \frac{h \cdot d_h}{k}. \tag{59}$$

The Nusselt number is usually empirically determined by a Nusselt function that is dependent on dimensionless flow numbers that describe different phenomena in a process according to:

$$\mathrm{Nu} = f(\mathrm{Re}, \mathrm{Pr}, \mathrm{Gr}, \mathrm{Ja}, \mathrm{Bo}, \mathrm{We} \ldots),$$

where the Prandtl number is defined according to equation (68), the Reynolds number is defined by equation (87), the Grashof number is defined according to equation (73), the Jakob number is defined by equation (74), the Bond number is defined according to equation (71) and the Weber number is defined by equation (79) in a system according to:

$$\mathrm{Pr} = \frac{v}{\alpha} = \frac{c_p \mu}{k}$$

$$\mathrm{Re} = \frac{\rho u d_h}{\mu_l} = \frac{\dot{m} d_h}{A_c \mu_l} = \frac{u d_h}{v_l}$$

$$\mathrm{Gr} = \frac{g\beta(T_s - T_\infty)L^3}{v^2}$$

$$\mathrm{Ja} = \frac{c_p(T_s - T_{sat})}{i_{fg}}$$

$$\mathrm{Bo} = \frac{g(\rho_l - \rho_v)L^2}{\sigma}$$

$$\mathrm{We} = \frac{\rho d_h u^2}{\sigma}.$$

The least complicated Nusselt function usually presented in the literature, is of type:

$$\mathrm{Nu} = a\mathrm{Re}^b\mathrm{Pr}^c, \tag{82}$$

where a, b and c are parameters that are empirically determined in order to adapt the function to a measured data set.

There are countless of different variants of the Nusselt function, all of them tailored to some specified reference data. The only common things in the empirical equations, are that they are built to account for different phenomena (represented by the dimensionless numbers) by adding weight to the empirically determined parameters (Mahmoud & Karayiannis, 2013).

The Reynolds number describes the ratio between inertia forces and viscous forces in a flowing fluid. The Prandtl number describes the ratio between momentum and thermal diffusivities in a fluid at given thermodynamic conditions. The Grashof number represents the ratio between the viscous forces and the buoyancy forces that induces fluid motion during heat transfer in a system (often heat transfer in the context of natural convection). The Jakob number defines the ratio of sensible heat to latent heat absorbed during a liquid-vapor phase change in a fluid. The Bond number represents the buoyancy motion that is induced during a liquid-vapor phase change, and is defined as the ratio between gravitational and surface tension forces. The Weber number describes the motion that is induced during nucleate boiling and is defined as the ratio between inertia and surface tension forces (Incropera F.P. *et al.* 2007).

According to the boiling theory presented in the previous chapter, five models have been proposed in order to describe the boiling phenomena. The empirical correlations are created based on an analysis of the dimensionless groups that accounts for different phenomena that

occur during the boiling process. Assumptions directly related to bubble behavior will not be considered due to lack of knowledge about bubble sizes, growth rate and departure frequency. The bubble behavior will therefore be taken into consideration indirectly via the Grashof number, Reynolds number, Prandtl number, Weber number, Bond number and Jakob number. The boiling number will not be considered, because the mass flux of the refrigerant was not accurately measured in the experiments and is therefore calculated based on the latent heat of the fluids at given saturation pressures. All the thermodynamic fluid properties used in the calculations in the experiments are gathered with the Standard Reference Data Program of the National Institute of Standards and Technology (Lemmon *et al.* 2018).

First, an attempt was made to adapt the parameters in equation (82) to the measured experimental data sets. The result of the optimization showed a poor level of accuracy, which resulted in natural convection being taken into consideration as a phenomenon that influences the boiling behavior of the refrigerant. Natural convection and the buoyant motion is represented by the Grashof number. The Grashof number was included in equation (82). This resulted in the first proposed empirical correlation. The first empirical correlation accounts for buoyancy forces, the ratio between inertia and viscous forces and the ratio between momentum diffusivities and thermal diffusivities according to:

$$\mathrm{Nu} = a\mathrm{Gr}_l^b \mathrm{Re}_l^c \mathrm{Pr}_l^d. \tag{I}$$

The next phenomena that was considered to have an impact on the boiling mechanisms was the surface superheat compared to the saturation temperature of the refrigerant, without accounting for buoyant motion and natural convection. The surface superheat was a term included in the Jakob number, which also considered the latent heat and the specific heat capacity as refrigerant properties according to equation (73). This resulted in a modified correlation of equation (82), which accounts for the ratio between inertia and viscous forces, the ratio between momentum diffusivities and thermal diffusivities and the maximum energy needed to maintain the refrigerant at the state of saturation according to:

$$\mathrm{Nu} = a\mathrm{Re}_l^b \mathrm{Pr}_l^c \mathrm{Ja}_l^d. \tag{II}$$

The following thought was to account for both the influence of wall superheat and natural convection with its buoyant motion. As presented previously, the Grashof number represents the natural convection and the Jakob number accounts for wall superheat. This led to a new

proposed correlation that was based on equation (82) which, in turn, accounts for buoyancy forces, the ratio between inertia and viscous forces, the ratio between momentum diffusivities and thermal diffusivities and the maximum energy needed to maintain the refrigerant at the state of saturation according to:

$$\mathrm{Nu} = a\mathrm{Gr}_l^b \mathrm{Re}_l^c \mathrm{Pr}_l^d \mathrm{Ja}_l^e. \quad \text{(III)}$$

The three first empirical correlations had an improving impact on the level of accuracy against the measured values in the experiments. The Jakob number was recognized to have the largest impact on the accuracy this far when equation (82) had been modified. The proposed empirical correlation (II) had this far indicated to be the most accurate proposed correlation. This, in turn, led to the idea of neglecting natural convection but including buoyant fluid motion. The buoyant fluid motion was, in turn, included in the dimensionless Bond number. This led to a modification of correlation (II). The new proposed correlation takes into account the ratio between inertia and viscous forces, the ratio between gravitational and surface tension forces, the ratio between momentum diffusivities and thermal diffusivities and the maximum energy needed to maintain the refrigerant at the state of saturation according to:

$$\mathrm{Nu} = a\mathrm{Re}_l^b \mathrm{Bo}^c \mathrm{Pr}_l^d \mathrm{Ja}_l^e. \quad \text{(IV)}$$

The last attempt to improve the accuracy of the empirical correlation was the thought that viscous forces had a negligible impact on the two-phase flow conditions compared to the surface tension forces. In order to account for these aforementioned phenomena the Reynolds number was replaced with the Weber number. This resulted in correlation (V) being proposed. Correlation (V) accounts for the ratio between inertia and surface tension forces, the ratio between gravitational and surface tension forces, the ratio between momentum diffusivities and thermal diffusivities and the maximum energy needed to maintain the refrigerant at the state of saturation according to:

$$\mathrm{Nu} = a\mathrm{We}_l^b \mathrm{Bo}^c \mathrm{Pr}_l^d \mathrm{Ja}_l^e. \quad \text{(V)}$$

The parameters (a, b, c, d and e) in the proposed correlations were adapted to the measured data points by minimizing the quadratic deviation between the calculated values and measured values using the GRG-optimization tool in Microsoft excel.

5.1 Thermosiphon experiment

The subject of interest in this experiment was the operating conditions of a plate and shell evaporator in a thermosiphon configuration. A visual scheme of the system is illustrated in figure 8. The evaporator and the condenser were of “flooded” plate and shell type. The heat source was warm water that was set to temperatures between 30℃ and 60℃. The volume stream of the warm water was set to be between 1 l/s and 3.5 l/s. The cold source, used in the condenser was water at temperatures between 8℃ and 30℃. The volume stream of the cold water was set to be between 1 l/s and 3 l/s. With adjustments of the volume flows and temperatures in the cold water stream and hot water stream, the operating pressures and temperatures of the intermediate medium (propane) were changed, resulting in different thermophysical properties of the refrigerant and in different operation modes of the evaporator. Adjustments in the cold water stream were recognized to have the largest impact on the system, because the saturation pressures and temperatures of the refrigerant were adjusted according to the cooling capacity of the condenser, and the system was designed to operate only near and around the saturation curve of the refrigerant. Temperature meters were installed at the entrance of the condenser and at the entrance of the evaporator. Pressure meters were installed at the entrance and exit of the evaporator as well as inside the condenser and inside the evaporator, in order to gather information about the states of the refrigerant at different points of the system. The properties of the propane were gathered according to the pressure inside the evaporator, in order to gather information about boiling conditions. In order to investigate the impact of the height of refrigerant in the evaporator, different amounts of refrigerant were provided to the system at different test dates. Refrigerant height level meters were installed inside the evaporator and inside the condenser, in order to observe the impact of utilized heat transfer area. The height of the refrigerant in the evaporator could be controlled to a certain extent by the operating conditions but the level was mostly dependent on the hydrostatic pressure in the system that was dependent on the amount of propane provided into the system.

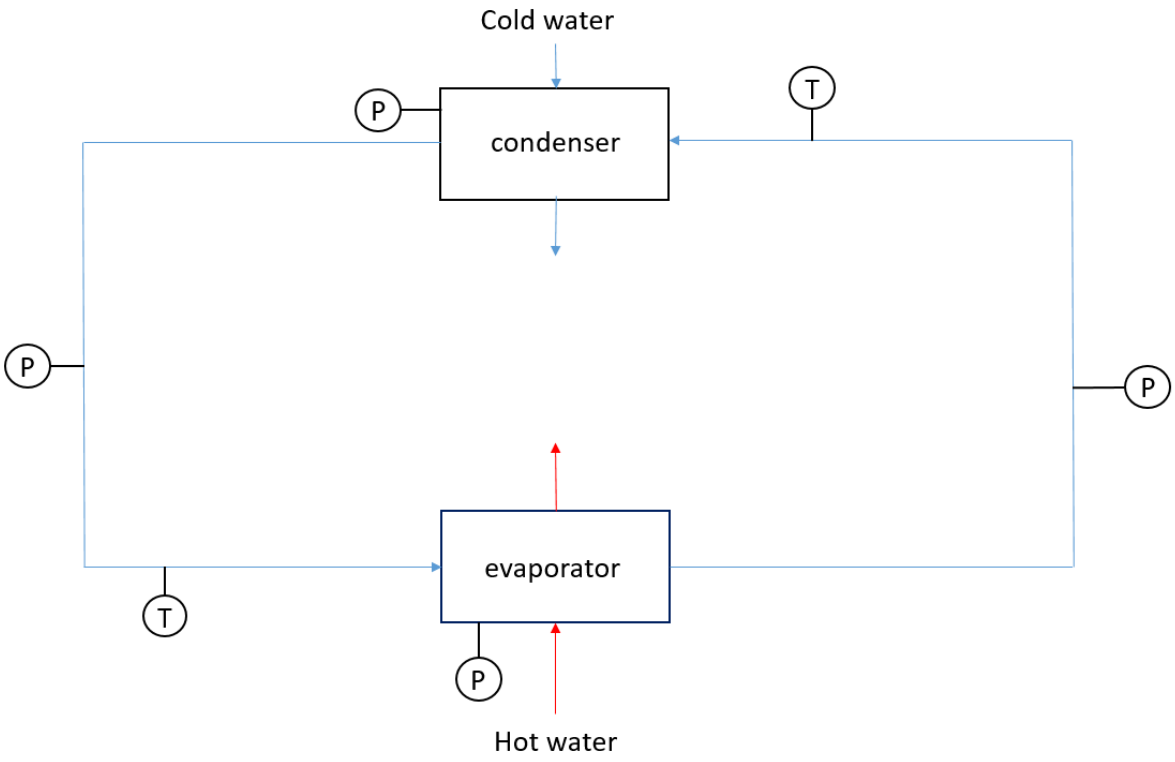

Figure 8: Visual scheme of the thermosiphon configuration.

The heating power input was calculated based on the water side in the heat exchanger with equation (98) according to:

$$q = \dot{m}_w c_p \Delta T_w.$$

The mass stream of refrigerant was calculated based on the latent heat at measured pressures in the evaporator with equation (97) according to:

$$\dot{m}_{ref} = \frac{q}{i_{fg}}.$$

The logarithmic mean temperature difference was defined by equations (101), (104) and (105) according to:

$$\Delta T_{lm} = \frac{(T_{w,in} - T_{sat,ref}) - (T_{w,out} - T_{sat,ref})}{ln\left(\frac{(T_{w,in} - T_{sat,ref})}{(T_{w,out} - T_{sat,ref})}\right)},$$

with the assumption that the propane was saturated vapor at the discharge of the evaporator. In other words, heat transferred to the vapor was neglected in the calculations.

The overall heat transfer coefficient U was calculated with equation (100) according to:

$$U = \frac{q}{A\Delta T_{lm}}.$$

The measured boiling heat transfer coefficient h_{ref} was calculated with equation (13) according to:

$$h_{ref} = \left(\frac{1}{U} - \frac{L}{k} - \frac{1}{h_w}\right)^{-1},$$

where the thermal conductivity of the heat transfer plates, k, had been determined previously as well as the thickness of the plates, L. An empirical correlation for the heat transfer coefficient h_w on the heating water side had been determined accurately in other experiments.

5.1.1 Determined empirical correlations and their accuracy

In this section, the optimization results will be presented graphically as well as in table form. The accuracy of empirical correlation (I)-(V) is presented in figures 9-13. Table 1, which represents the accuracy of the proposed empirical correlations compared to the experimental data, is presented after the graphical illustrations. The accuracy limits are expressed as the percentage deviation from the measured values. The numbers presented in the table are the number of calculated values compared to the total number of values that are present in the aforementioned error limits.

$$\mathrm{Nu} = \mathrm{Gr}_l^{-1.622}\mathrm{Re}_l^{2.207}\mathrm{Pr}_l^{30.064}$$

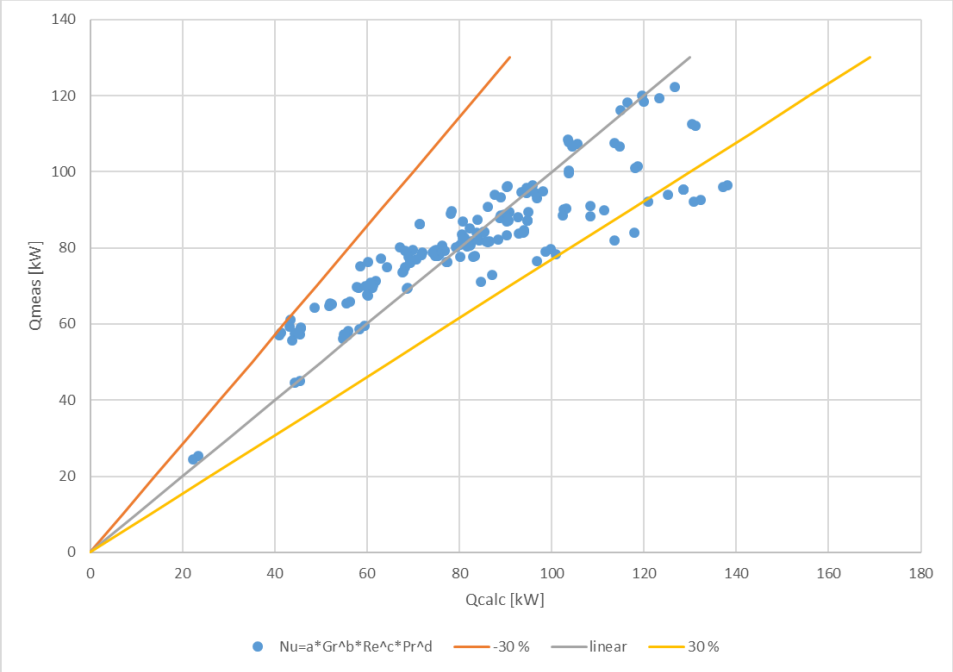

Figure 9: Accuracy of empirical correlation (I) adapted to the data gathered in the thermosiphon experiment.

$$\mathrm{Nu} = 1.99 \cdot 10^{-6}\mathrm{Re}_l^{1.796}\mathrm{Pr}_l^{1.05}\mathrm{Ja}_l^{-2.044}$$

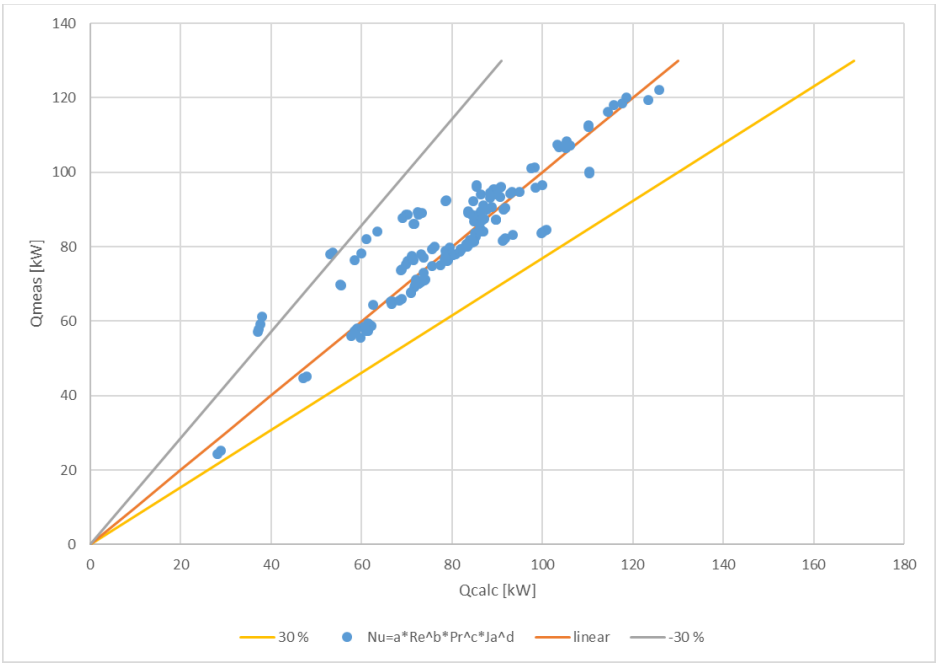

Figure 10: Accuracy of empirical correlation (II) adapted to the data gathered in the thermosiphon experiment.

$$\mathrm{Nu} = 0.000129\mathrm{Gr}_l^{-0.243}\mathrm{Re}_l^{1.881}\mathrm{Pr}_l^{2.853}\mathrm{Ja}_l^{-1.863}$$

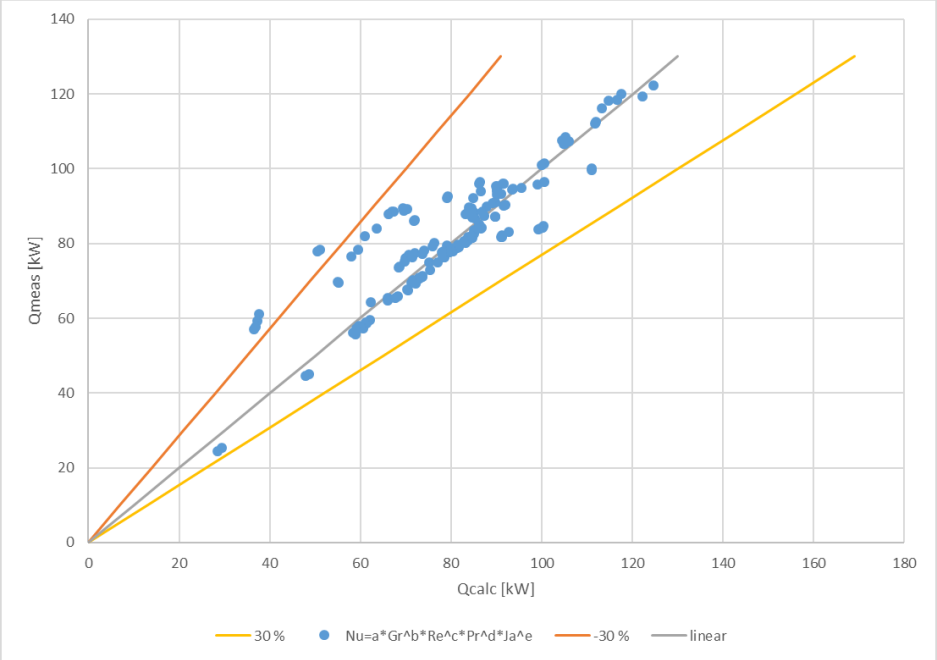

Figure 11: Accuracy of empirical correlation (III) adapted to the data gathered in the thermosiphon experiment.

$$\mathrm{Nu} = 0.000227\mathrm{Re}_l^{1.88}\mathrm{Bo}^{-0.665}\mathrm{Pr}_l^{-2.55}\mathrm{Ja}_l^{-2.11}$$

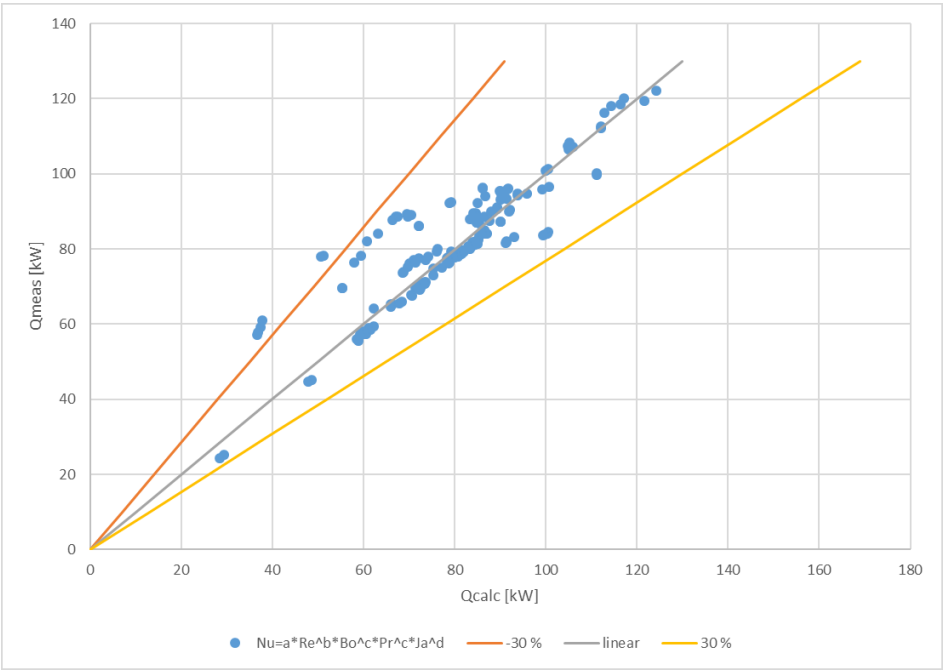

Figure 12: Accuracy of empirical correlation (IV) adapted to the data gathered in the thermosiphon experiment.

$$Nu = 3.58We_l^{0.941}Bo^{-0.267}Pr_l^{5.101}Ja_l^{-2.105}$$

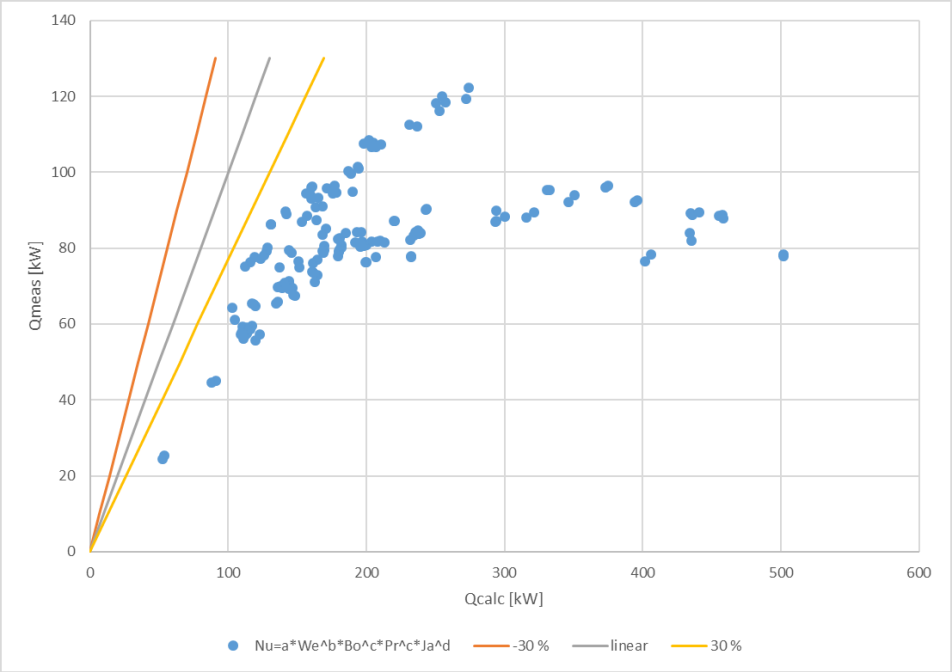

Figure 13: Accuracy of empirical correlation (V) adapted to the data gathered in the thermosiphon experiment.

Table 1: Accuracy of the empirical correlations proposed to the gathered thermosiphon experimental data.

	± 30%	± 20%	± 15%	± 10%	± 5%
$\mathrm{Nu} = \mathrm{Gr}_l^{-1.622}\mathrm{Re}_l^{2.21}\mathrm{Pr}_l^{30.64}$	94%	82%	71%	57%	38%
$\mathrm{Nu} = 1.99 \cdot 10^{-6}\mathrm{Re}_l^{1.796}\mathrm{Pr}_l^{1.05}\mathrm{Ja}_l^{-2.044}$	96%	91%	85%	78%	63%
$\mathrm{Nu} = 0.000129\mathrm{Gr}_l^{-0.243}\mathrm{Re}_l^{1.881}\mathrm{Pr}_l^{2.853}\mathrm{Ja}_l^{-1.863}$	96%	89%	84%	78%	65%
$\mathrm{Nu} = 0.000227\mathrm{Re}_l^{1.88}\mathrm{Bo}^{-0.665}\mathrm{Pr}_l^{-2.55}\mathrm{Ja}_l^{-2.11}$	96%	89%	84%	78%	66%
$\mathrm{Nu} = 3.58\mathrm{We}_l^{0.941}\mathrm{Bo}^{-0.267}\mathrm{Pr}_l^{5.101}\mathrm{Ja}_l^{-2.11}$	0%	0%	0%	0%	0%

5.1.2 Conclusions made of the thermosiphon experiment

It was recognized that the proposed correlations showed the largest deviation from the measured values, when the volume flows in the hot water stream were low as well as when the cold water intake temperatures were between 25°C and 30°C (at high pressures and temperatures of the refrigerant). It was determined that the inaccuracies occurred because of low wall superheat resulting in an unpredicted worse heat transfer between the refrigerant and the heated wall which, in turn, affect the vapor bubble behavior on the surface. The level of the propane did not have any impact on the accuracy of the empirical correlations. The

results indicate that buoyancy motion, the ratio between inertia and viscous forces, the ratio between momentum diffusivities and thermal diffusivities and the maximum energy needed to maintain the refrigerant at the state of saturation are all phenomena that need to be considered, in the thermosiphon configuration, when determining the heat transfer coefficient due to low flow rates of the refrigerant. Low flow rates result in an increased significance of buoyancy motion and vapor bubble behavior on the heated surface. Due to the low flow rates of the refrigerant, nucleate boiling was determined to be the dominating boiling mechanism in the experiment. The most suitable empirical correlation was correlation (IV):

$$\mathrm{Nu} = 0.000227\mathrm{Re}_l^{1.88}\mathrm{Bo}^{-0.665}\mathrm{Pr}_l^{-2.55}\mathrm{Ja}_l^{-2.11}$$

5.2 Cascade refrigeration cycle experiment

A plate and shell evaporator has been tested with several refrigerants, in order to gather comprehensive data and adapt it to an empirical formula. A visual scheme of the system is presented in figure 14. The configuration consists of two cycles with their own intermediate medium. The subject of interest was the evaporator connected to the warm water stream. The warm water stream was set to be between 6.5 l/s and 7 l/s. The warm water inlet temperature was set to 13℃. The operating pressures were measured before and after the evaporator in the primary cycle. The operating pressures and temperatures of the refrigerant in the primary cycle were controlled by the compressor input power and the temperature and volume flow of the cold water stream in the secondary cycle. The operating conditions of the refrigerant in the primary cycle was mostly dependent on the temperature of the cold source, namely the state of the refrigerant in the secondary cycle. The temperature in the secondary cycle controlled the saturation temperature and operating temperatures of the refrigerant in the primary cycle connected to the hot water stream. The tested refrigerants were: propane, R134a, R507 and ammonia. R507 is a mixture of two refrigerants. Both of the refrigerants in the mixture have nearly the same boiling point at the operating conditions in the experiment. Because of the nearly similar boiling point, only convective heat transfer was taken into consideration, although in theory, convective mass transfer also should be accounted for in this case, when a refrigerant mixture is considered.

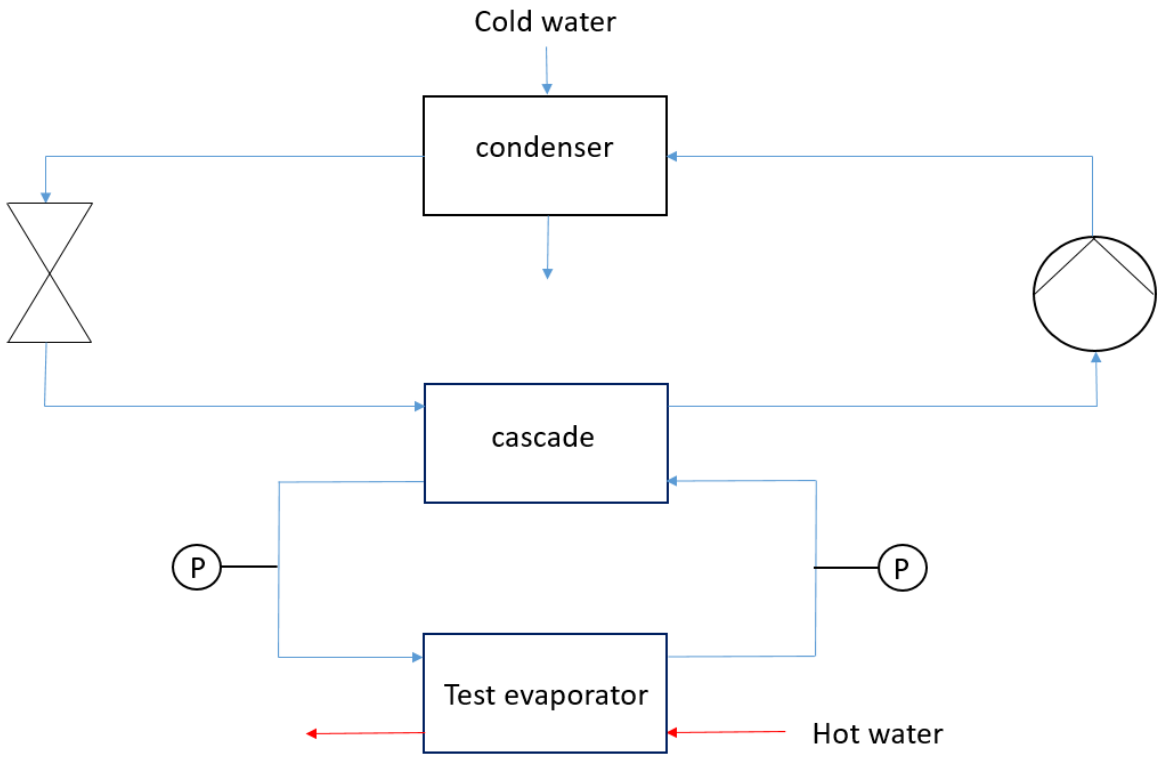

Figure 14: Visual scheme of the cascade refrigeration cycle.

Similarly to the thermosiphon experiment, the heating power input, q, was calculated based on the water side in the tested evaporator with equation (98). After the heating power input was calculated, the mass stream of refrigerant, $\dot{m}_{ref}$, was obtained with equation (97). The latent heat, i_{fg}, used in equation (97) was assumed with the measured pressures in the primary cycle.

The logarithmic mean temperature difference, ΔT_{lm}, was equally to the thermosiphon experiment defined by equations (101), (104) and (105), with the assumption that the fluids are saturated vapor at the discharge of the evaporator. In other words heat transferred to the vapor is neglected in the calculations. The refrigerants were assumed to be saturated liquid at the inlet of the test evaporator and saturated vapor at the discharge of the evaporator. The overall heat transfer coefficient, U, was obtained in the same way as in the thermosiphon experiment with equation (100). The measured boiling heat transfer coefficient, h_{ref}, was also in this case calculated with equation (13). The thermal conductivity, k, of the heat transfer plates was known as well as the thickness of the plates L. An empirical correlation for the heat transfer coefficient h_w on the heating water side had been determined in other experiments accurately.

5.2.1 Determined empirical results and correlations

In this section the optimization results will be presented graphically as well as in table form. The accuracy of empirical correlation (I)-(V) is presented in figures 15-19. Table 2, which represents the accuracy of the empirical correlations proposed for the experimental data, is presented after the graphical illustrations. The accuracy limits are expressed as the percentage deviation from the measured values. The numbers presented in the table are the number of calculated values compared to the total number of values that are present in the aforementioned error limits.

$$\mathrm{Nu} = 2066064\mathrm{Gr}_l^{-0.612}\mathrm{Re}_l^{0.741}\mathrm{Pr}_l^{0.496}$$

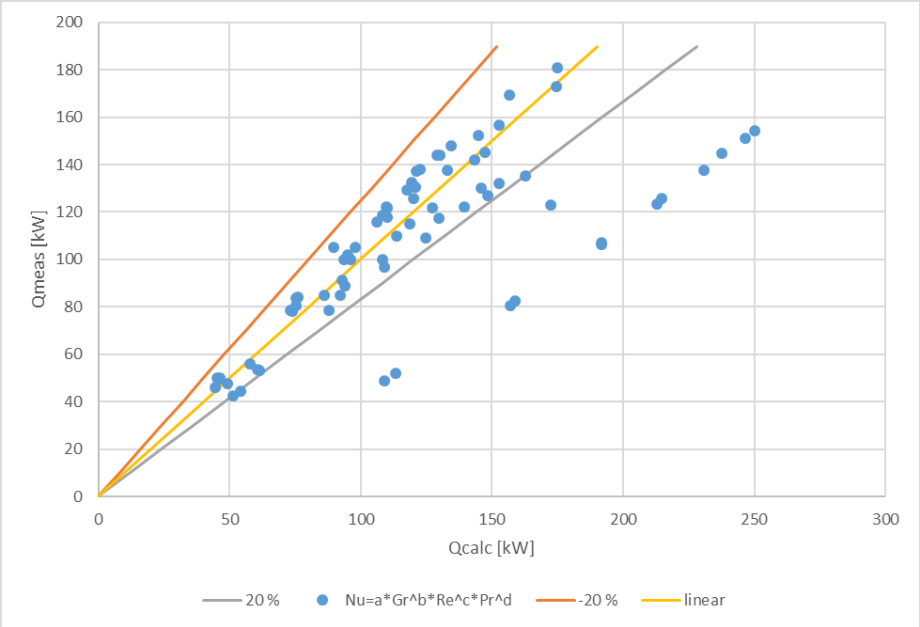

Figure 15: Accuracy of empirical correlation (I) adapted to the data gathered in the cascade refrigeration cycle experiment.

$$\mathrm{Nu} = 0.00174\mathrm{Re}_l^{1.268}\mathrm{Pr}_l^{0.234}\mathrm{Ja}_l^{-1.103}$$

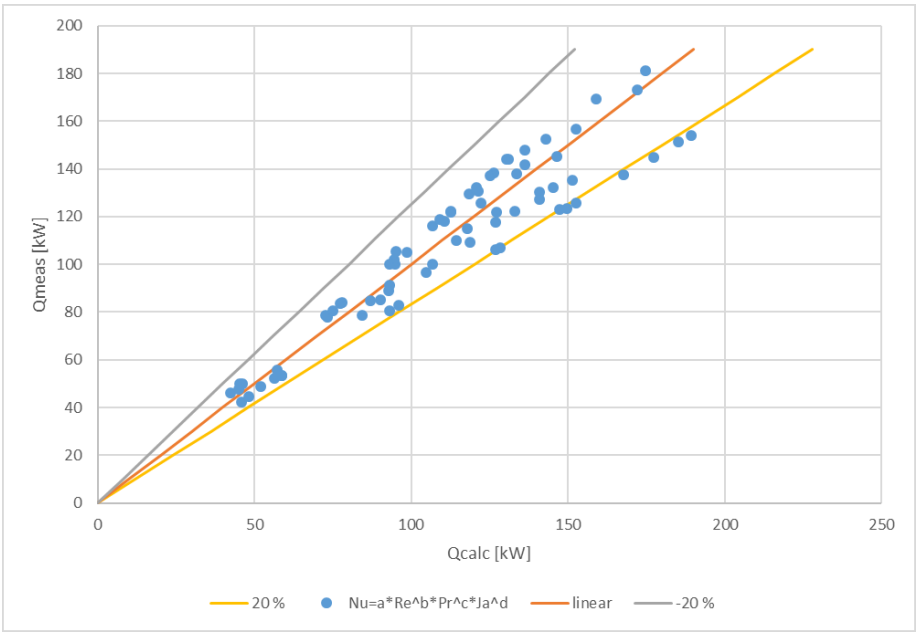

Figure 16: Accuracy of empirical correlation (II) adapted to the data gathered in the cascade refrigeration cycle experiment.

$$Nu = 1.97 \cdot 10^{-6} Gr_l^{0.232} Re_l^{1.344} Pr_l^{0.205} Ja_l^{-1.365}$$

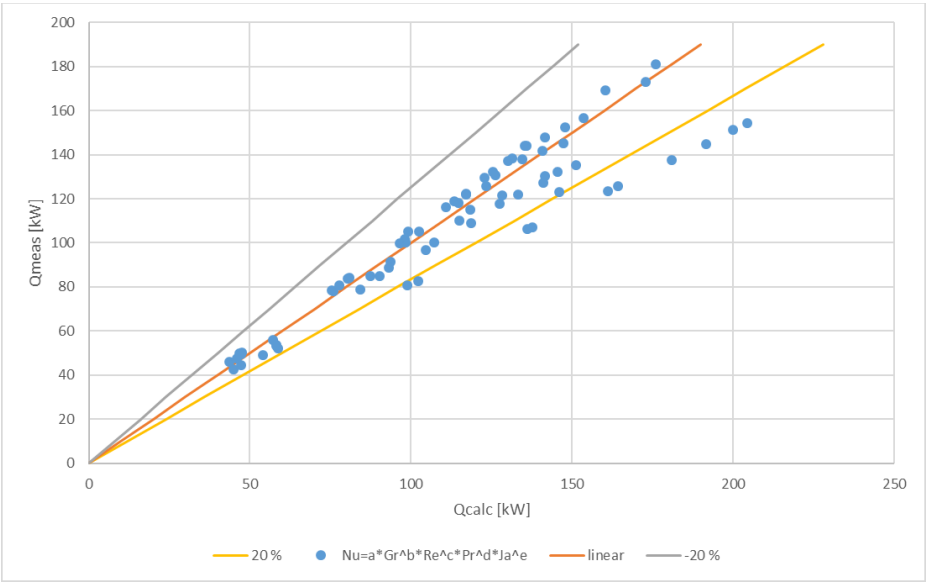

Figure 17: Accuracy of empirical correlation (III) adapted to the data gathered in the cascade refrigeration cycle experiment.

$$\mathrm{Nu} = 0.000224\mathrm{Re}_l^{1.46}\mathrm{Bo}^{0.169}\mathrm{Pr}_l^{0.0586}\mathrm{Ja}_l^{-1.36}$$

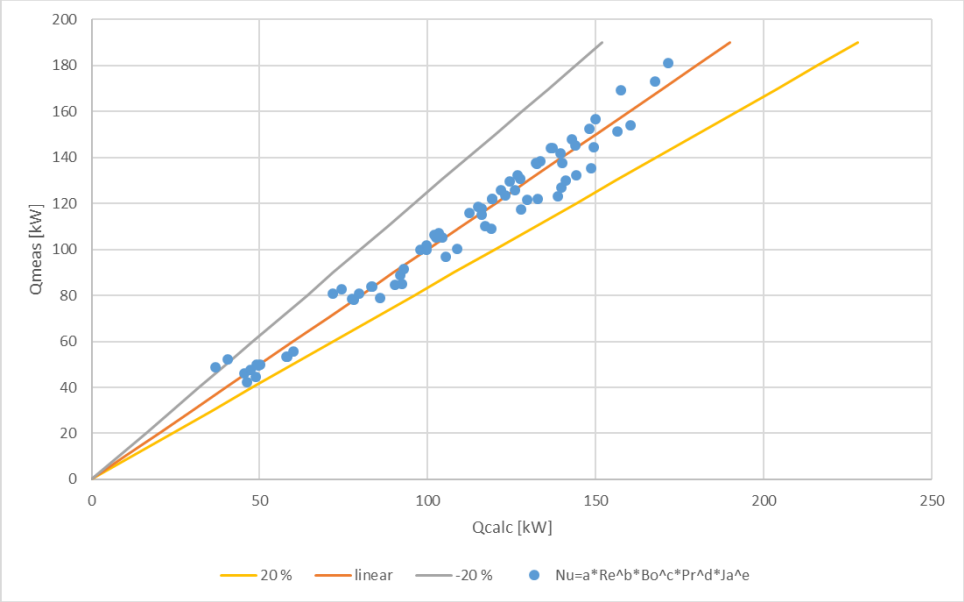

Figure 18: Accuracy of empirical correlation (IV) adapted to the data gathered in the cascade refrigeration cycle experiment.

$$\mathrm{Nu} = 19.31\mathrm{We}_l^{0.893}\mathrm{Bo}^{0.448}\mathrm{Pr}_l^{-1.661}\mathrm{Ja}_l^{-1.528}$$

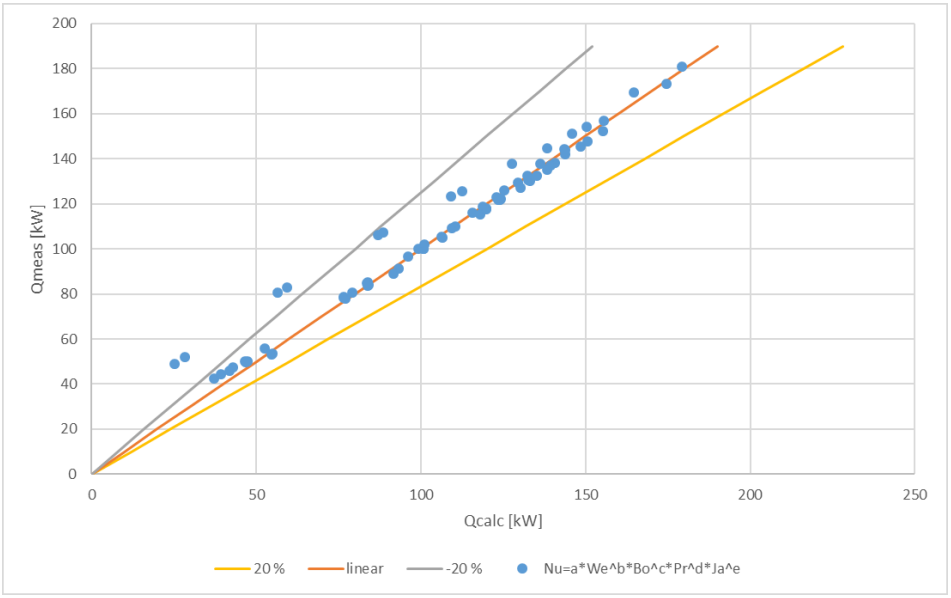

Figure 19: Accuracy of empirical correlation (V) adapted to the data gathered in the cascade refrigeration cycle experiment.

Table 2: Accuracy of the empirical correlations proposed for the cascade refrigeration cycle.

	$\pm 30\%$	$\pm 20\%$	$\pm 15\%$	$\pm 10\%$	$\pm 5\%$
$\mathrm{Nu} = 2066064\mathrm{Gr}_l^{-0.612}\mathrm{Re}_l^{0.741}\mathrm{Pr}_l^{0.496}$	82%	78%	75%	56%	24%
$\mathrm{Nu} = 0.00174\mathrm{Re}_l^{1.268}\mathrm{Pr}_l^{0.234}\mathrm{Ja}_l^{-1.103}$	100%	92%	85%	82%	19%
$\mathrm{Nu} = 1.97 \cdot 10^{-6}\mathrm{Gr}_l^{0.232}\mathrm{Re}_l^{1.344}\mathrm{Pr}_l^{0.205}\mathrm{Ja}_l^{-1.365}$	82%	78%	75%	56%	24%
$\mathrm{Nu} = 0.000224\mathrm{Re}_l^{1.46}\mathrm{Bo}^{0.169}\mathrm{Pr}_l^{0.0586}\mathrm{Ja}_l^{-1.36}$	100%	97%	97%	93%	63%
$\mathrm{Nu} = 19.31\mathrm{We}_l^{0.893}\mathrm{Bo}^{0.448}\mathrm{Pr}_l^{-1.661}\mathrm{Ja}_l^{-1.528}$	97%	94%	92%	86%	76%

5.2.2 Conclusions made of the cascade refrigeration cycle experiment

The results indicate that the ratio between inertia and surface tension forces, the ratio between gravitational and surface tension forces, the ratio between momentum diffusivities and thermal diffusivities and the maximum energy needed to maintain the refrigerant at the state of saturation are phenomena that need to be accounted for when a plate evaporator of this type operating at saturated conditions is considered according to proposed correlation (V). Low flow rates in the evaporator result in an increased importance of buoyancy motion and surface tension of the fluid. The wall superheat was considered to be low, which indicate that the dominating boiling regime was also here nucleate boiling. The most suitable empirical correlation was determined to be empirical correlation (V):

$$\mathrm{Nu} = 19.31\mathrm{We}_l^{0.893}\mathrm{Bo}^{0.448}\mathrm{Pr}_l^{-1.661}\mathrm{Ja}_l^{-1.528}$$

It is noticeable that empirical correlation (IV) that accounts for the ratio between inertia and surface tension forces, the ratio between gravitational and surface tension forces, the ratio between momentum diffusivities and thermal diffusivities and the maximum energy needed to maintain the refrigerant at the state of saturation shows a better level of accuracy than correlation (V) that was determined to be the most accurate one. When the results were analyzed it was determined that the points predicted to be outliers in figure 19 are in fact from the same refrigerant R507. The measured data points for refrigerant R507 was even in the empirical determination somewhat questionable, because the compound of the refrigerant mixture was unknown and therefore assumed to be a 50-50 mass percent mixture of both of the pure fluids. Depending on the compound of the refrigerant R507, the thermophysical

properties will change, resulting in totally different predictions for the heat transfer and a new empirical correlation must be applied for the measured data points. Other possible reasons for the inaccuracies, when considering refrigerant R507, may originate from that the refrigerants in the mixture flow separately, which in turn may cause computational problems in the calculations. Because of the aforementioned reasons the empirical correlation (IV)

$$\mathrm{Nu} = 0.000224\mathrm{Re}_l^{1.46}\mathrm{Bo}^{0.169}\mathrm{Pr}_l^{0.0586}\mathrm{Ja}_l^{-1.36}$$

was determined to be somewhat more inaccurate than the selected one, according to figure 18 and 19. Figure 20 shows the accuracy of correlation (V) when refrigerant R507 is neglected in the measurements.

$$\mathrm{Nu} = 19.31\mathrm{We}_l^{0.893}\mathrm{Bo}^{0.448}\mathrm{Pr}_l^{-1.661}\mathrm{Ja}_l^{-1.528}$$

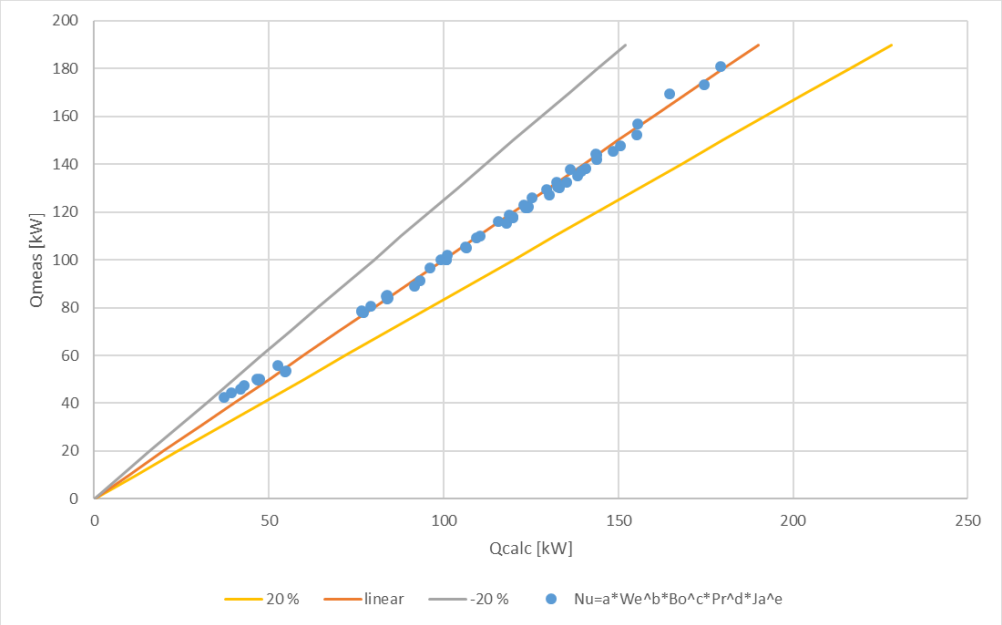

Figure 20: Accuracy of empirical correlation (V) adapted to the data gathered in the cascade refrigeration cycle experiment. R507 is in this case neglected.

5.3 Ammonia refrigeration cycle

A plate and shell evaporator in a refrigeration cycle has been tested with ammonia as working fluid according to the visual scheme presented in figure 21. In these experiments the working fluid entered the evaporator as a liquid-vapor mixture, because of throttling after the discharge of the condenser. The condensing pressure and the evaporating pressure where measured as well as the temperature at the discharge of the evaporator. The volume flow and

the inlet and discharge temperature were measured in the warm water stream in the evaporator.

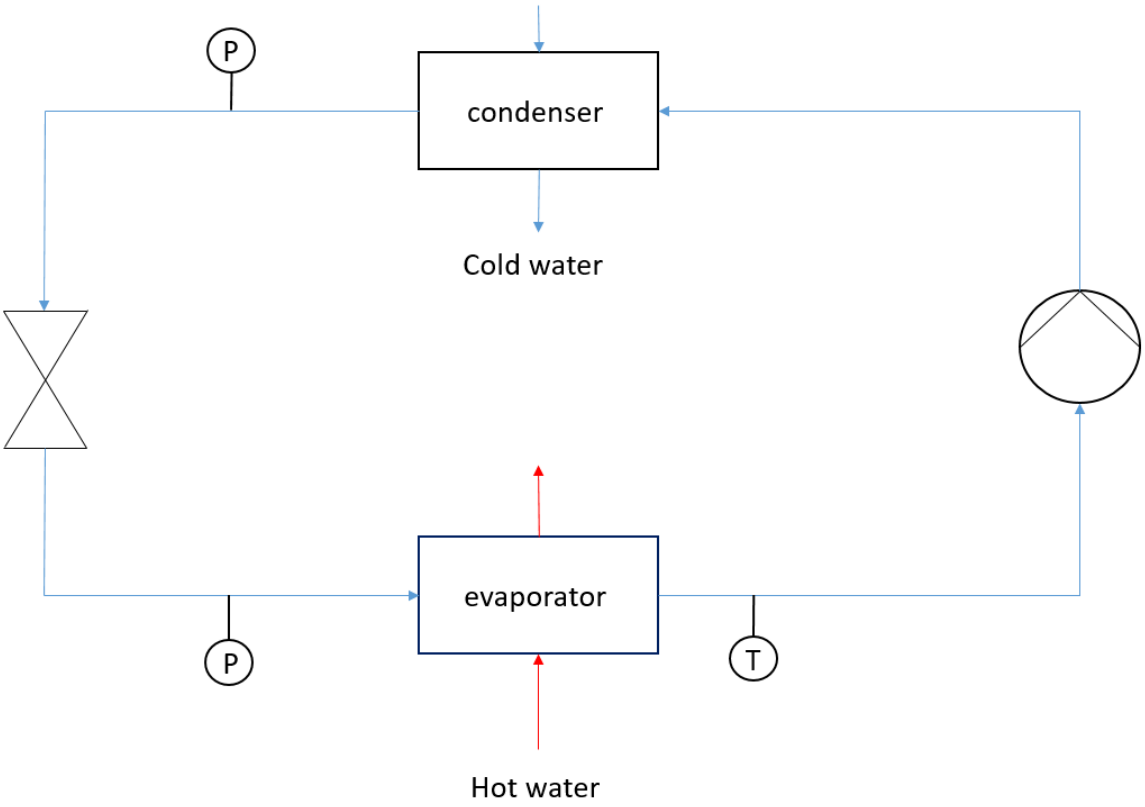

Figure 21: Visual scheme of the NH_3 refrigeration cycle.

The heating power input, q, was calculated with equation (98) based on the hot water stream as in the previous experiments. The mass stream of refrigerant was calculated according to equation (97). In this case equation (97) is presented as:

$$\dot{m}_{ref} = \frac{q}{i_{fg}+c_{p,ref}\Delta T_{superheat}},$$

because of the presence of superheat in the system.

The logarithmic mean temperature difference was also in this experiment defined by equation (101), (104) and (105):

$$\Delta T_{lm} = \frac{(T_{w,in}-T_{sat,ref})-(T_{w,out}-T_{sat,ref})}{ln\left(\frac{(T_{w,in}-T_{sat,ref})}{(T_{w,out}-T_{sat,ref})}\right)},$$

again with the assumption that the ammonia is close to the saturation point at the discharge of the evaporator, resulting in a small impact on the logarithmic temperature difference. The

logarithmic mean temperature difference calculated with the saturation temperatures are assumed to be closer to the reality than logarithmic mean temperature differences calculated with the real inlet and discharge temperatures. In other words, heat transferred after the total phase change from liquid to vapor is neglected in the calculations.

The properties of the refrigerant at the inlet of the evaporator were obtained by observing the throttling valve. An energy balance was created around the throttling valve, with the assumptions that heat loss to the surroundings can be neglected, resulting in:

$$i_{cond,out} = i_{evap,in} \, .$$

All the thermodynamic properties that could not directly be obtained based on the vapor fractions are determined with properties from the liquid saturated state because of low vapor fractions at the inlet of the evaporator.

The overall heat transfer coefficient U was obtained with equation (100). The measured boiling heat transfer coefficient, h_{ref}, was calculated according to equation (13). Again, the thermal conductivity, k, of the heat transfer plates was known as well as the thickness of the heat transfer plates L. An empirical correlation for the heat transfer coefficient h_w on the heating water side had been determined in other experiments accurately.

5.3.1 Accuracy of the determined empirical correlations

This section will present the accuracy of the empirical correlations (I)-(V), proposed for the experimental data set. Graphically the correlations will be presented in figures 22-26. After the results have been graphically presented, the accuracy will again be summarized in a table, in this case table 3. The values and error limits presented in the table are calculated similarly compared to the values in table 1-2 presented previously.

$$\mathrm{Nu} = 8.9 \cdot 10^{11} \mathrm{Gr}_l^{-1.297} \mathrm{Re}_l^{1.178} \mathrm{Pr}_l^{-1.491}$$

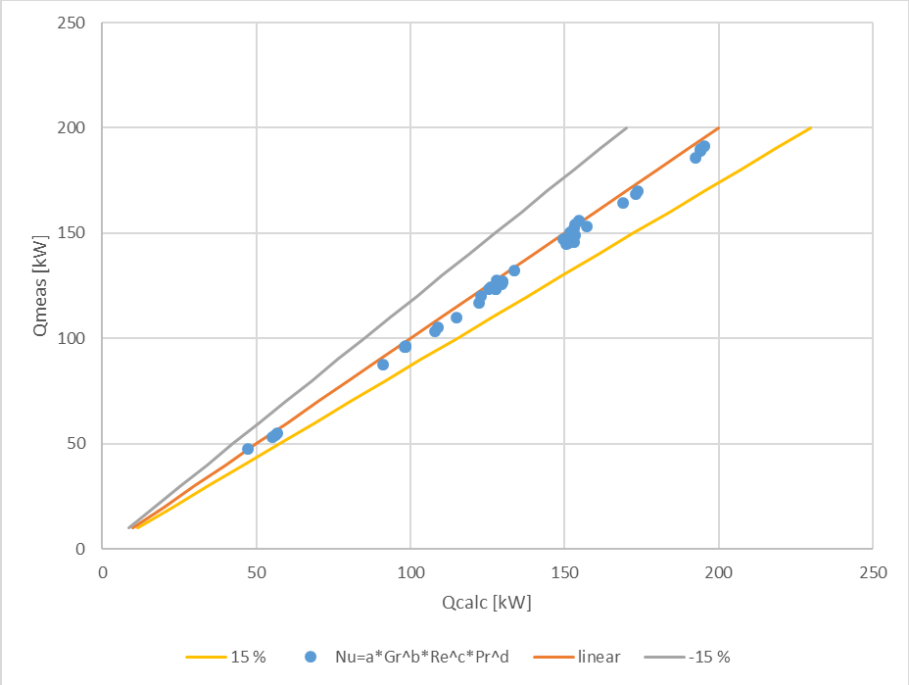

Figure 22: Accuracy of empirical correlation (I) adapted to the data gathered from the NH_3 refrigeration cycle experiment.

$$\mathrm{Nu} = 3.36 \cdot 10^{-5} \mathrm{Re}_l^{1.171} \mathrm{Pr}_l^{4.07} \mathrm{Ja}_l^{-1.417}$$

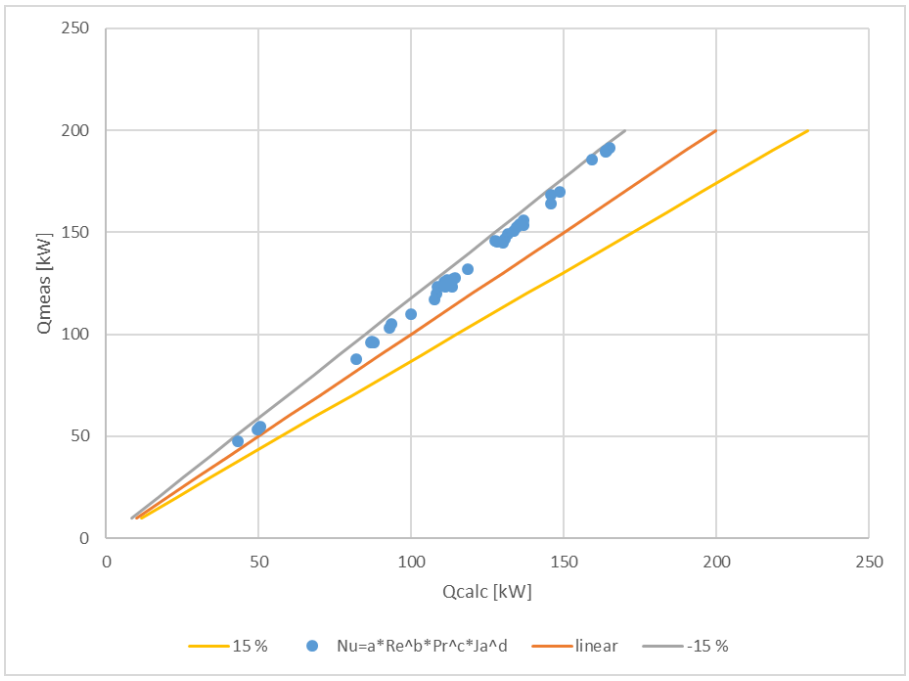

Figure 23: Accuracy of empirical correlation (II) adapted to the data gathered from the NH_3 refrigeration cycle experiment.

$$\mathrm{Nu} = 1.033\mathrm{Gr}_l^{-0.371}\mathrm{Re}_l^{1.164}\mathrm{Pr}_l^{3.318}\mathrm{Ja}_l^{-1.077}$$

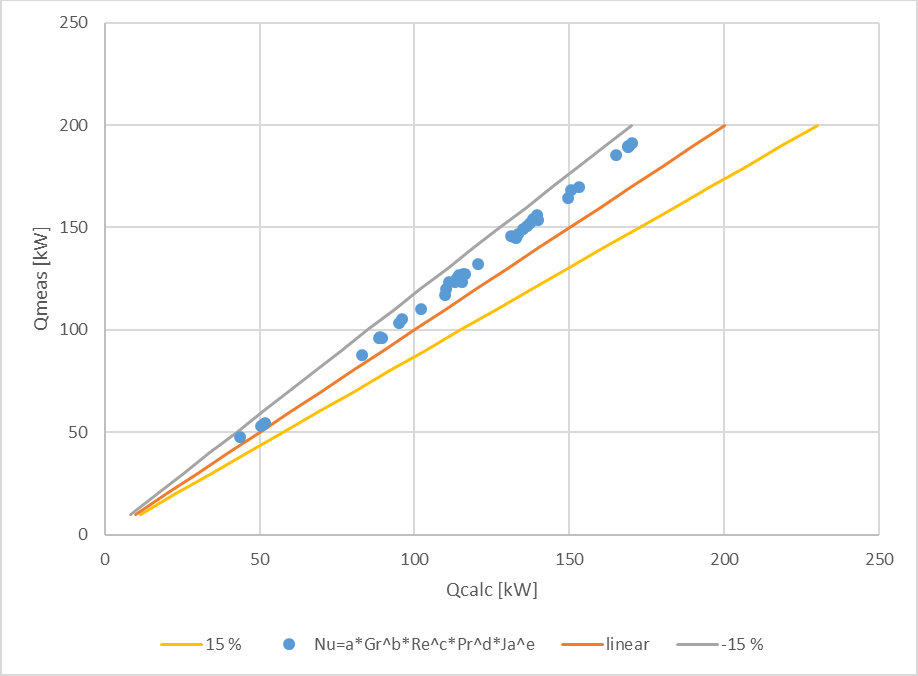

Figure 24: Accuracy of empirical correlation (III) adapted to the data gathered from the NH_3 refrigeration cycle experiment.

$$\mathrm{Nu} = 0.0639\mathrm{Re}_l^{1.16}\mathrm{Bo}^{-4.36}\mathrm{Pr}_l^{0.165}\mathrm{Ja}_l^{-1.47}$$

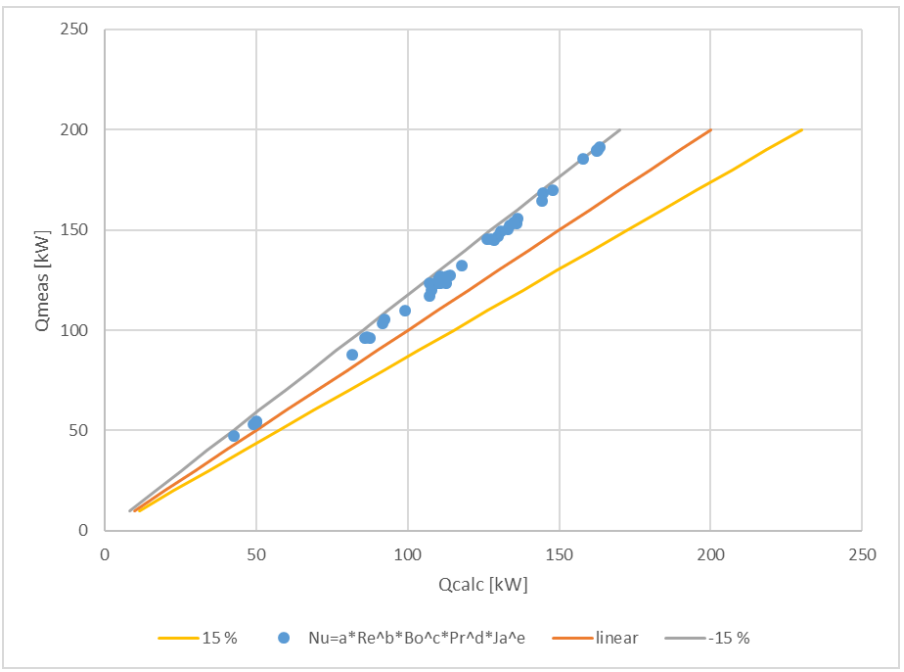

Figure 25: Accuracy of empirical correlation (IV) adapted to the data gathered from the NH_3 refrigeration cycle experiment.

$$\mathrm{Nu} = 0.158\mathrm{We}_l^{0.583}\mathrm{Bo}^{0.123}\mathrm{Pr}_l^{3.720}\mathrm{Ja}_l^{-1.459}$$

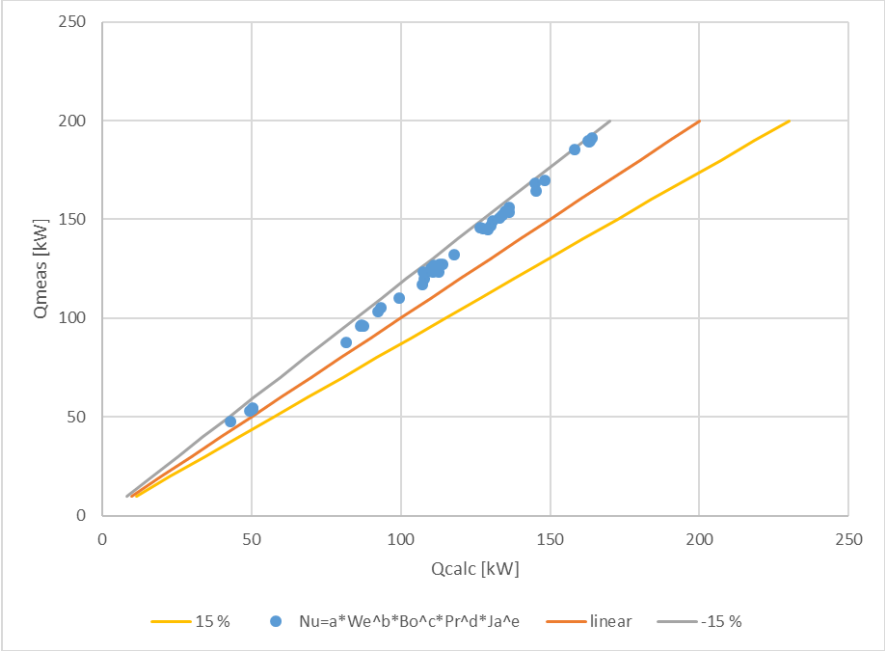

Figure 26: Accuracy of empirical correlation (V) adapted to the data gathered from the NH_3 refrigeration cycle experiment.

Table 3: Accuracy of the empirical correlations proposed for the NH_3 refrigeration cycle.

	$\pm 30\%$	$\pm 20\%$	$\pm 15\%$	$\pm 10\%$	$\pm 5\%$
$\mathrm{Nu} = 8.9 \cdot 10^{11}\mathrm{Gr}_l^{-1.297}\mathrm{Re}_l^{1.178}\mathrm{Pr}_l^{-1.491}$	100%	100%	100%	100%	98%
$\mathrm{Nu} = 3.36 \cdot 10^{-5}\mathrm{Re}_l^{1.171}\mathrm{Pr}_l^{4.07}\mathrm{Ja}_l^{-1.417}$	100%	100%	100%	32%	0%
$\mathrm{Nu} = 1.033\mathrm{Gr}_l^{-0.371}\mathrm{Re}_l^{1.164}\mathrm{Pr}_l^{3.318}\mathrm{Ja}_l^{-1.077}$	100%	100%	100%	80%	0%
$\mathrm{Nu} = 0.0639\mathrm{Re}_l^{1.16}\mathrm{Bo}^{-4.36}\mathrm{Pr}_l^{0.165}\mathrm{Ja}_l^{-1.47}$	100%	100%	100%	22%	0%
$\mathrm{Nu} = 0.158\mathrm{We}_l^{0.583}\mathrm{Bo}^{0.123}\mathrm{Pr}_l^{3.720}\mathrm{Ja}_l^{-1.459}$	100%	100%	100%	27%	0%

5.3.2 Conclusions made of the of the ammonia refrigeration cycle

The results indicate that buoyancy forces, the ratio between inertia and viscous forces and the ratio between momentum diffusivities and thermal diffusivities are considerable parameters when observing these kinds of refrigeration configurations. The results are reasonable because of the superheating that results in large temperature and density gradients in the system according to the theory about buoyancy behavior presented in chapter 4. Large temperature and density gradients result in a larger impact of natural convection and

buoyancy motion of the fluid. The most suitable empirical correlation was empirical correlation (I):

$$\mathrm{Nu} = 8.9 \cdot 10^{11} \mathrm{Gr}_l^{-1.297} \mathrm{Re}_l^{1.178} \mathrm{Pr}_l^{-1.491}$$

5.4 Determined empirical correlations tested on data gathered from other experiments

In this section, the suitability of some of the determined correlations will be tested on data gathered from the other conducted experiments. This is made in order to investigate if same phenomena occur in the different evaporators and to verify the conclusions made in the other conducted experiments. The most accurate ones in each experiment will be tested. The most accurate ones in the thermosiphon experiment, were empirical correlations (II), (III) and (IV). The most accurate empirical correlations in the cascade refrigeration cycle experiment were (II), (IV) and (V). Empirical correlations (I) and (III) showed the highest level of accuracy in the ammonia refrigeration cycle experiment.

5.4.1 Empirical correlations tested on the thermosiphon experimental data

In this section, the most accurate empirical correlations determined for the cascade refrigeration cycle and the ammonia refrigeration cycle have been tested on the thermosiphon data set. The accuracy of the empirical correlations determined for the thermosiphon data set will function as a reference when a comparison between the different determined correlations is made. The test results and the conclusions made in previous sections will be discussed and verified.

The accuracy of empirical correlations (II), (IV) and (V) proposed for the cascade refrigeration cycle experimental data as well as empirical correlations (I) and (III) proposed for the ammonia refrigeration cycle experimental data will be tested on the data gathered from the thermosiphon experiment. The test results are presented in table 4. Visually the suitability is presented in figures 27-31.

Table 4: Comparison of the accuracy of the most accurate empirical correlations, proposed for the other experiments and applied to the data from the thermosiphon experiment.

	$\pm 30\%$	$\pm 20\%$	$\pm 15\%$	$\pm 10\%$	$\pm 5\%$
$\mathrm{Nu} = 0.00174\mathrm{Re}_l^{1.268}\mathrm{Pr}_l^{0.234}\mathrm{Ja}_l^{-1.103}$	88%	82%	73%	59%	34%
$\mathrm{Nu} = 0.000224\mathrm{Re}_l^{1.46}\mathrm{Bo}^{0.169}\mathrm{Pr}_l^{0.0586}\mathrm{Ja}_l^{-1.36}$	94%	78%	68%	55%	29%
$\mathrm{Nu} = 19.31\mathrm{We}_l^{0.893}\mathrm{Bo}^{0.448}\mathrm{Pr}_l^{-1.661}\mathrm{Ja}_l^{-1.528}$	76%	53%	36%	20%	13%
$\mathrm{Nu} = 8.9 \cdot 10^{11}\mathrm{Gr}_l^{-1.297}\mathrm{Re}_l^{1.178}\mathrm{Pr}_l^{-1.491}$	0%	0%	0%	0%	0%
$\mathrm{Nu} = 1.033\mathrm{Gr}_l^{-0.371}\mathrm{Re}_l^{1.164}\mathrm{Pr}_l^{3.318}\mathrm{Ja}_l^{-1.077}$	85%	30%	5%	1%	1%

$$\mathrm{Nu} = 0.00174 \cdot \mathrm{Re}_l^{1.268} \cdot \mathrm{Pr}_l^{0.234} \cdot \mathrm{Ja}_l^{-1.103}$$

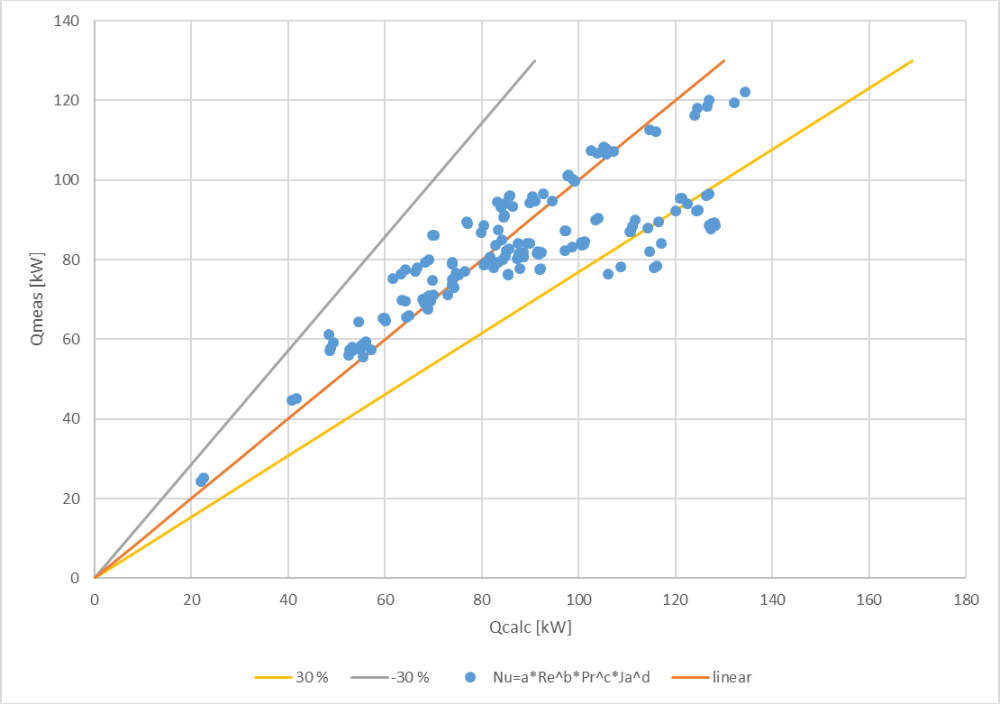

Figure 27: Accuracy of empirical correlation (II) proposed for the cascade refrigeration cycle, applied to the thermosiphon data.

$$\mathrm{Nu} = 0.000224\mathrm{Re}_l^{1.46}\mathrm{Bo}^{0.169}\mathrm{Pr}_l^{0.0586}\mathrm{Ja}_l^{-1.36}$$

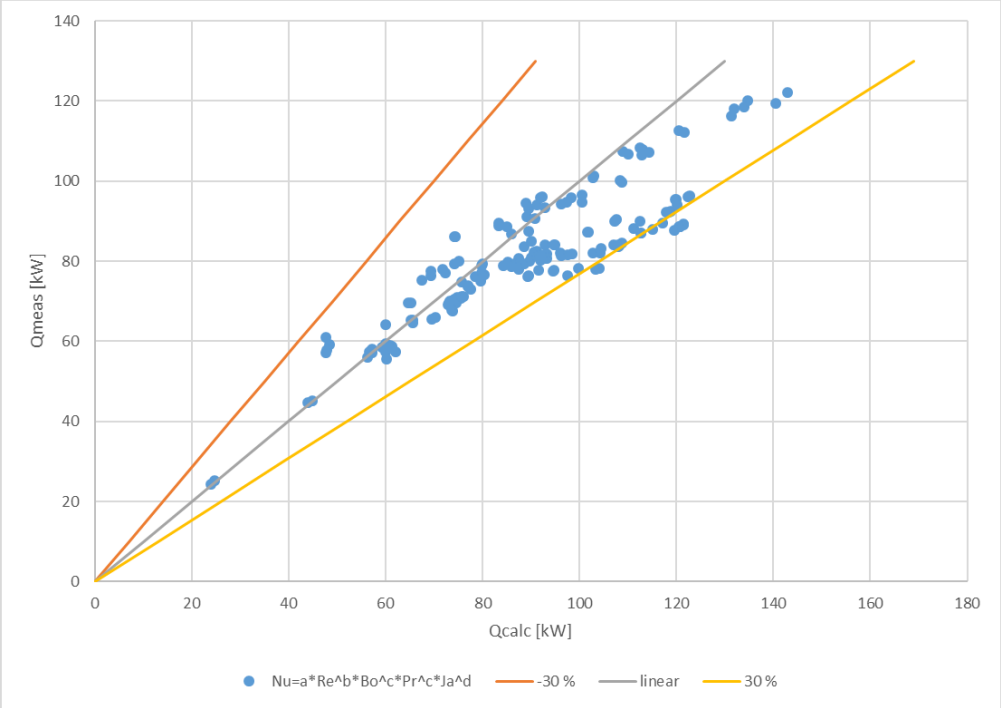

Figure 28: Accuracy of empirical correlation (IV) proposed for the cascade refrigeration cycle, applied to the thermosiphon data.

$$\mathrm{Nu} = 19.31\mathrm{We}_l^{0.893}\mathrm{Bo}^{0.448}\mathrm{Pr}_l^{-1.661}\mathrm{Ja}_l^{-1.528}$$

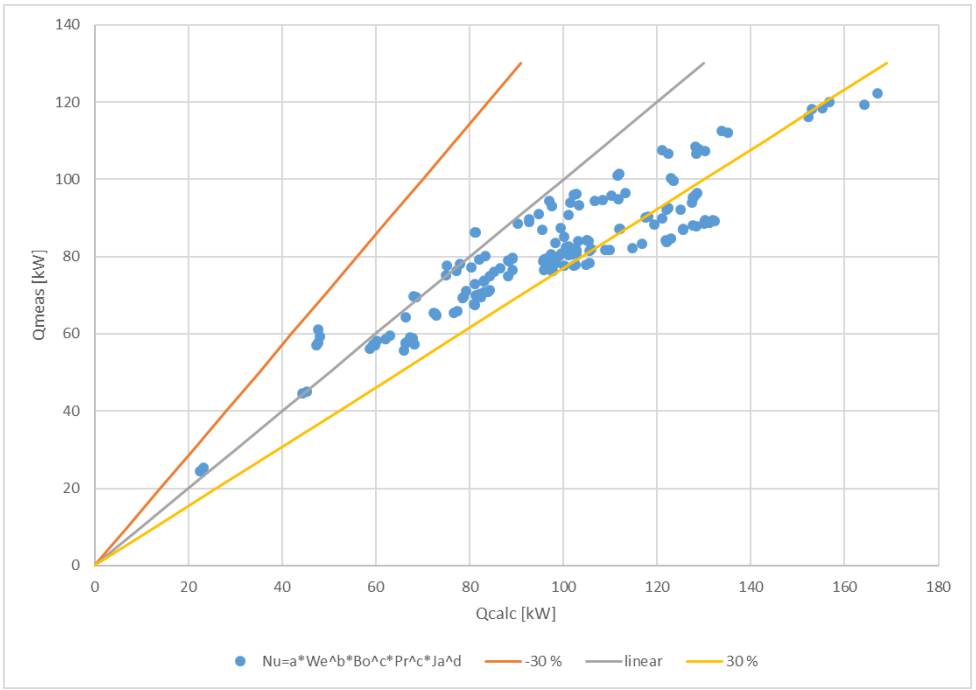

Figure 29: Accuracy of empirical correlation (V) proposed for the cascade refrigeration cycle, applied to the thermosiphon data.

$$\mathrm{Nu} = 8.9 \cdot 10^{11} \mathrm{Gr}_l^{-1.297} \mathrm{Re}_l^{1.178} \mathrm{Pr}_l^{-1.491}$$

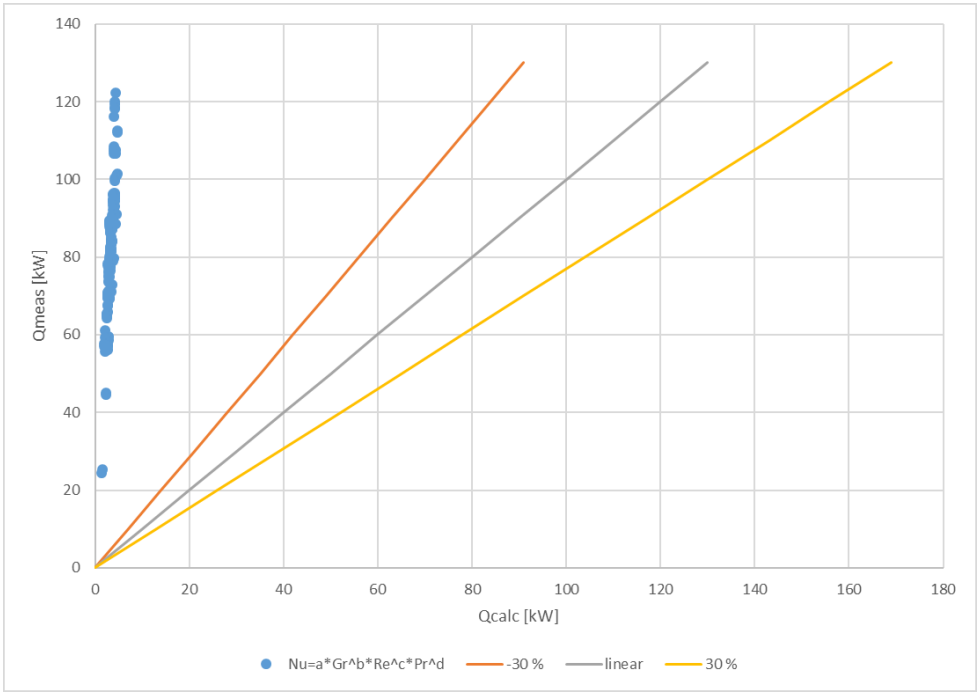

Figure 30: Accuracy of empirical correlation (I) proposed for the NH_3 refrigeration cycle, applied to the thermosiphon data.

$$\mathrm{Nu} = 1.033 \mathrm{Gr}_l^{-0.371} \mathrm{Re}_l^{1.164} \mathrm{Pr}_l^{3.318} \mathrm{Ja}_l^{-1.077}$$

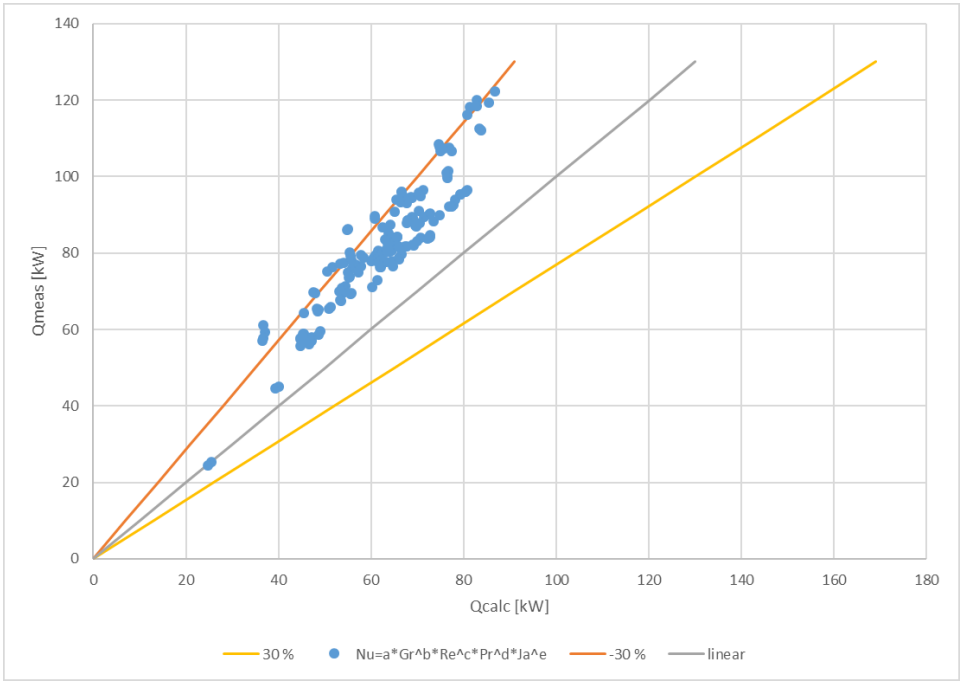

Figure 31: Accuracy of empirical correlation (III) proposed for the NH_3 refrigeration cycle data, applied to the thermosiphon data.

Not surprisingly, the empirical correlations adapted for the experiments with many refrigerants in the cascade refrigeration cycle reach the highest level of accuracy. One of the best suiting correlations for the cascade refrigeration cycle was also the most appropriate for this data set. The most appropriate correlation included phenomena such as motion created by buoyancy forces, surface superheat and density gradients, which indicate that the impact is significant and that conclusions made based on the correlations proposed directly to the thermosiphon data can be verified. The most appropriate correlation proposed for data gathered in other experiments was empirical correlation (IV):

$$\mathrm{Nu} = 0.000224\mathrm{Re}_l^{1.46}\mathrm{Bo}^{0.169}\mathrm{Pr}_l^{0.0586}\mathrm{Ja}_l^{-1.36},$$

which was originally adapted to data gathered in the cascade refrigeration cycle experiment. Empirical correlation (III) proposed for the ammonia refrigeration cycle also shows a high level of accuracy, for the reason that it partly accounts for the same phenomena, such as buoyancy motion, wall superheat and density gradients. This can be noticed, if a dimension analysis is made on the empirical correlation (III) based on the dimensionless groups included in the correlation.

5.4.2 Empirical correlations tested on the cascade refrigeration cycle

In this section, the most accurate empirical correlations proposed for the evaporators in the thermosiphon configuration and the ammonia refrigeration cycle have been tested on the cascade refrigeration cycle data set. The accuracy of the empirical correlations proposed for the cascade refrigeration cycle data set will function as a reference when a comparison between the different determined correlations is made. The test results and the conclusions made in previous sections will be discussed and verified.

The accuracy of the empirical correlations (II), (III) and (IV) proposed for the thermosiphon configuration as well as empirical correlations (I) and (III) proposed for the ammonia refrigeration cycle have been tested on the data set gathered from the cascade refrigeration cycle experiment. The accuracy is presented in table 5. Visually the suitability is presented in figures 32-36.

Table 5: Comparison of the accuracy of the most accurate empirical correlations, proposed for the other experiments and applied to the data from the cascade refrigeration cycle experiment.

	$\pm 30\%$	$\pm 20\%$	$\pm 15\%$	$\pm 10\%$	$\pm 5\%$
$\mathrm{Nu} = 1.99 \cdot 10^{-6}\mathrm{Re}_l^{1.796}\mathrm{Pr}_l^{1.05}\mathrm{Ja}_l^{-2.044}$	83%	68%	57%	40%	19%
$\mathrm{Nu} = 0.000129\mathrm{Gr}_l^{-0.243}\mathrm{Re}_l^{1.881}\mathrm{Pr}_l^{2.853}\mathrm{Ja}_l^{-1.863}$	29%	6%	1%	0%	0%
$\mathrm{Nu} = 0.000227\mathrm{Re}_l^{1.88}\mathrm{Bo}^{-0.665}\mathrm{Pr}_l^{-2.55}\mathrm{Ja}_l^{-2.11}$	25%	19%	13%	4%	1%
$\mathrm{Nu} = 8.9 \cdot 10^{11}\mathrm{Gr}_l^{-1.297}\mathrm{Re}_l^{1.178}\mathrm{Pr}_l^{-1.491}$	0%	0%	0%	0%	0%
$\mathrm{Nu} = 1.033\mathrm{Gr}_l^{-0.371}\mathrm{Re}_l^{1.164}\mathrm{Pr}_l^{3.318}\mathrm{Ja}_l^{-1.077}$	25%	19%	11%	0%	0%

$$\mathrm{Nu} = 1.99 \cdot 10^{-6}\mathrm{Re}_l^{1.796}\mathrm{Pr}_l^{1.05}\mathrm{Ja}_l^{-2.044}$$

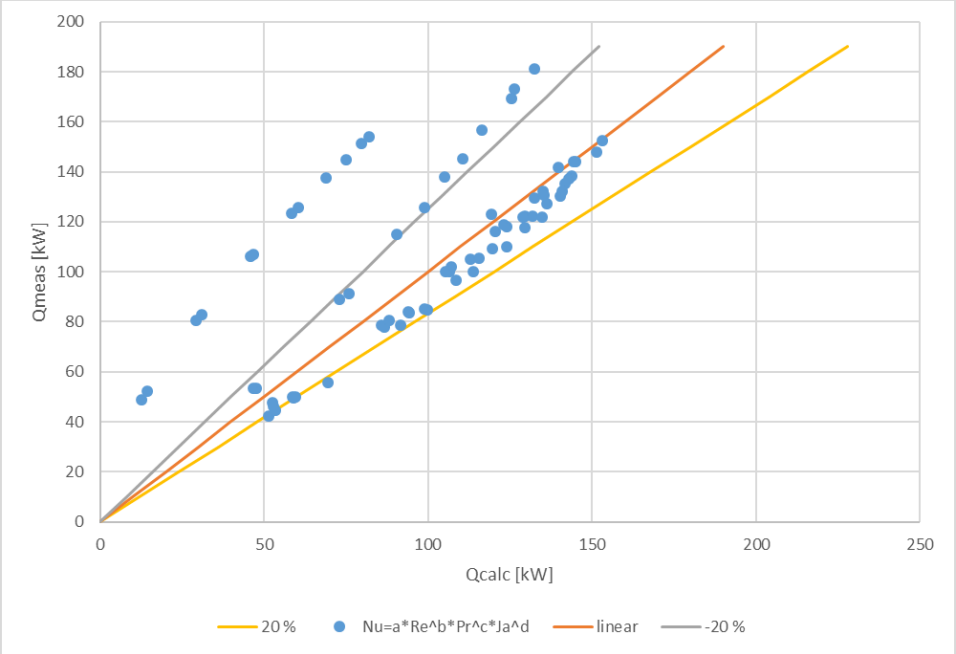

Figure 32: Accuracy of proposed correlation (II) adapted to the thermosiphon experimental data and applied to the cascade refrigeration cycle data.

$$\mathrm{Nu} = 0.000129\mathrm{Gr}_l^{-0.243}\mathrm{Re}_l^{1.881}\mathrm{Pr}_l^{2.853}\mathrm{Ja}_l^{-1.863}$$

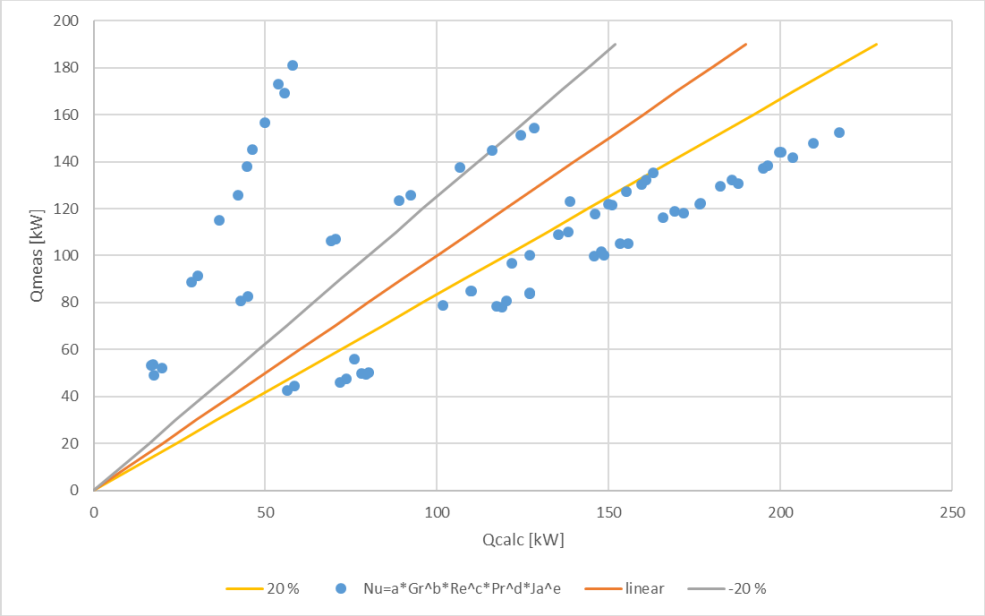

Figure 33: Accuracy of proposed correlation (III) adapted to the thermosiphon experimental data and applied to the cascade refrigeration cycle data.

$$\mathrm{Nu} = 0.000227\mathrm{Re}_l^{1.88}\mathrm{Bo}^{-0.665}\mathrm{Pr}_l^{-2.55}\mathrm{Ja}_l^{-2.11}$$

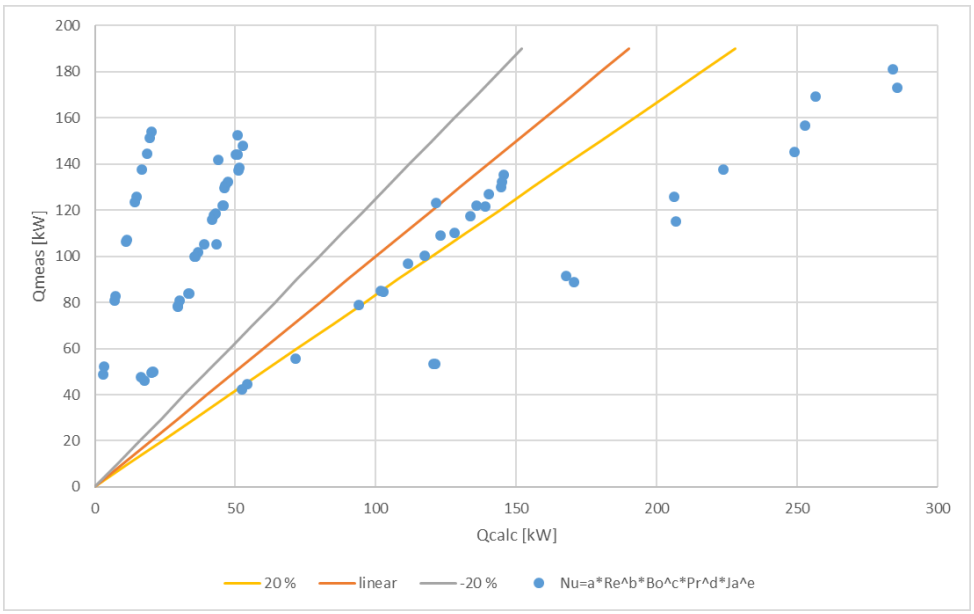

Figure 34: Accuracy of proposed correlation (IV) adapted to the thermosiphon experimental data and applied to the cascade refrigeration cycle data.

$$\mathrm{Nu} = 8.9 \cdot 10^{11} \mathrm{Gr}_l^{-1.297} \mathrm{Re}_l^{1.178} \mathrm{Pr}_l^{-1.491}$$

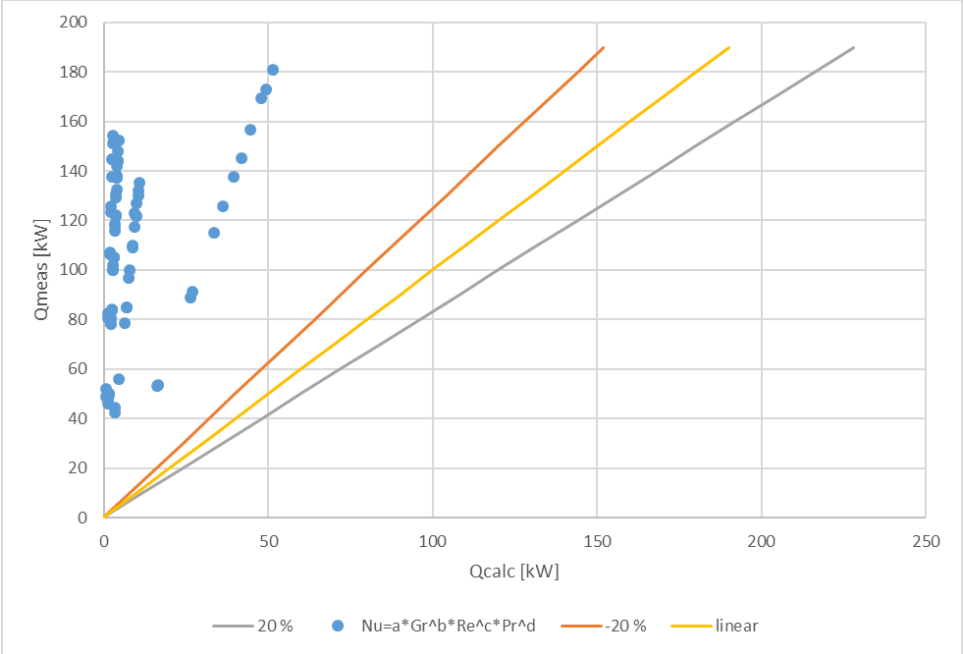

Figure 35: Accuracy of correlation (I) proposed for the NH_3 refrigeration cycle data and applied to the cascade refrigeration data.

$$\mathrm{Nu} = 1.033 \mathrm{Gr}_l^{-0.371} \mathrm{Re}_l^{1.164} \mathrm{Pr}_l^{3.318} \mathrm{Ja}_l^{-1.077}$$

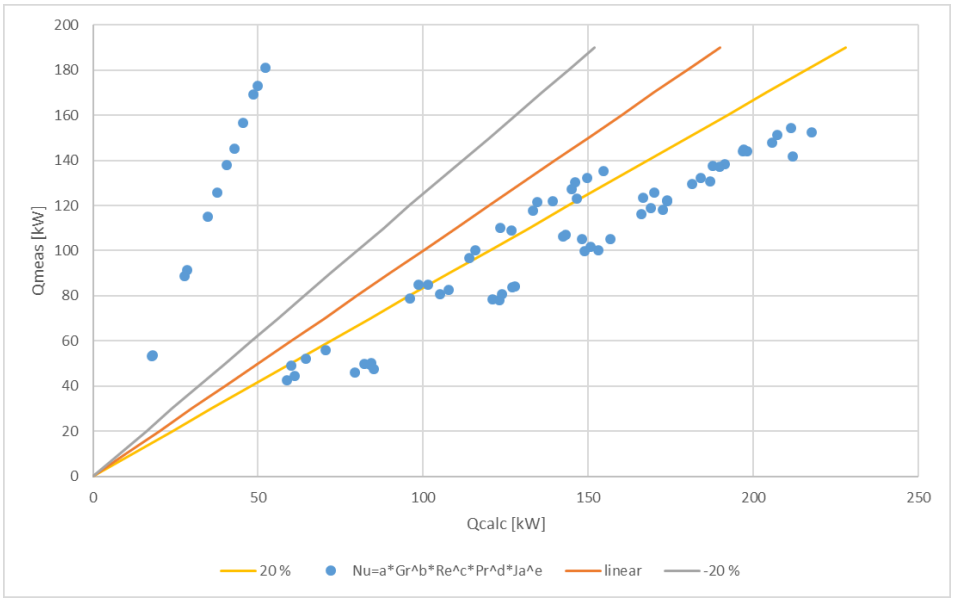

Figure 36: Accuracy of correlation (III) proposed for the NH_3 refrigeration cycle data and applied to the cascade refrigeration data.

Surprisingly, the empirical correlations that account for the same phenomena as the most accurate ones for the cascade refrigeration cycle do not show a satisfactory level of accuracy at all. Empirical correlation (II), proposed for the thermosiphon data that accounts for inertia and viscous forces, momentum and thermal diffusivities and the heat required to maintain

the refrigerant at the state of saturation proposed for the thermosiphon experimental data is the most appropriate for the cascade refrigeration cycle data. The corresponding correlation that accounts for the same phenomena and was adapted to the cascade refrigeration cycle data did also show a reasonable level of accuracy. This means that the conclusions about the dominant phenomena occurring in the process can be questioned. Empirical correlation (II) proposed for the cascade refrigeration cycle may have the same level of accuracy and describe the phenomena occurring in the process as good as empirical correlations (IV) and (V) suggested to be the most accurate ones. The correlations proposed for the superheating direct expansion evaporator in the ammonia refrigeration cycle are not appropriate at all for the cascade refrigeration data set, due to large differences in refrigerant properties between the refrigerants used in this configuration. Other remarkable reasons for poor accuracy in the empirical correlations proposed for the ammonia refrigeration cycle are the presence of superheat and the operating conditions. The presence of superheat can indicate on a totally dry evaporator surface which in turn can affect the bubble behavior. The operating conditions in the ammonia refrigeration cycle were at some extent outside the state of saturation. The most suitable correlation created for the data gathered in the other experiments was empirical correlation (II):

$$\mathrm{Nu} = 1.99 \cdot 10^{-6} \mathrm{Re}_l^{1.796} \mathrm{Pr}_l^{1.05} \mathrm{Ja}_l^{-2.044},$$

which was originally optimized for the thermosiphon data.

5.4.3 Empirical correlation tested on the ammonia refrigeration cycle

In this section, the most accurate proposed empirical correlations for the evaporators in the thermosiphon configuration and the cascade refrigeration cycle have been tested on the ammonia refrigeration cycle data set. The accuracy of the empirical correlations determined for the ammonia refrigeration cycle data set will function as a reference when a comparison between the different determined correlations is made. The test results and the conclusions made in previous sections will be verified.

The accuracy of empirical correlations (II), (III) and (IV) proposed based on data from the thermosiphon experiment and the correlations (II), (IV) and (V) proposed based on data from the cascade refrigeration cycle data will be tested on the data set gathered from the ammonia

refrigeration cycle experiment. The results are presented in table 6. Visually the suitability is presented in figures 37-42.

Table 6: Comparison of the accuracy of the most accurate empirical correlations proposed for the other experiments and tested on the data gathered from the NH_3 refrigeration cycle experiment.

	$\pm 30\%$	$\pm 20\%$	$\pm 15\%$	$\pm 10\%$	$\pm 5\%$
$\mathrm{Nu} = 1.99 \cdot 10^{-6}\mathrm{Re}_l^{1.796}\mathrm{Pr}_l^{1.05}\mathrm{Ja}_l^{-2.044}$	0%	0%	0%	0%	0%
$\mathrm{Nu} = 0.000129\mathrm{Gr}_l^{-0.243}\mathrm{Re}_l^{1.881}\mathrm{Pr}_l^{2.853}\mathrm{Ja}_l^{-1.863}$	41%	19%	17%	12%	7%
$\mathrm{Nu} = 0.000227\mathrm{Re}_l^{1.88}\mathrm{Bo}^{-0.665}\mathrm{Pr}_l^{-2.55}\mathrm{Ja}_l^{-2.11}$	0%	0%	0%	0%	0%
$\mathrm{Nu} = 0.00174\mathrm{Re}_l^{1.268}\mathrm{Pr}_l^{0.234}\mathrm{Ja}_l^{-1.103}$	0%	0%	0%	0%	0%
$\mathrm{Nu} = 0.000224\mathrm{Re}_l^{1.46}\mathrm{Bo}^{0.169}\mathrm{Pr}_l^{0.0586}\mathrm{Ja}_l^{-1.36}$	0%	0%	0%	0%	0%
$\mathrm{Nu} = 19.31\mathrm{We}_l^{0.893}\mathrm{Bo}^{0.448}\mathrm{Pr}_l^{-1.661}\mathrm{Ja}_l^{-1.528}$	0%	0%	0%	0%	0%

$$\mathrm{Nu} = 1.99 \cdot 10^{-6}\mathrm{Re}_l^{1.796}\mathrm{Pr}_l^{1.05}\mathrm{Ja}_l^{-2.044}$$

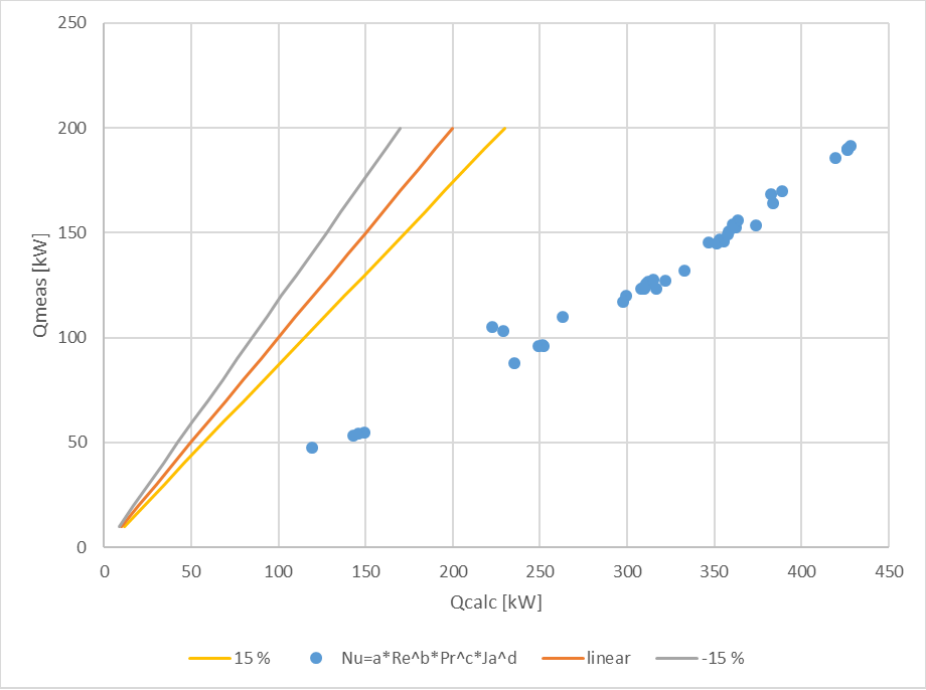

Figure 37: Accuracy of correlation (II), proposed for the thermosiphon experimental data and applied to the NH_3 refrigeration cycle data.

$$\mathrm{Nu} = 0.000129\mathrm{Gr}_l^{-0.243}\mathrm{Re}_l^{1.881}\mathrm{Pr}_l^{2.853}\mathrm{Ja}_l^{-1.863}$$

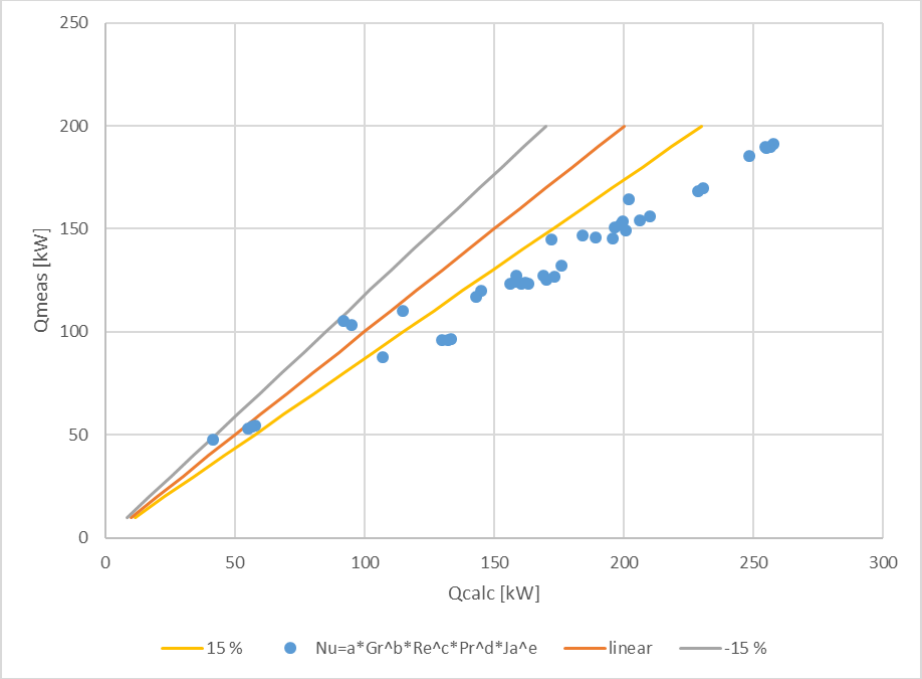

Figure 38: Accuracy of correlation (III), proposed for the thermosiphon experimental data and applied to the NH_3 refrigeration cycle data.

$$\mathrm{Nu} = 0.000227\mathrm{Re}_l^{1.88}\mathrm{Bo}^{-0.665}\mathrm{Pr}_l^{-2.55}\mathrm{Ja}_l^{-2.11}$$

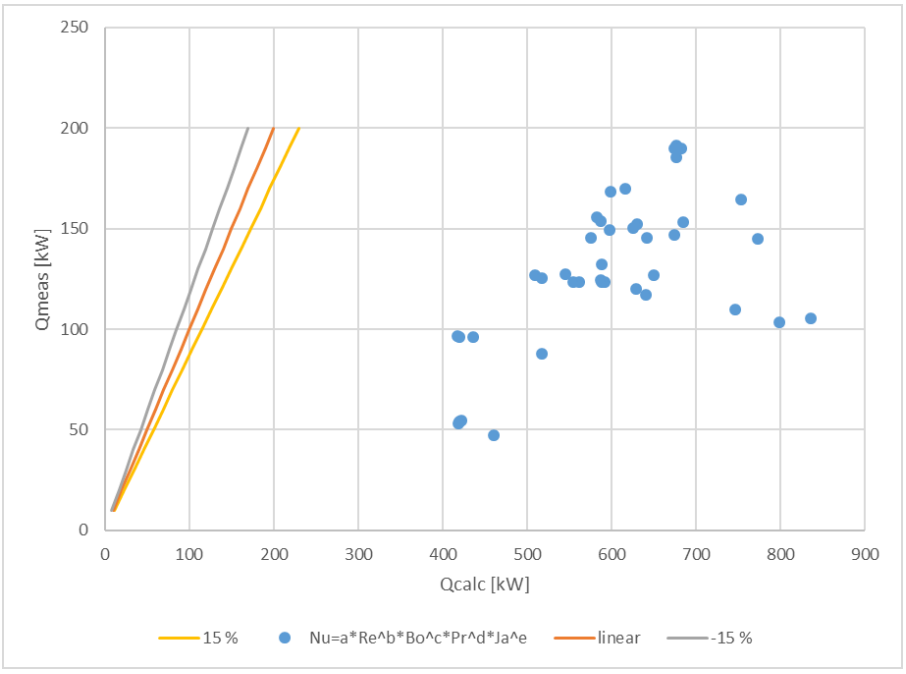

Figure 39: Accuracy of correlation (IV), proposed for the thermosiphon experimental data and applied to the NH_3 refrigeration cycle data.

$$\mathrm{Nu} = 0.00174\mathrm{Re}_l^{1.268}\mathrm{Pr}_l^{0.234}\mathrm{Ja}_l^{-1.103}$$

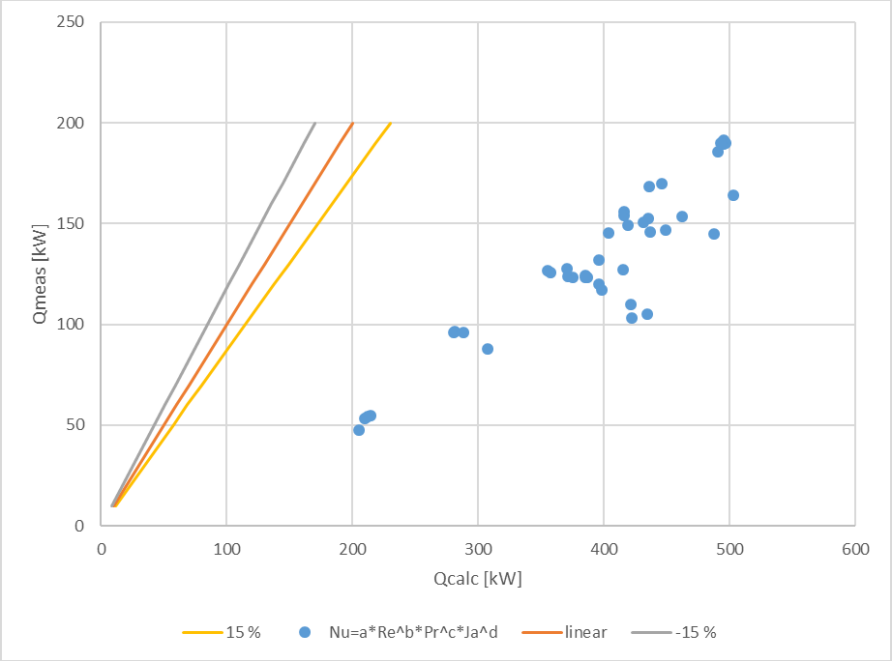

Figure 40: Accuracy of correlation (II), proposed for the cascade refrigeration cycle experimental data and applied to the NH₃ refrigeration cycle data.

$$\mathrm{Nu} = 0.000224\mathrm{Re}_l^{1.46}\mathrm{Bo}^{0.169}\mathrm{Pr}_l^{0.0586}\mathrm{Ja}_l^{-1.36}$$

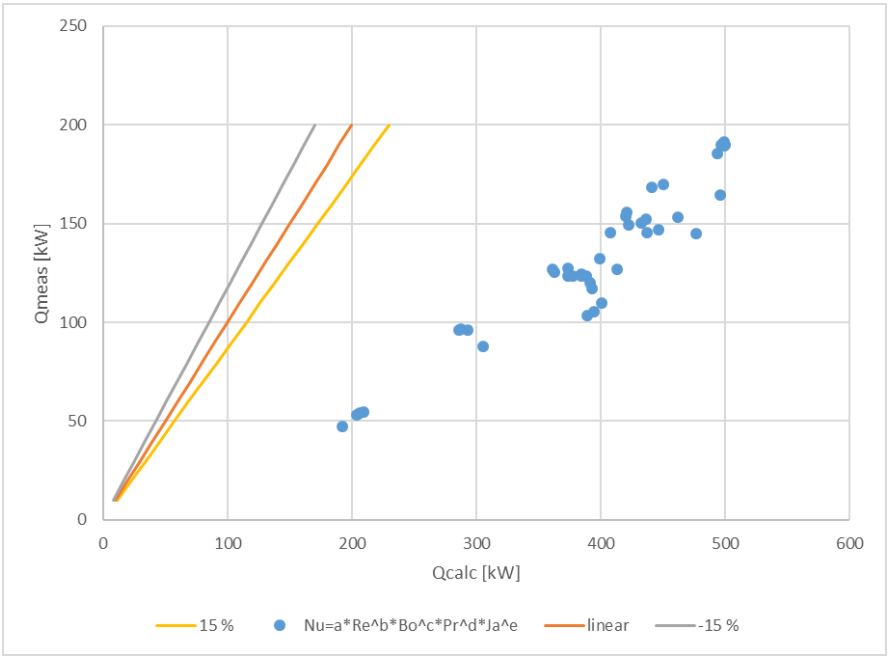

Figure 41: Accuracy of correlation (IV), proposed for the cascade refrigeration cycle experimental data and applied to the NH₃ refrigeration cycle data.

$$\mathrm{Nu} = 19.31\mathrm{We}_l^{0.893}\mathrm{Bo}^{0.448}\mathrm{Pr}_l^{-1.661}\mathrm{Ja}_l^{-1.528}$$

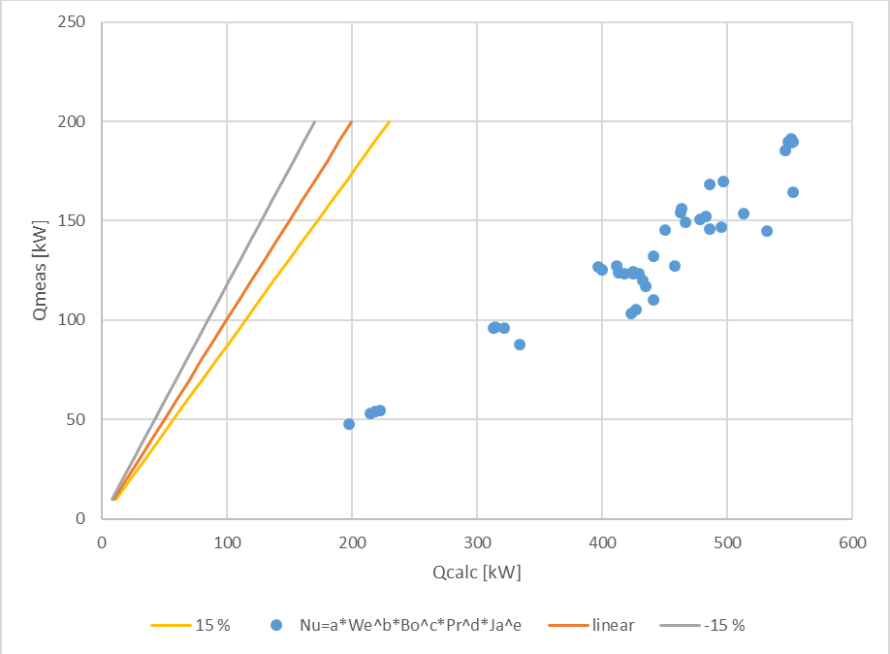

Figure 42: Accuracy of correlation (V), proposed for the cascade refrigeration cycle experimental data and applied to the NH_3 refrigeration cycle data.

None of the empirical correlations proposed for the other configurations show a satisfactory level of accuracy, as presented in table 6 and figures 37-42, due to totally different operation modes. The refrigerant enters as a vapor-liquid mixture and exits as superheated vapor. The increased vapor fraction in the fluid results in a larger impact of fluid motion created by the density and temperature gradients which, in turn, results in a larger impact of natural convection. The bubble behavior does not therefore correspond to the other empirical correlations satisfactorily. The most appropriate correlation created for the other data sets accounts partially for the same phenomena as the ammonia refrigeration cycle. The unsatisfactory level of accuracy may also originate from differences in the properties between the refrigerants used in the other experiments. The most accurate empirical correlation proposed for the data sets in the other experiments was correlation (III):

$$\mathrm{Nu} = 0.000129\mathrm{Gr}_l^{-0.243}\mathrm{Re}_l^{1.881}\mathrm{Pr}_l^{2.853}\mathrm{Ja}_l^{-1.863}$$

which was originally optimized to the thermosiphon data set.

6 Conclusions

Basic theory about heat transfer has been presented, with the emphasis on two-phase heat transfer in plate heat exchangers. The mechanisms of the phase change of a fluid have been the main subject of interest. Multiple theories about phase change of a fluid have been presented in the literature, but the theories are often in conflict with each other. The boiling mechanisms are dependent on the environment the phase change occurs in and the geometry of the surface that the fluid is boiled on. Many theoretical models have been proposed in the literature, but all of them are either tailored to a specific data set with their own operating conditions or just simulations that include variables that are not possible to measure efficiently during a boiling experiment. Such variables are vapor fractions in the fluid and bubble diameters, for example. Three experiments were conducted in order to gather boiling data for plate and shell evaporators. After the experiments were conducted, the boiling heat transfer coefficients were attempted to be predicted through empirical correlations that account for different boiling phenomena occurring in the different types of processes. The heat transfer geometry was similar in all of the experiments which, in turn, allowed to focus only on the phenomena occurring in the process and on the conditions the boiling took place in. Buoyancy behavior, flow conditions, boundary layer conditions and wall superheat were phenomena that were determined to be considerable when predicting a heat transfer coefficient during a liquid-vapor phase change during boiling. The empirical correlations indicated that the boiling mechanisms are totally different if the boiled fluid exits as superheated vapor or enters as a vapor-liquid mixture. The correlations proposed for the flooded evaporator in the thermosiphon configuration and the evaporator in the cascade refrigeration cycle indicate that the same fundamental phenomena occur in the boiling processes. The flooded evaporator in the thermosiphon configuration indicated the governance of the nucleate boiling regime, although it is generally considered that the dominating boiling regime in such evaporators is convective boiling. The dominating boiling regime in the evaporator in the cascade refrigeration cycle was also determined to be nucleate boiling. The deviation in the parameters optimized for the thermosiphon experiment as well as for the cascade refrigeration cycle experiments may originate from the differences in the operating conditions, refrigerant properties, as well as from the fact that one of them was of “flooded” type and the other of “direct expansion” type. The third experiment, where the refrigerant entered as a liquid-vapor mixture and exited as superheated vapor, deviated from

the behavior of the other conducted experiments which, in turn, indicated that different boiling heat transfer mechanisms govern at different operating modes of the same type of heat exchangers.

7 Sources

Ayub, Z.H., Ayub, A.H., Khan, T.S, Salam, S. & Nawaz, K. (2019). Literature survey and universal evaporation correlation for plate type heat exchangers. *International Journal of Refrigeration*, Vol. 99, p. 408-418.

Bell, K. J & Mueller, A.C. (2001). *Wolverine Engineering Data book II*. Wolverine Tube Inc.

Brooks, S.C. & Hibiki, T. (2015). Wall nucleation modeling in subcooled boiling flow. *International Journal of Heat and mass Transfer*, Vol. 86, p. 183-196.

Chen, J.C. (1966). Correlation for boiling heat transfer to saturated fluids in convective flow. *Ind. Eng. Chem. Process Des. Dev.*, 5 (3), p. 322-329.

Chen, S., Liu, D., Xiao, Y. & Gu, H. (2019). Experimental study on onset of nucleate boiling and flow boiling heat transfer in a 5x5 rod bundle at low flow rates. *International Journal of Heat and Mass Transfer*, Vol. 137, p. 727-739.

Clark, J. A. (1969). *Cryogenic Heat Transfer*. Advances in Heat Transfer, Vol. 5, p. 325-517

Coulson, J.M, Richardson, J.F., Backhurst, J.R. & Harker, J.H. (2000). *Coulson & Richardson's chemical engineering*. 6th edition. Butterworth Heinemann. Vol. 1.

Ebrahimi-Mamaghani, A., Sotudeh-Gharebagh, R., Zarghami, R. & Moustoufi, N. (2019). Dynamics of two-phase flow in vertical pipes. *Journal of Fluids and Structures*, Vol. 87, p. 150-173

Eldeeb, R., Aute, V. & Radermacher, R. (2016). A survey of correlations for heat transfer and pressure drop for evaporation and condensation in plate heat exchangers. *International Journal of Refrigeration*, Vol. 65, p. 12-26.

Hall, S.M. (2018). *Rules of Thumb for Chemical Engineers*. Elsevier Inc., 6th edition, p. 197-230.

Hartwig, J., Darr, S. & Asencio, A. (2016). Assessment of existing two phase heat transfer coefficient and critical heat flux correlations for cryogenic flow boiling in pipe quenching experiments. *International Journal of Heat and Mass Transfer*, Vol. 93, p. 441-463.

Hesselgreaves, J.E. (2001). *Compact heat exchangers – Selection, Design and Operation*. Elsevier Ltd, Vol.1, p. 125-153, 201-273, 275-302.

Incropera, F.P., Dewitt, D.P, Bergman T.L & Lavine A.S (2007). *Fundamentals of Heat and Mass Transfer*. John Wiley & Sons Inc., 6th edition.

Khan, T.S., Khan, M.S, Chyu, M.C. & Ayub, Z.H. (2010). Experimental investigation of single phase convective heat transfer coefficient in a corrugated plate heat exchanger for multiple plate configurations. *Applied Thermal Engineering*, Vol. 30, p.1058-1065.

Koyama, K., Arima, H., Ikegami, Y. & Chiyoda, H. (2014). Experimental study on thermal characteristics of ammonia flow boiling in a plate evaporator at low mass flux. *International Journal of Refrigeration*, Vol. 38, p. 227-235.

Kumar Singh, G., Pradhan, S. & Tanna, V. (2018). Experimental studies of two phase flow characteristics and void fraction predictions in steady state two phase nitrogen flow. *Cryogenics*, Vol. 100, p. 77-84

Lemmon, E.W., Bell, I.H., Huber, M.L., McLinden, M.O. NIST Standard Reference Database 23: Reference Fluid Thermodynamic and Transport Properties-REFPROP, Version 10.0, National Institute of Standards and Technology, Standard Reference Data Program, Gaithersburg, 2018.

Mahmoud, M.M. & Karayiannis, T.G. (2013). Heat transfer correlation for flow boiling in small to micro tubes. *International Journal of Heat and Mass Transfer*. Vol. 66, p. 553-574.

Nitsche, M. & Gbadamosi, R.O. (2016). Chapter 10-Design of Thermosiphon Reboilers. *Heat Exchanger Design Guide – A Practical Guide for Planning, Selecting and Designing of Shell and Tube Exchangers*. Butterworth Heinemann, p. 181-227

Perry, R.H., Green, D.W & Maloney, J.O. (1997). *Perry's chemical engineers' handbook*. 7th edition. McGraw-Hill.

Shah, R.K. & Sekulic, D.P. (2003). *Fundamentals of heat exchanger design*. United States of America: John Wiley & Sons Inc. Vol.10.

Táboas F., Vallès, M., Bourouis, M. & Coronas A. (2010). Flow boiling heat transfer of ammonia/water mixture in a plate heat exchanger. *International Journal of Refrigeration*, Vol. 33, p. 695-705

Tovazhnyanskyy, L.L., Kapustenko, P.O., Arsenyeva, O. P., Khavin, G.L., Yuzbashyan, A.P. & Arsenyev, P.Y. (2016). Two types of welded plate heat exchangers for efficient heat recovery industry. *Applied Thermal Engineering*, Vol. 105, p.763-773